DIFFERENTIAL SCANNING CALORIMETRY IN HIGH

TEMPERATURE CHEMISTRY

By

PAUL DEAN GWINUP

Bachelor of Science

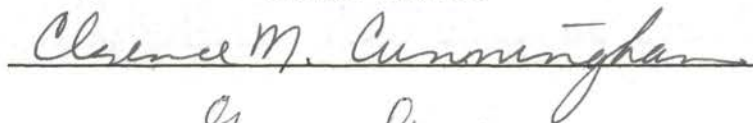Oklahoma State University

Stillwater, Oklahoma

1957

Submitted to the Faculty of the Graduate College
of the Oklahoma State University
in partial fulfillment of the requirements
for the degree of
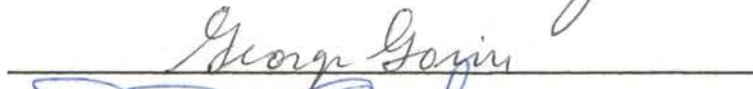DOCTOR OF PHILOSOPHY
July, 1967
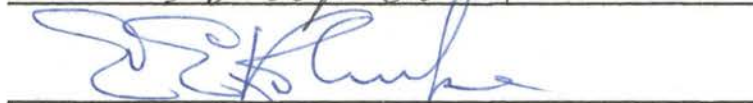
DIFFERENTIAL SCANNING CALORIMETRY IN HIGH

TEMPERATURE CHEMISTRY

Thesis Approved:

_____
Thesis Adviser

Clarence M. Cunningham

George Gorin

_____

J. Paul Devlin

_____
Dean of the Graduate College

ii

ACKNOWLEDGMENTS

TABLE OF CONTENTS

TABLE OF CONTENTS (Continued)

LIST OF TABLES

LIST OF FIGURES

CHAPTER I

INTRODUCTION

Differential scanning calorimetry is similar in many respects to
an older technique, differential thermal analysis (DTA), which was in-
vented in 1887 by Le Chatelier (1). In DTA any thermal effects in the
sample of interest are compared with the null effect in an inert ma-
terial as the temperature of both the sample and inert substance is in-
creased. This comparison is accomplished by placing one junction of a
differential thermocouple in the sample and the other junction in the
inert reference material. The temperature of the furnace surrounding
the sample and reference material is increased linearly with time. If
the sample undergoes a heat effect, its net rate of temperature rise
will be different from that of the reference material; the resulting
temperature difference will cause a voltage to appear across the dif-
ferential thermocouple. This voltage increases slowly as the sample
begins to extract energy from the sample holder; then more rapidly as
the reaction speeds up, reaches a maximum, and then returns to the
base line as the reaction is completed. The data obtained from the re-
sulting peaks indicate whether the reaction is endothermic or exother-
mic and the temperature range over which the reaction occurs. This
qualitative information is rather specific for a given substance, and
has been used extensively by ceramists for identification purposes.

The possibility that DTA might be used to obtain information about

1

the quantity of energy involved in thermal effects has such potential that several attempts have been made to bring it about (2-9). These attempts divide themselves into computational and calibration methods. The computational methods attempt to relate the enthalpy change for the reaction to the characteristic height, area, and shape of the DTA peak. The calibration methods utilize a reaction, similar to the reaction of interest, of known enthalpy change to obtain peak area calibration. These methods have proven to be only moderately successful.

Differential scanning calorimetry (DSC) utilizes the basic DTA equipment. In DSC, however, the sample is surrounded by a small heater which supplies the energy required by the reacting sample (3, 10). Electrical energy is supplied to the heater by an electronic control system at a rate that will just keep the sample and reference thermocouples at the same temperature. Speros and Woodhouse (10) have developed the conditions necessary for equating the enthalpy of the reaction to the amount of energy supplied by the heater. When these conditions are met, the kinetics of the reaction can be obtained from the rate of energy input, and the enthalpy change for the reaction from the integral of the rate vs. time curve. These conditions are satisfied by adjusting the instrument and, thus, are not specific to any particular type of reaction.

The purpose of this study was to design and construct a differential scanning calorimeter with which to investigate the kinetic and thermodynamic properties of temperature-induced solid decomposition and disproportionation reactions. These reactions are of the following general type,

$$A_{(solid)} + Energy \longrightarrow B_{(solid)} + C_{(gas)} \quad .$$
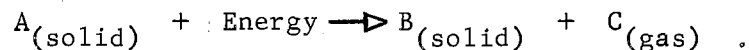
In such reactions, in which the product gas is a molecular species different from that which exists in the solid phase, equilibrium is seldom established; therefore, measurements by the usual techniques, i.e., Knudsen effusion, transpiration, or static pressure measurement, have been difficult or impossible (11). Many collisions of $C_{(gas)}$ with the solid surface are required before the reverse reaction occurs. In the Knudsen or transpiration techniques the gaseous molecule usually has a higher probability of leaving the vessel containing the solid phase than of colliding favorably with the surface; equilibrium is therefore never achieved. A static pressure measurement, while not suffering from these disadvantages, also presents difficulties when one considers container materials and pressure transducers for high temperature applications. Differential scanning calorimetry is amenable to closed-cell reactions in self-generated atmospheres, or open-cell reactions in controlled atmospheres, with a wide variety of cell materials. Since differential scanning calorimetry measures energy changes directly, it should also be useful in non-gas-producing reactions such as solid-solid transitions or reactions in solutions.

CHAPTER II

THEORETICAL BASIS FOR DIFFERENTIAL

SCANNING CALORIMETRY

Speros and Woodhouse (10) developed the equations that placed dif-
ferential scanning calorimetry on a sound theoretical basis. The
analysis that follows is essentially theirs, except for the order of
presentation. For the analysis the model chosen to represent the DSC
system consists of a metal block with high thermal conductivity im-
mersed in a gas; a dimensionless heat source $\underline{H}$ (the sample heater),
heat sink $\underline{S}$ (a melting sample), and sample thermocouple TC_S are embedded
in the metal block; the reference structure consists of a thermocouple
TC_R embedded in a metal block identical to the sample structure. The
sample and reference structures are shown diagrammatically in Figure 1.

The temperature of the gas, $\underline{T}_g$, in which the sample and reference
structures are immersed is increased linearly with time. When the gas
temperature reaches the melting point of the sample, $\underline{T}_m$, melting be-
gins. At this point energy must be supplied by the sample heater to
prevent the temperature of the sample structure from lagging behind
that of the reference structure. The conditions that must be met for
the energy supplied by the sample heater to be equal to the enthalpy
change for the fusion can be developed from two considerations: (1)
temperature balance between the sample and reference thermocouples,
and (2) thermal balance within the sample structure.

4

Temperature balance between the sample and reference thermocouples is maintained by supplying energy from the heater to the sample thermocouple. When steady state conditions have been established, the rate at which energy is supplied to the sample thermocouple by the heater is equal to the rate at which energy is extracted from the sample thermocouple by the melting sample. The condition of temperature balance between the sample and reference structures can be expressed by

$$T_S = T_R = T_g . \tag{1}$$

From the steady state assumption one can write for the <u>sample thermocouple</u>,

$$\left(\frac{dQ}{dt}\right)_{in} = \left(\frac{dQ}{dt}\right)_{out} \tag{2}$$

where Q represents the quantity of energy involved. For one dimensional energy flow one can write (see Figure $\underline{1}$)

$$\left(\frac{dQ}{dt}\right)_{in} = -\frac{1}{r'D'}\left(T_S - T_h\right) \tag{3}$$

$$\left(\frac{dQ}{dt}\right)_{out} = -\frac{1}{rD}\left(T_m - T_S\right) \tag{4}$$

in which $\underline{r}'$, $\underline{r}$ are "thermal resistance" constants (i.e., reciprocal thermal conductivities), $\underline{T}_h$ is the heater temperature, and $\underline{D}'$, $\underline{D}$ are the distances from heater to sample thermocouple and from thermocouple to sample, respectively ($\underline{12}$). Combination of (2), (3), (4) gives

$$\frac{T_h - T_S}{r'D'} = \frac{T_S - T_m}{rD} \tag{5}$$
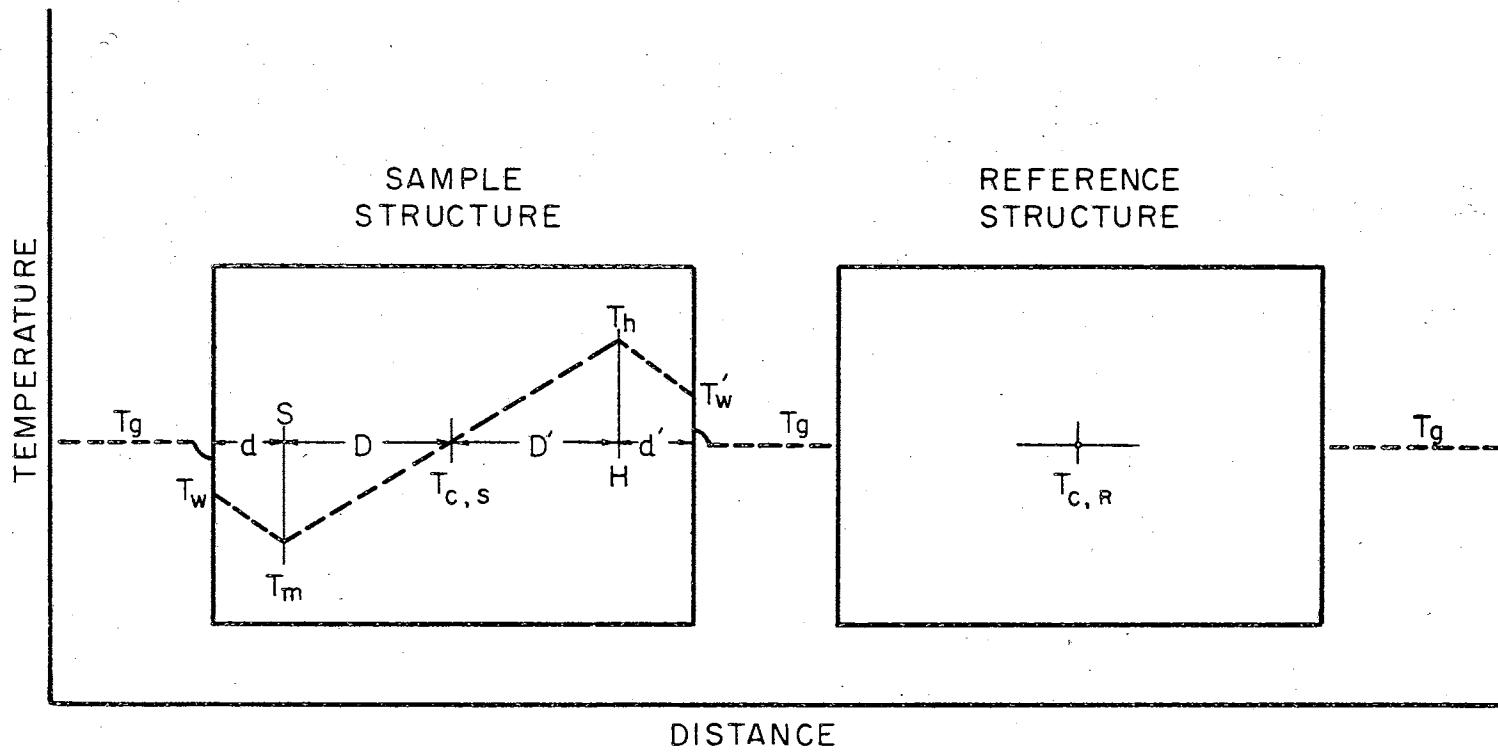
Figure 1. Model Representing DSC System

which can be arranged to obtain

$$\frac{T_S - T_m}{T_h - T_S} = \frac{rD}{r'D'} \tag{6}$$

Substitution of (1) into (6) gives

$$\frac{T_g - T_m}{T_h - T_g} = \frac{rD}{r'D'} = \frac{D}{D'} = \Delta \tag{7}$$

since, for a homogeneous solid, $\underline{r}' = \underline{r}$. The term on the left in equation (7) must be a constant independent of the nature of the melting sample, because $\underline{D}$ and $\underline{D}'$ are constant for a given sample structure. Even though $\underline{T}_m$ and the enthalpy change per gram vary from sample to sample, $\underline{T}_h$ and $\underline{T}_g$ may also vary to maintain temperature balance between sample and reference structures. Thus, equation (7) will hold when temperature balance and steady state conditions exist.

Again referring to Figure 1, one can write the following energy flow equations for the sample structure. The heater loses energy at a rate given by

$$\frac{dQ}{dt} = \left(\frac{-1}{rD + r'D'}\right)\left(T_m - T_h\right) + \frac{dL}{dt} \tag{8}$$

where (dL/dt) is the rate of energy loss to the surroundings. The melting sample absorbs energy at a rate given by

$$\frac{dH}{dt} = \left(\frac{-1}{rD + r'D'}\right)\left(T_m - T_h\right) + \frac{dG}{dt} \tag{9}$$

where (dG/dt) is the rate of energy absorption by the sample from the surroundings.

Equations (8) and (9) indicate that energy balance, $\Delta Q = \Delta H$, can be achieved if the energy lost to the surroundings by the heater is equal to the energy gained from the surroundings by the melting sample, i.e., if

$$\frac{dL}{dt} = \frac{dG}{dt} \, . \tag{10}$$

Expressions for these energy transfers can be obtained by assuming steady state conditions at the walls of the sample structure. The energy gained by the sample from the surroundings is

$$\frac{dG}{dt} = -\frac{1}{rd}\left(T_m - T_w\right) = -\frac{1}{R}\left(T_w - T_g\right) \tag{11}$$

in which r and R are "thermal resistance" constants for the metal and gas respectively; T_w the wall temperature adjacent to the sample, and d the distance from sample to wall. The expression on the right in (11) is the rate at which energy is transmitted to the wall from the gas, and the middle term is the rate of energy flow away from the wall to the sample. Separation of the equality in (11) gives.

$$\frac{dG}{dt} = -\frac{1}{rd}\left(T_m - T_w\right), \tag{12}$$

and

$$\frac{dG}{dt} = -\frac{1}{R}\left(T_w - T_g\right), \tag{13}$$

which may be rewritten as

$$rd\left(\frac{dG}{dt}\right) = -\left(T_m - T_w\right) , \tag{14}$$

and

$$R\left(\frac{dG}{dt}\right) = -\left(T_w - T_g\right) .$$ (15)

Addition of (14) and (15) with subsequent rearrangement gives

$$\frac{dG}{dt} = \frac{T_g - T_m}{R + rd} .$$ (16)

The energy lost by the heater to the surroundings is (cf. equation (11))

$$\frac{dL}{dt} = -\frac{1}{r'd'}\left(T'_w - T_h\right) = -\frac{1}{R'}\left(T_g - T'_w\right)$$ (17)

where r' is the metal "thermal resistance" constant, R' is the gas "thermal resistance" constant, d' is the distance from heater to the wall, and T'_w is the temperature of the wall adjacent to the heater. Separation of the equality and repetition of the sequence of (12) - (16) gives

$$\frac{dL}{dt} = \frac{T_h - T_g}{R' + r'd'} .$$ (18)

From equations (16) and (18) it follows that the condition expressed by equation (10) is satisfied if

$$\frac{T_g - T_m}{R + rd} = \frac{T_h - T_g}{R' + r'd'} .$$ (19)

Rearrangement gives

$$\frac{T_g - T_m}{T_h - T_g} = \frac{R + rd}{R' + r'd'} ,$$ (20)

and the term on the left is identical with that obtained in equation
(7) from consideration of temperature balance between sample and ref-
erence structures; therefore

$$\frac{R + rd}{R' + r'd'} = \Delta = \frac{D}{D'} ,$$

(21)

Equations (7), (20), and (21) indicate the restrictions that must
be met if the energy supplied by the heater is to be equal to the en-
thalpy change. If $\frac{R + rd}{R' + r'd'} \neq \Delta$, then ΔQ will not equal ΔH even
though temperature balance is maintained between sample and reference
structures. Fortunately, one anticipates that it should be possible
to satisfy the restrictions of equation (21) since the distances $\underline{d}$, $\underline{d}'$,
$\underline{D}$, $\underline{D}'$ and the thermal resistance constants $\underline{r}$, $\underline{r}'$, $\underline{R}$, $\underline{R}'$, can be varied
by design of the sample structure and choice of materials, respective-
ly. The technique used by Speros and Woodhouse and in this work to
effect the balancing is to vary the sample structure, by adjusting
the distance between sample, heater, and thermocouple, until the
measured energy input is equal to the known enthalpy of fusion of a
pure metal sample. If the analysis above is valid, once this balance
is achieved no further adjustment is necessary regardless of the type
of reaction to be studied.

Kinetics From Differential Scanning Calorimetry

Determination of reaction rates from differential thermal analysis
and from thermogravimetric analysis (TGA) has been the subject of many
papers (4,13-16). These methods consist of relating the various
parameters of the DTA or TGA curve to the terms in an assumed rate

expression. In DSC the method is much the same, except that for a balanced sample structure one can reasonably assume that the rate of reaction is proportional to the rate of energy input. This constitutes a rather fundamental difference between DSC and DTA; the peaks obtained by these two techniques are quite similar, but in DSC the ordinate represents directly the rate of energy input to the sample.

For reactions of the type

$$A_{(solid)} \longrightarrow B_{(solid)} \quad + \quad C_{(gas)} \tag{22}$$
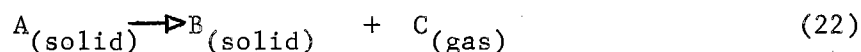
the kinetics are described in many cases (17) by

$$\frac{dx}{dt} = k(1-x)^{\alpha} \tag{23}$$

where x is the fraction of product that exists at any time t, and α is the order. It has been pointed out, however, that this equation has no general validity for heterogeneous solid state reactions (16); other rate expressions have been proposed (19,20).

When the sample structure is balanced (cf. equation (21)), the absorption of energy, dH, in a small time interval is proportional to the number of moles reacting, dn, in that time interval. This can be expressed mathematically as

$$dn = KdH \tag{24}$$

By integrating (24) one can obtain the proportionality constant K,

$$\int_{m=o}^{m=n} dn = K \int_{H_1}^{H_2} dH \tag{25}$$

$\underline{N}$ is the number of moles of product formed and, with the stoichiometry of (22), is also the initial number of moles of reactant. The second integral in (25) represents the total enthalpy change ΔH_r for the reaction as it occurs in the cell. Integration of (25) therefore gives

$$N = K\Delta H_r \quad , \tag{26}$$

or

$$K = \frac{N}{\Delta H_r} \quad .$$

Substitution of (26) into (24), the initial equation, yields

$$dn = \frac{N}{\Delta H_r} \, dH. \tag{27}$$

Differentiation with respect to time and substitution of $\underline{x}$ for $\underline{n}/\underline{N}$ give

$$\frac{dx}{dt} = \frac{1}{\Delta H_r} \frac{dH}{dt} \quad . \tag{28}$$

From equation (28) $\underline{x}$ at any time $\underline{t}_1$ can be obtained by integration,

$$\int_{x = o}^{x = x} dx = \int_{t = t_o}^{t = t_1} \left(\frac{1}{\Delta H_r} \frac{dH}{dt} \right) dt \quad , \tag{29}$$

or

$$x = \frac{1}{\Delta H_r} \int_{H_o \text{ at } t_o}^{H_1 \text{ at } t_1} dH = \frac{a}{\Delta H_r} \quad . \tag{30}$$

The expression

$$a = \int_{H = H_o}^{H = H_1} dH \qquad (31)$$

represents the area of the DSC peak at a given time $\underline{t}_1$. Integration of (31) from $\underline{H}_o$ at $\underline{t} = \underline{t}_o$ to $\underline{H}_\infty$ at $\underline{t} = \underline{t}_\infty$ (i.e., when the reaction is complete) gives, as in (25) and (26),

$$A = \int_{H = H_o}^{H = H_\infty} dH = \Delta H_r \; ; \qquad (32)$$

hence, $\underline{A}$ represents the total area of the DSC peak. Substitution into (23) from equations (28), (30), and (32) gives

$$\frac{1}{A} \frac{dH}{dt} = k \left(1 - \frac{a}{A}\right)^{\alpha} \qquad (33)$$

which may be solved for the specific rate constant $\underline{k}$,

$$k = \frac{1}{A} \frac{dH}{dt} \left(1 - \frac{a}{A}\right)^{-\alpha} \qquad (34)$$

All of the quantities on the right side of (34) except $\underline{\alpha}$ are obtainable at a given temperature from the DSC curve. Figure 2 shows a typical curve with these quantities indicated.

The order $\underline{\alpha}$ of the reaction may be obtained by the method proposed by Borchardt and Daniels ($\underline{4}$). In this method one divides the DSC peak into a series of intervals. At the end of each interval one has values for $\underline{a}$, $d\underline{H}/d\underline{t}$, and $\underline{T}$, the absolute temperature. A value for $\underline{\alpha}$ is then assumed, and $\underline{k}$ is calculated from data at the end of each
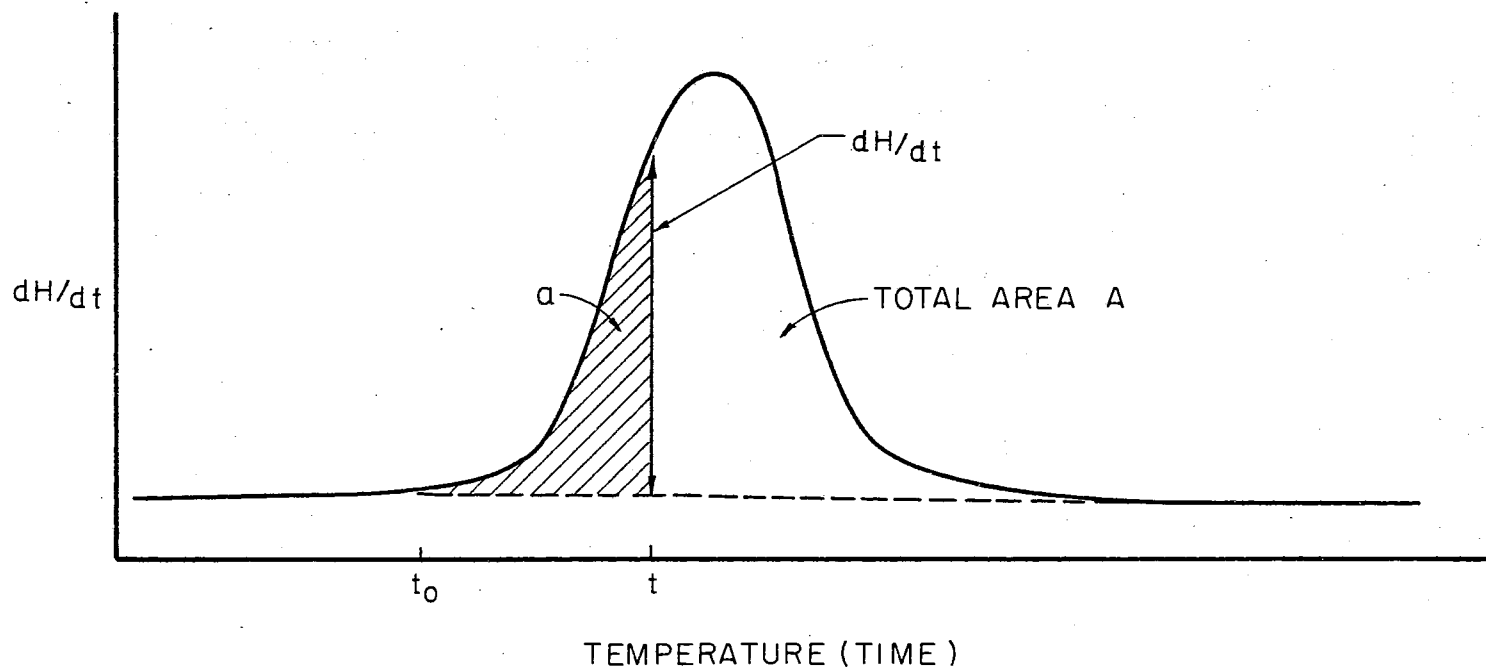
Figure 2. Typical DSC Peak

interval using equation (34). Thus, at the end of each interval a value for $\underline{T}$ and $\underline{k}$ are obtained. A least-squares linear analysis of the $(1/\underline{T}, \ln \underline{k})$ data obtained is then made. The process is repeated with other assumed values of $\underline{\alpha}$, and usually a range of values for $\underline{\alpha}$ is covered. The value of $\underline{\alpha}$ that produces the least scatter of the data about a least-squares line through the $(1/\underline{T}, \ln \underline{k})$ points is assumed to be the correct value. The activation energy may then be obtained from the slope of this Arrhenius plot.

CHAPTER III

EXPERIMENTAL APPARATUS

Introduction

The differential scanning calorimeter consists of two essentially identical sample and reference structures mounted in a furnace, and two electronic control systems which control the power input to the furnace and to the sample heater. The sample and reference structures are surrounded by a Vycor envelope, which allows investigations in controlled atmospheres. The furnace control system, Figure 3, allows the temperature of the furnace to be programmed at the desired rate. This control system senses the difference between the programmed emf and the emf of the furnace thermocouple, and regulates power to the furnace to keep the difference equal to zero. The sample heater control system, Figure 16, senses the difference in emf between the sample and reference thermocouples, and supplies power to the sample heater to maintain this difference at zero. The power thus required is measured with a Hall multiplier. The output of the Hall device is displayed on a time-base strip chart recorder. The ordinate of the strip chart is power, the absissa time; thus the area of a peak is energy supplied to the sample heater. These two control systems allow the temperature of a sample to be increased linearly until the sample undergoes a thermal effect, and a measurement of the instantaneous power and the total energy required by the sample.

16
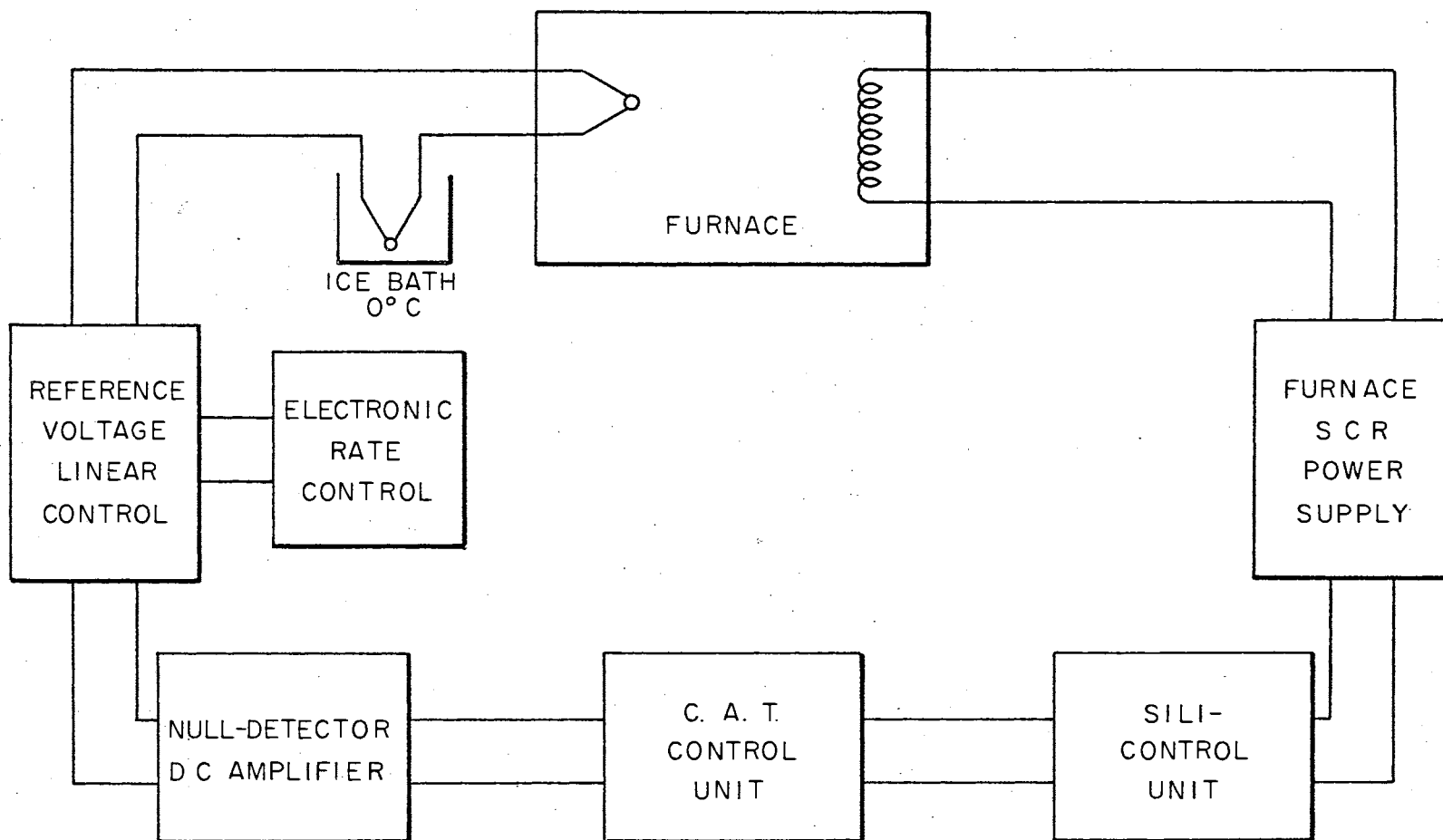
Figure 3. Furnace Control System

The various sub-systems of the apparatus are described in the following sections. Components are described with the minimal nomenclature required for identification of the item in the comprehensive listing of apparatus and supplies in Appendix B.

Furnace Control System

The purpose of the furnace control system, Figure 3, is to control the furnace at a fixed temperature or to increase the temperature linearly with time. The difference in emf between the furnace thermocouple and a reference junction at zero degrees Celsius is opposed by a known voltage from a potentiometer. When the temperature of the furnace is such that the emf from the thermocouples is equal to the voltage of the potentiometer, there is no error signal. When the two voltages differ, the resulting error signal is sensed by the Null-Detector, amplified, and transmitted to a Current Adjusting Type (C.A.T.) control unit which has three-action control: (a) proportional band, (b) rate, and (c) reset; these are described in detail in a subsequent section entitled "C.A.T. Control Unit." The output of the C.A.T. control unit, 0-5 mA, drives the Silicontrol which impresses on the gate of a silicon controlled rectifier (SCR) a positive pulse once each 180 degrees of the 60 Hz signal from the building power lines. When its gate is made sufficiently positive, the SCR conducts and thus delivers power to the furnace; the amount of power can be controlled by shifting the phase of the gate pulse with respect to the 60 Hz power signal. In the Silicontrol a saturable reactor and a phase shifting network shifts the phase of the pulse from 0 to 180 degrees as the dc input current to the reactor is increased from 0 to 5 mA. The Silicontrol-SCR combination

controls power input to the furnace very smoothly since current can be made to flow during any desired fraction of the total possible conduction angle.

Reference Voltage and Linear Voltage Control

The reference voltage circuit, Figure 4, provides an accurate voltage which can be varied linearly with time or set at a predetermined value. The linear variation of voltage is obtained with two ten-turn potentiometers, either of which can be driven by a common mechanical drive. The 1000-ohm potentiometer provides rapid voltage increase, the 10-ohm potentiometer provides slow voltage increase.

The Reference Voltage Circuit was standardized initially by adjusting the current in the circuit until the voltage across the 10-kohm standard resistor was 1.0000 V as measured with a Leeds and Northrup portable potentiometer (Serial No. 89461). The 500-ohm potentiometer was then adjusted until the voltage across the 10-kohm standard plus the voltage to the wiper of the 500-ohm resistor was equal to the standard cell voltage, 1.0194 V at 25°C. This adjustment is made only once, after which the 500-ohm potentiometer is locked in position.

Routine calibration of the linear voltage circuit is accomplished by moving switch S-2 to the "calibrate" position which removes the thermocouple from the circuit and impresses the error voltage between the standard cell and the wiper of the 500-ohm potentiometer onto the input of the Null-Detector. The current-adjust rheostat is adjusted until no error voltage appears across the input to the Null-Detector, as determined by the panel meter on the Null-Detector. Switch S-2 is then released, which places the thermocouple back in the circuit. The
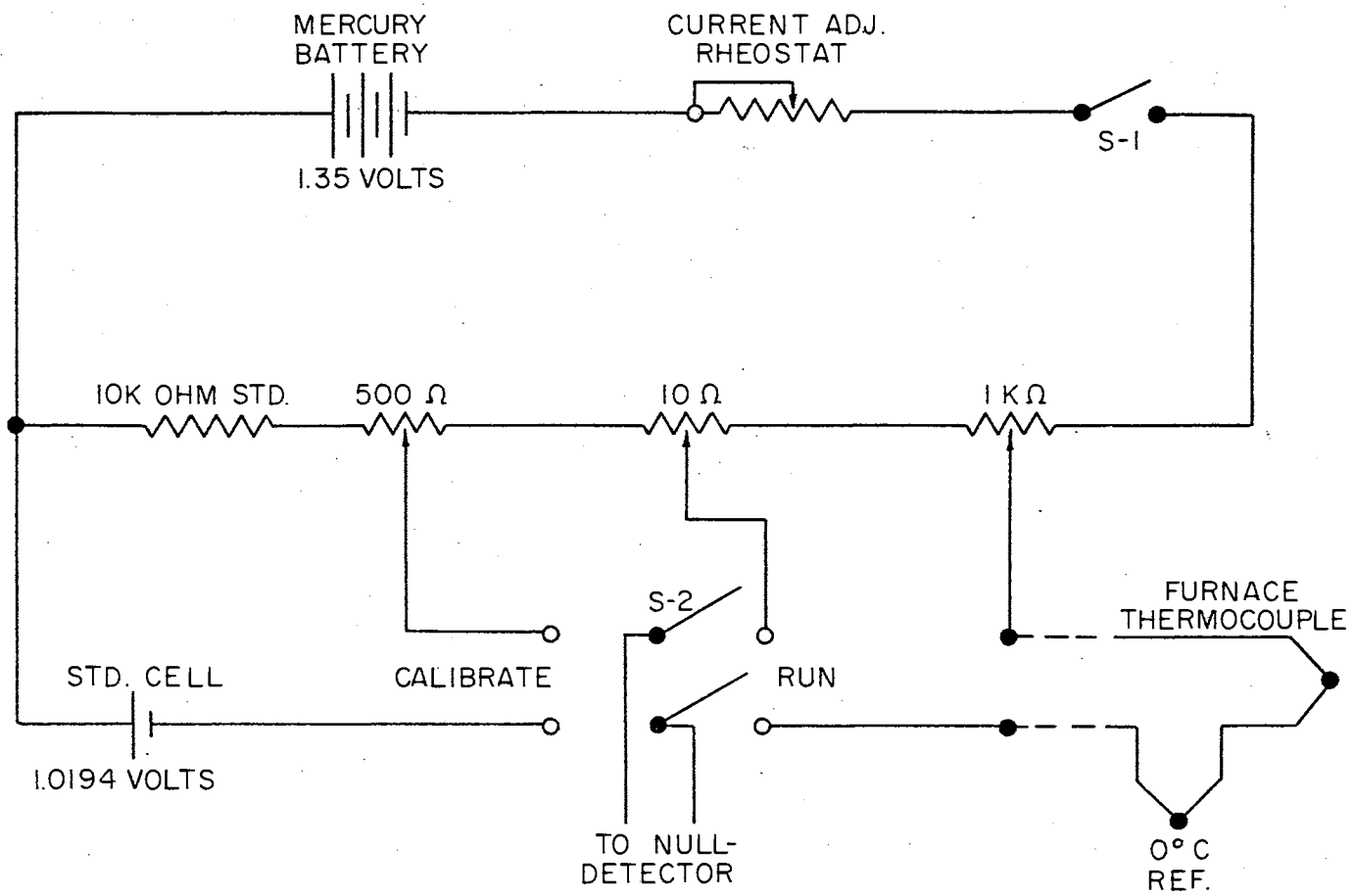
Figure 4. Reference and Linear Voltage Control Circuit

input to the Null-Detector in the "Run" position is the difference be-
tween the emf of the furnace thermocouple and the voltage between the
wipers of the 10-ohm and 1-kohm potentiometers.

Electro-Mechanical Drive

Rotation of the 10-ohm and 1-kohm potentiometers, in the reference
voltage circuit Figure 4, is accomplished by a pulse-operated stepping
motor. Pulses for stepping the motor at the desired rate are generated
by a preset counter which provides an output pulse for a given, but
arbitrary, preset number of input pulses from a 1000 Hz tuning fork
oscillator. The output of the preset counter, after passing through a
suitable impedance matching circuit, is fed into the "Translator Mod-
ule" or "stepping board", where the pulse is shaped and amplified
sufficiently to drive the stepping motor.

The stepping motor drives a speed reducer which has a reduction of
1000 to 1. The output shaft of the reducer is coupled through anti-
backlash gears to idlers of electric clutches. The electric clutches
are connected to the shafts of the potentiometers. Ten-turn dials
which indicate the position of the potentiometers are driven by gears
attached to the potentiometer shafts. The reading of these dials gives
the voltage between the sliders of the motor-driven potentiometers. A
preset voltage can be obtained by disengaging the electric clutch and
manually rotating the dial to the desired voltage. The furnace can be
regulated at the temperature corresponding to this fixed voltage or,
if the electric clutch is engaged, the temperature of the furnace can
be increased linearly with time from this fixed point.

Tuning Fork Oscillator

The pulse source which ultimately drives the stepping motor is a Model T/f-O tuning fork oscillator. This oscillator vibrates with a fixed frequency of 1000 Hz. The four-volt output pulses are essentially square wave within 40-60 per cent duty cycle and have a rise time of less than 10 microseconds. A well-filtered and regulated 12-volt dc power supply, Figure 5, is required for the operation of this oscillator.

Preset Counter

The preset counter provides control of the stepping rate of the stepping motor by delivering to the motor one pulse for a given preset number of input pulses. The rate can be varied from 1000 pulses per second, the maximum output of the tuning fork oscillator, to one pulse per 10 seconds, i.e., the Model 512 counter has four decades, 1 to 10,000 count. Maximum input to the preset counter is 10 volts peak into an input impedance of 20,000 ohms. The standard output circuit of the counter has been modified (by the manufacturer) to give a 5 volt positive output pulse, which is 0.5-0.8 millisecond wide and has a rise time less than 0.1 millisecond, into 10-kohms impedance.

Common Emitter Pulse Amplifier

The rated output of the preset counter is 5 volt positive pulses into 10,000 ohms. The Translator Module requires a negative 10 volt pulse and has an input impedance of 3,000 ohms. A circuit to invert the pulse, amplify it from 5 to 10 volts, and match the impedances is
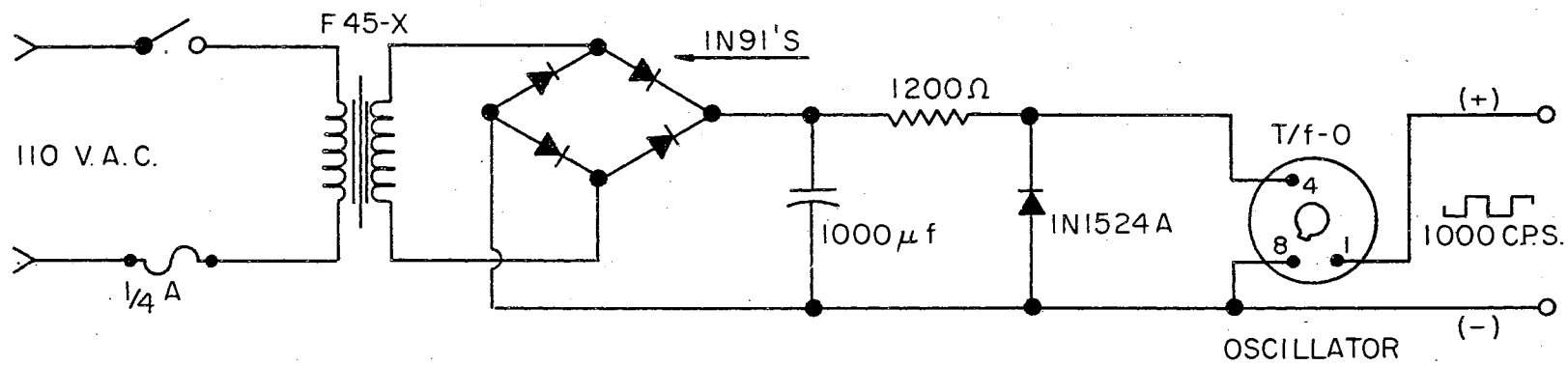
Figure 5. Power Supply for Tuning Fork Oscillator

therefore necessary. This circuit is shown in Figure 6.

The output of the preset counter is fed into a voltage divider. This divider reduces the input to the 2N508 to a value that does not overdrive it. The 2N508 inverts the pulse which is then fed into the Silicon Controlled Switch (SCS, 3N60 in Figure 6) circuit to "gate on" the SCS. The cathode gate and cathode of the SCS are connected so that the SCS turns itself off. The anode of the SCS is connected through a 47-kohm resistor to the Translator Module 12-volt power supply (see below) on the positive side of the voltage-dropping resistor; the voltage level at this point is 18 volts dc with 0.03-volt, 120 Hz ripple. The 6-volt power supply for the 2N508 transistor is a Burgess Z4 dry-cell battery. The output pulse from the SCS is shaped by a differentiating network composed of 0.1mfd capacitor and 270-ohm resistor, into a very sharp voltage spike which drives the Translator Module, which in turn operates the step motor.

Translator Module and Stepping Motor

The Slo-Syn Translator Module, Type STM250, is a plug-in printed circuit board with logic capabilities for stepping a Slo-Syn motor in one direction. The module is operated by a negative 10-volt pulse and has an input impedance of 3,000 ohms. The Translator Module requires two power supplies; 3 volts, 150 milliamps dc and 12 volts, 3 amps dc. The schematic diagrams of these power supplies are shown in Figure 7.

The Slo-Syn stepping motor, Type SS250, requires 200 pulses for one revolution. It is rated at 250 inch-ounces torque and has a maximum speed of 2 revolutions (400 steps) per second.
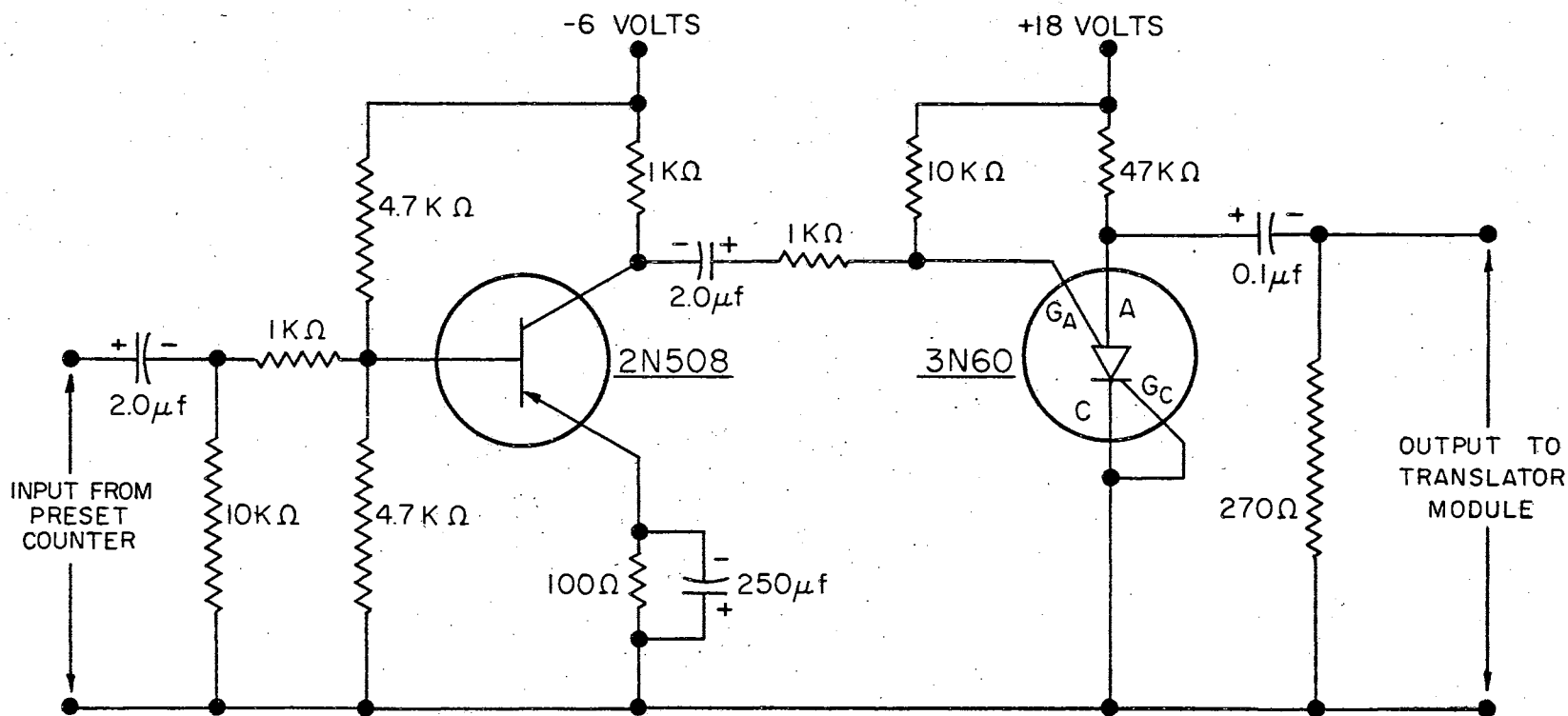
Figure 6. Common Emitter Pulse Amplifier
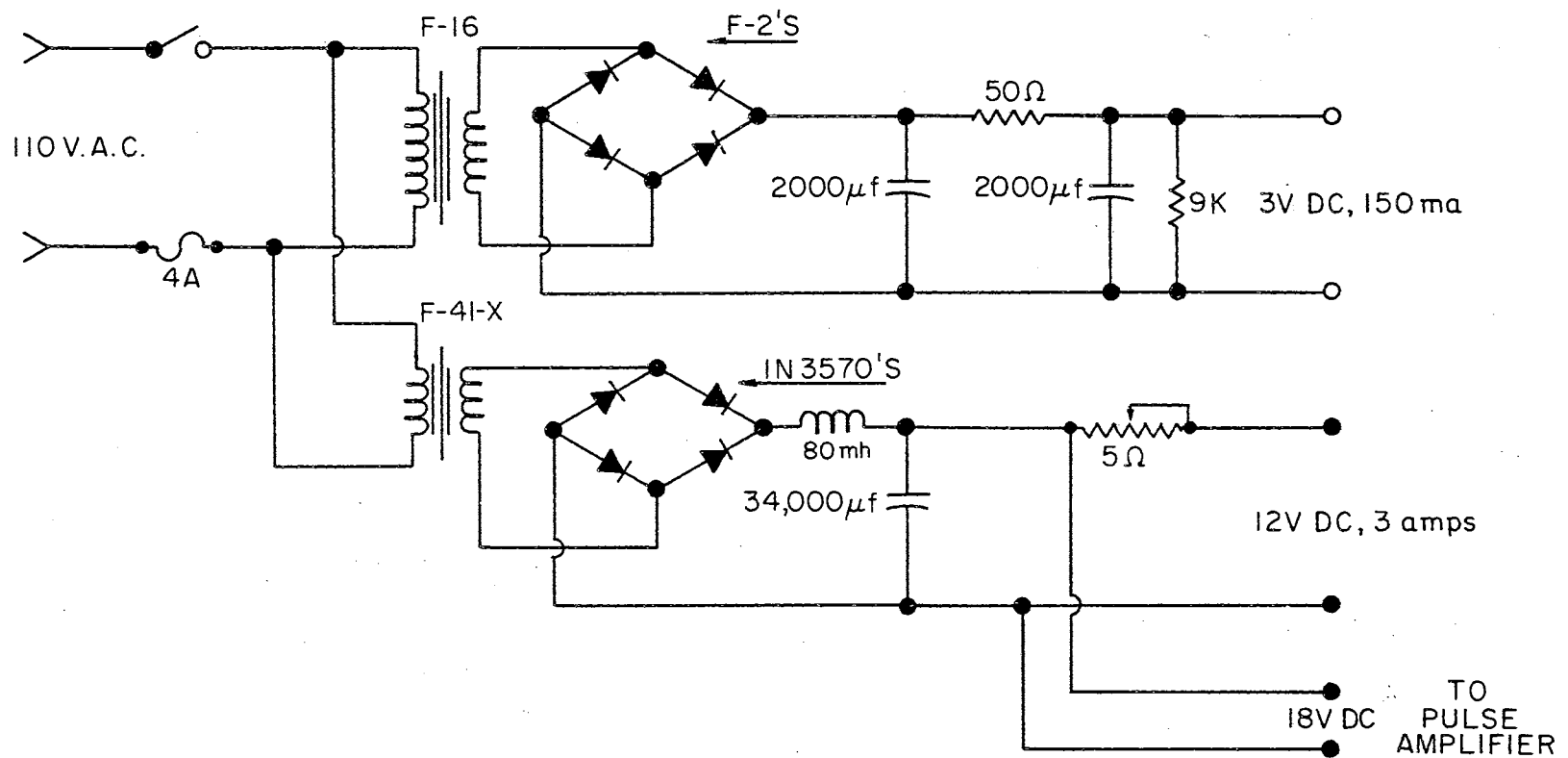
Figure 7. Power Supply for Translator Module

Mechanical Linkage

The Slo-Syn stepping motor is the prime mover for the operation of the motor-driven potentiometers, Figure 8. The variable-speed stepping motor drives a Bantam Speed Reducer, Type 11-c1000R, which has a reduction of 1000 to 1. The coupler has shaft sizes of 3/8 to 1/4 inch. The output shaft of the speed reducer is fitted with a precision 1 spur gear, which meshes with two antibacklash gear assemblies. The antibacklash gears are connected to the idlers of two electric clutches, Type FFC-30. When the electric clutches are engaged, the idlers drive the output of the clutches which are directly coupled to the potentiometer shafts. The potentiometer shafts are fitted with precision 1 spur gears which mesh with the same size precision 1 spur gears mounted on the 10-turn counter dial shafts. When the potentiometers are rotated, their positions are indicated by these counter dials.

Either of the potentiometers can be driven at a time, but not both at once. The 1000-ohm potentiometer provides fast scanning rates; the 10-ohm potentiometer slow scanning rates. The furnace can be regulated at a set point by disengaging the electric clutch of the 1000-ohm potentiometer and setting the indicator dial to the emf corresponding to the temperature desired. If the emf of the furnace thermocouple, with reference at $0^{\circ}C$, is different from this value, the error signal actuates the control system to increase or decrease the power input to the furnace until the emfs are the same. Since the emf-temperature curve for Chromel-Alumel thermocouples is very nearly linear, the temperature of the furnace will increase nearly linearly with time.

The two independently driven potentiometers make it possible to
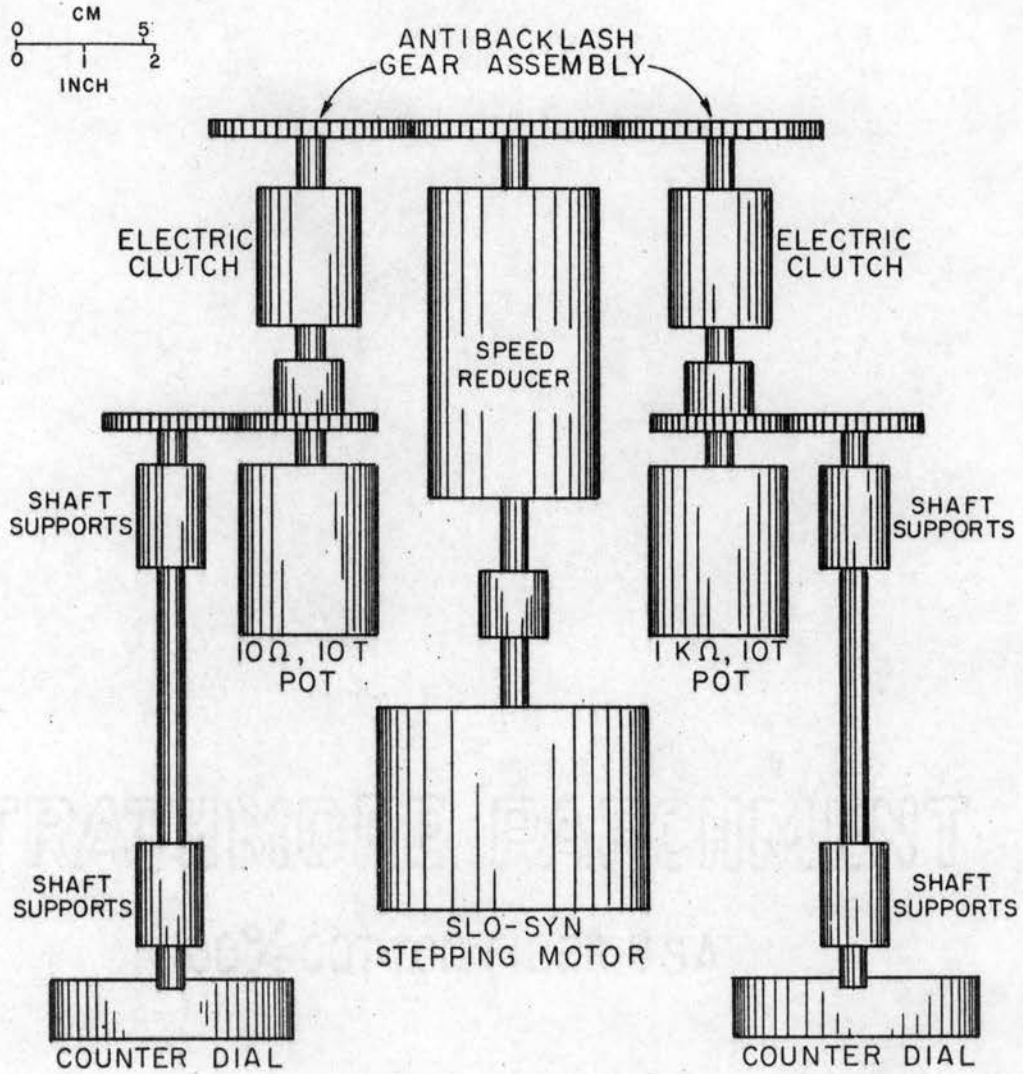
Figure 8. Mechanical Linkage for Linear Voltage Control

move rapidly to a given temperature, switch to the "slow" potentiometer, and move through a thermal transition at a very slow rate.

The electric clutches require a 24 volt 200 milliamp dc power supply, a schematic of which is shown in Figure 9. Power is applied to the appropriate clutch by a double-pole double-throw switch.

Electronic DC Null-Detector

Any error signal between the reference voltage and the emf of the furnace thermocouple is detected and amplified by a Leeds and Northrup Electronic DC Null-Detector, the output of which drives the C.A.T. control unit (see below). The Null-Detector has a maximum sensitivity of 1.0 microvolt per scale division, a very stable zero point, and a noise level less than 0.2 microvolt. The amplifier output is -0.5 to plus 0.5 volt into an impedance of 1000 ohms. More detailed information may be found in Leeds and Northrup information bulletin, Directions 177148.

C.A.T. Control Unit

A Leeds and Northrup Three-Action Current Adjusting Type (C.A.T.) Control Unit, Series 60 Model C-1, was used to provide three types of control over power supplied to the furnace: (a) proportional band, (b) reset action, and (c) rate action. Proportional band control provides power in proportion to the error signal. Reset action is an integrating function which increases (or decreases) the instantaneous power by an amount determined by the time-integral of the error signal. The third control is a derivative action which adds to power input, an amount dependent on the rate of change of the error signal. The rated
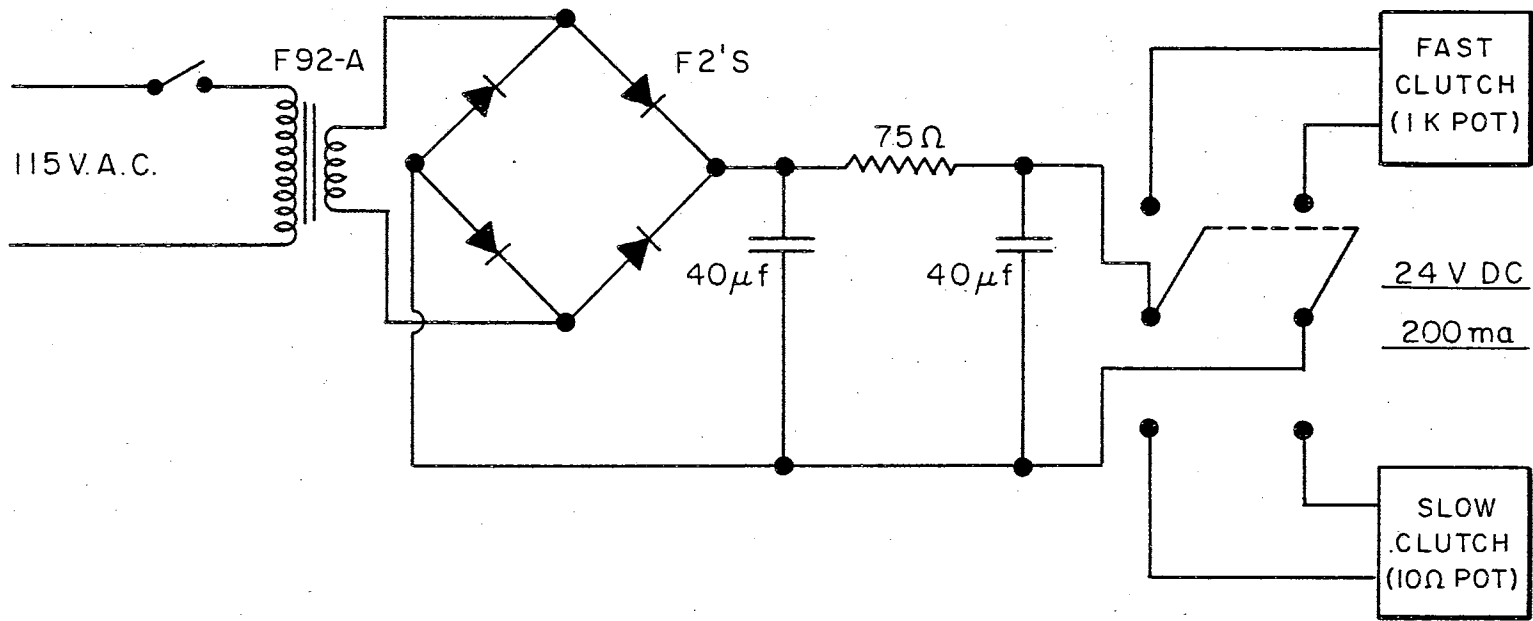
Figure 9. Power Supply for Electric Clutch

output of the C.A.T. unit is 0 to 5 milliamps into 3,000 ohms.

Silicontrol Unit

The Silicontrol provides a phase-variable pulse to the gate of the SCR in the furnace power supply. This provides smooth proportional power to the furnace by varying the conduction angle of the SCR from 0 to 180 degrees.

By varying the current in the dc windings of the saturable core reactor from 0 to 5 milliamps the pulse is shifted in phase from 0 to 180 degrees. The Silicontrol is designed to provide a pulse each 180 degrees of phase, thus allowing control of both portions of the ac cycle.

It was necessary to use a current divider at the dc terminals (winding 5-6) of the Silicontrol. The Silicontrol required only 3 milliamps for 180 degrees of phase shift. To allow the C.A.T. to operate over its full range of 0 to 5 milliamps into an impedance of 3,000 ohms a current divider-impedance matching circuit, Figure 10, was used.

The 6-volt output pulse of the Silicontrol, terminals G_1 and K_1, are connected to the gate and cathode, respectively, of the SCR in the furnace power supply. A suitable protection circuit is provided between the SCR and the Silicontrol to prevent ac leakage from the SCR into the Silicontrol. The circuit is shown in Figure 11.

Some difficulty was encountered with ac on the dc windings of the Silicontrol; the ac signal leaked back into the C.A.T. causing the control system to oscillate. The ac was eliminated by connecting a 250 microfarad capacitor across terminals 5 and 6, and shorting the other dc windings.
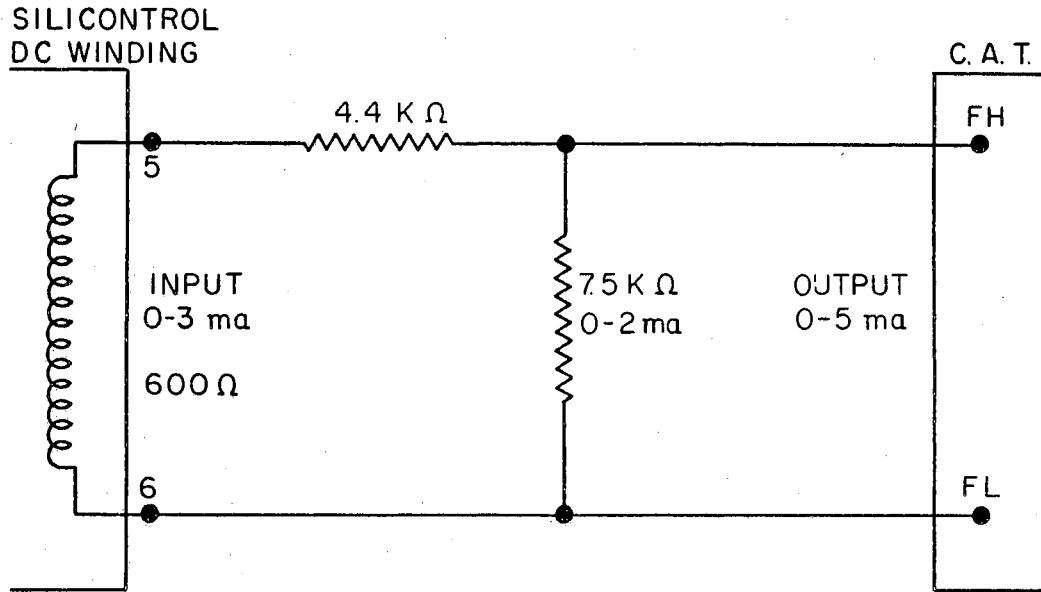
Figure 10. Impedance Matching Circuit Between CAT Unit
and Silicontrol
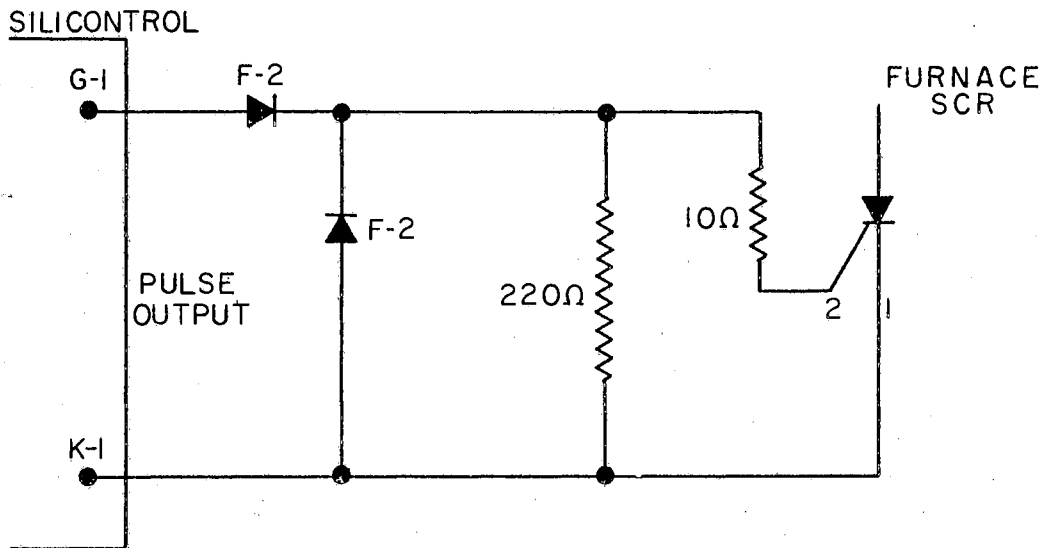
Figure 11. Protection Circuit for Silicontrol

Furnace Power Supply

Power for the furnace is provided by a SCR controlled ac power
supply, Figure 12. The power supply is capable of delivering 15 amps
at either 110 or 208 volts. Proportional power control is attained by
using one SCR in a diode bridge which provides unidirectional current
through the SCR and thereby allows one SCR to control both the positive
and negative portions of the ac cycle. This has the advantage of being
simple as well as more economical than two high-amperage SCR's.

The C40C SCR is protected by two 5D5 Thyrectors which break over
at peak inverse voltages below the rated value of the SCR. Only one
Thyrector is operative in the 110 volt mode, both are operative in the
208 volt mode. The diodes in the bridge are A40C's.

The power supply must be turned off before switching voltage
modes. This prevents any surge of voltage which might damage the com-
ponents of the power supply. The voltage mode and power-on are indi-
cated by lights on the front panel.

Furnace

The heating element of the furnace is a 1000-degree Celsius, non-
inductively wound, Hevi-duty unit, Type 2712SP. The $2\frac{1}{4}$ by 12-inch
unit is mounted on machinable ceramic discs both top and bottom, Figure
13. These discs are held in place by recesses in transite end plates.
These transite plates are held in place by three steel rods, which
effectively clamp the furnace together. One end of the furnace is
closed, the other open to allow entry of the calorimeter system. The
heating element leads are connected to terminals on the top of the
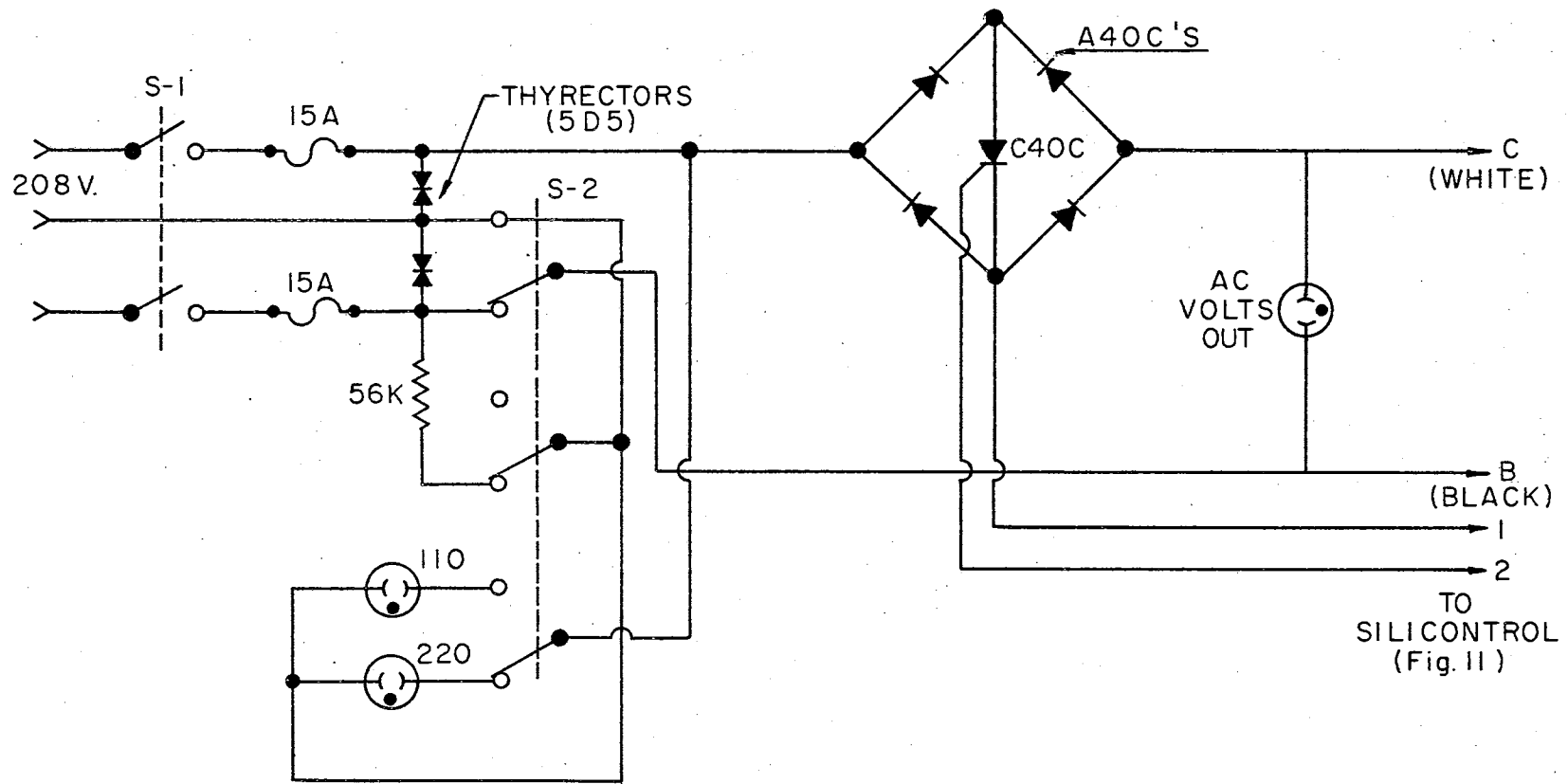
Figure 12. SCR Controlled Furnace Power Supply
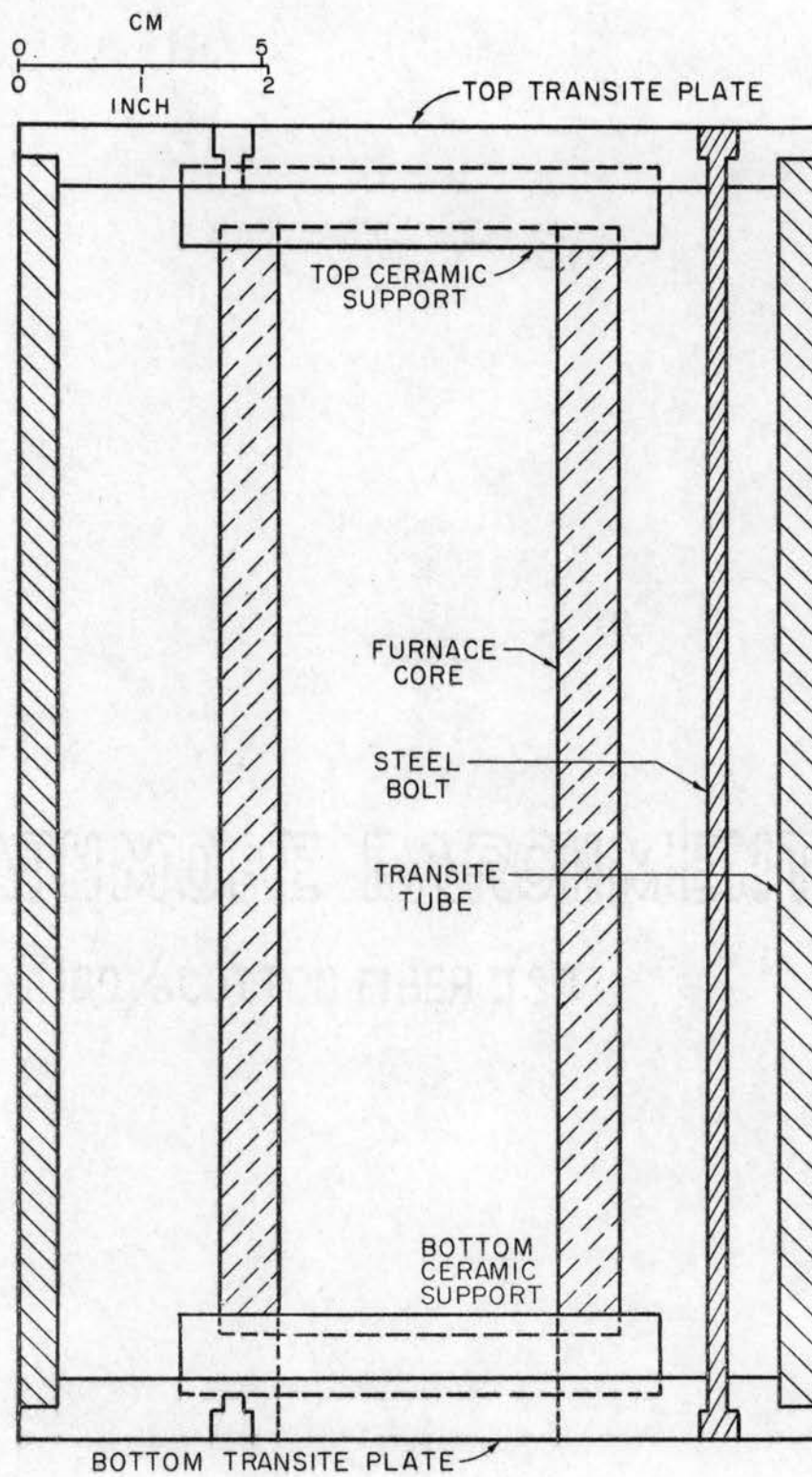
Figure 13. DTA - DSC Furnace

furnace. A Chromel-Alumel thermocouple is attached to the ceramic body
of the heating unit and the leads are brought out through two holes in
the top of the furnace. The temperature profile was measured with the
furnace vertical, closed end up, and is shown in Figure 14. The fur-
nace support, Figure 15, allows the furnace to be positioned about the
calorimeter system, or raised and rotated out of the way for sample in-
sertion.

Calorimeter Heater Control System

The purpose of this control system, Figure 16, is to detect any
thermal effects occurring in the sample and to supply energy at a rate
that will just keep the sample and reference structures at the same
temperature. One junction of a differential thermocouple is located
in the sample structure and the other in the reference structure. Any
thermal effects occurring in the sample will cause an emf to appear
across the differential thermocouple, the output of which is fed into
a dc Null-Detector where it is amplified. The amplifier drives a
C.A.T. control unit which in turn regulates a Silicontrol. The phase-
variable pulse of the Silicontrol is impressed on the gate of a SCR-
controlled dc power supply. The amount of power supplied to the heater
is determined by a Hall Multiplier, which can be independently cali-
brated. The Hall voltage which is directly proportional to the power
input to the sample heater, is recorded on a strip chart recorder. The
integral of Hall voltage vs. time is the amount of energy supplied to
the sample structure.

The system can be used for ordinary DTA by recording the output
of the dc Null-Detector after it has been disconnected from the control
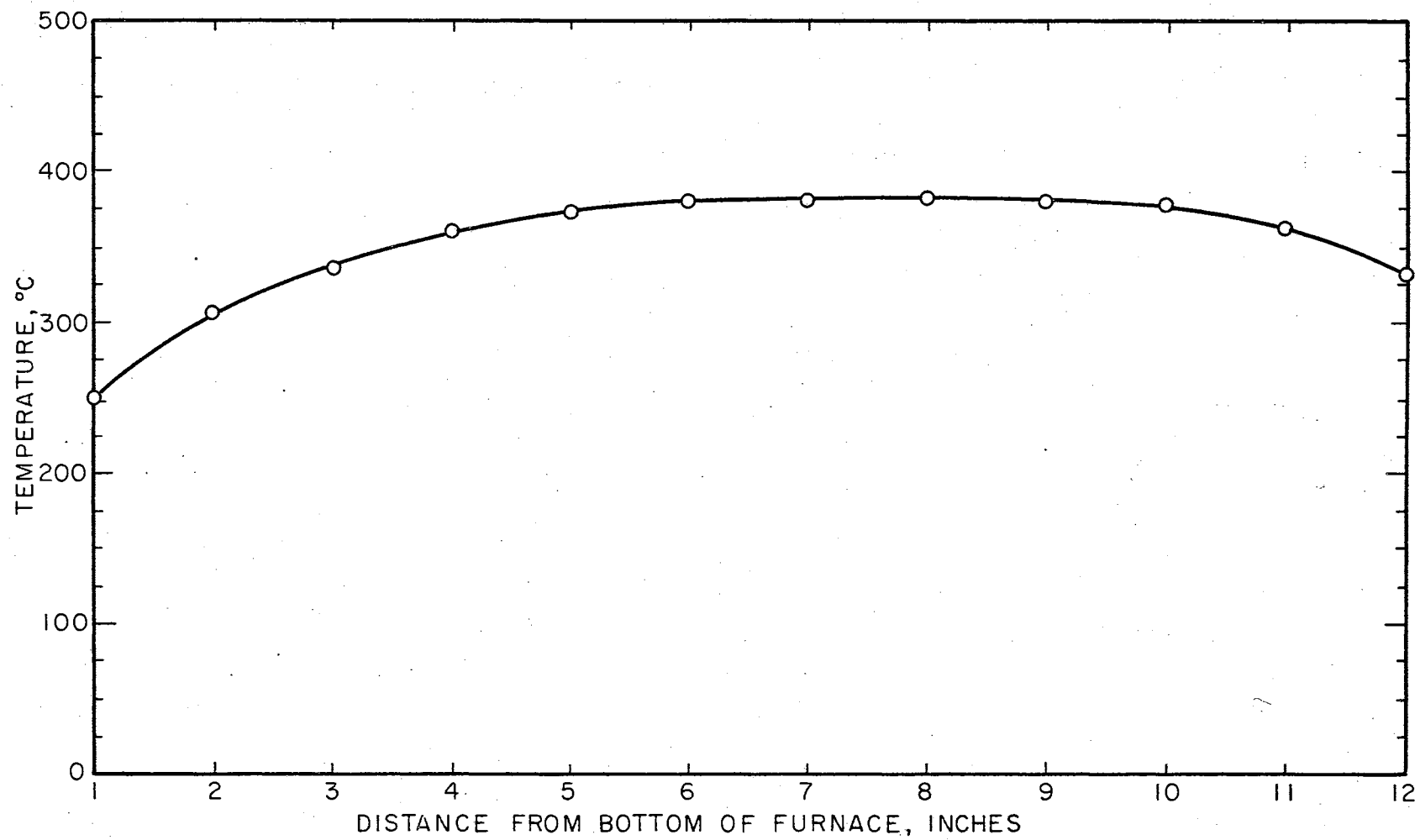
Figure 14. Temperature Profile for DTA - DSC Furnace
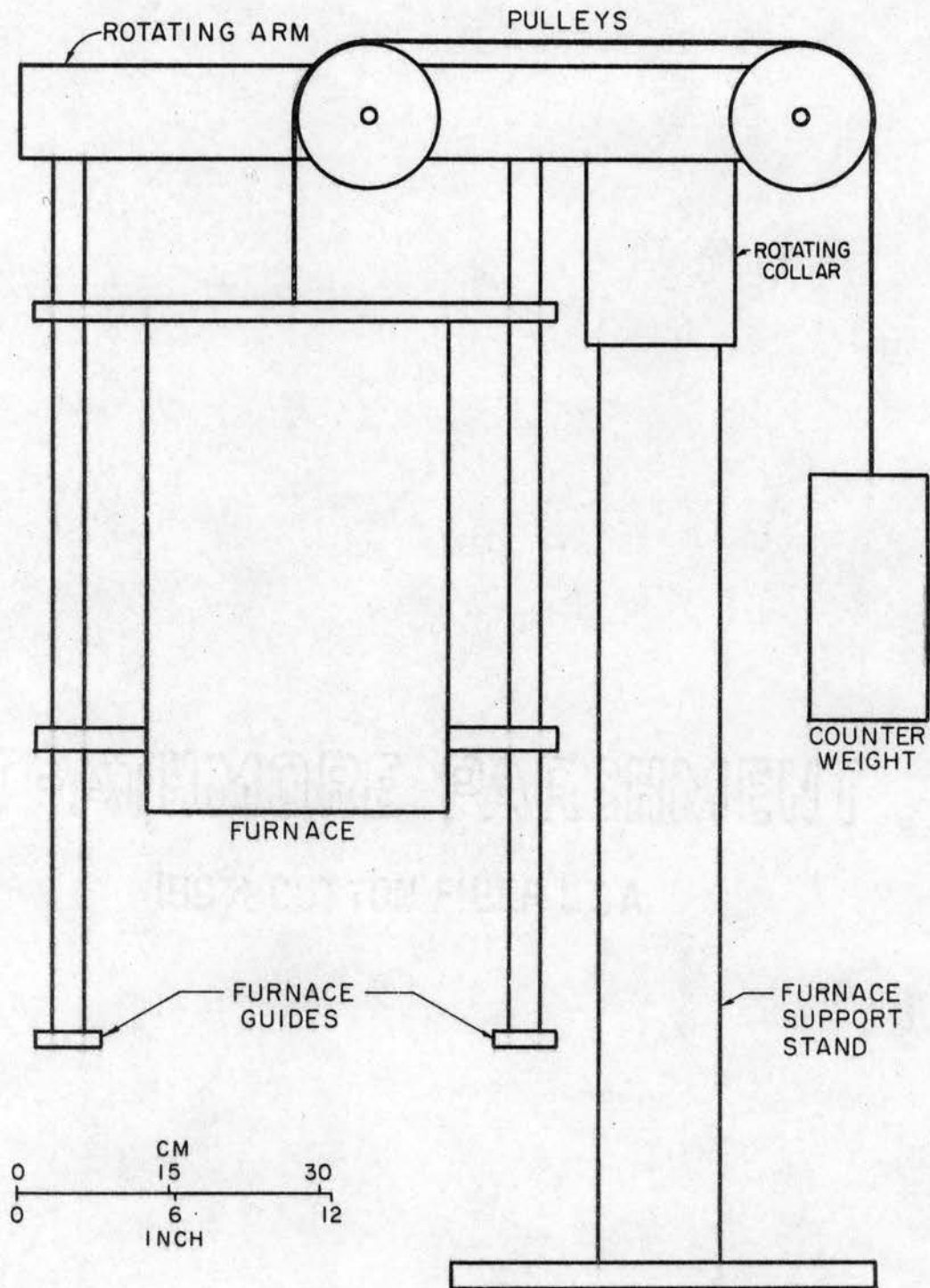
Figure 15.   DTA - DSC Furnace Support
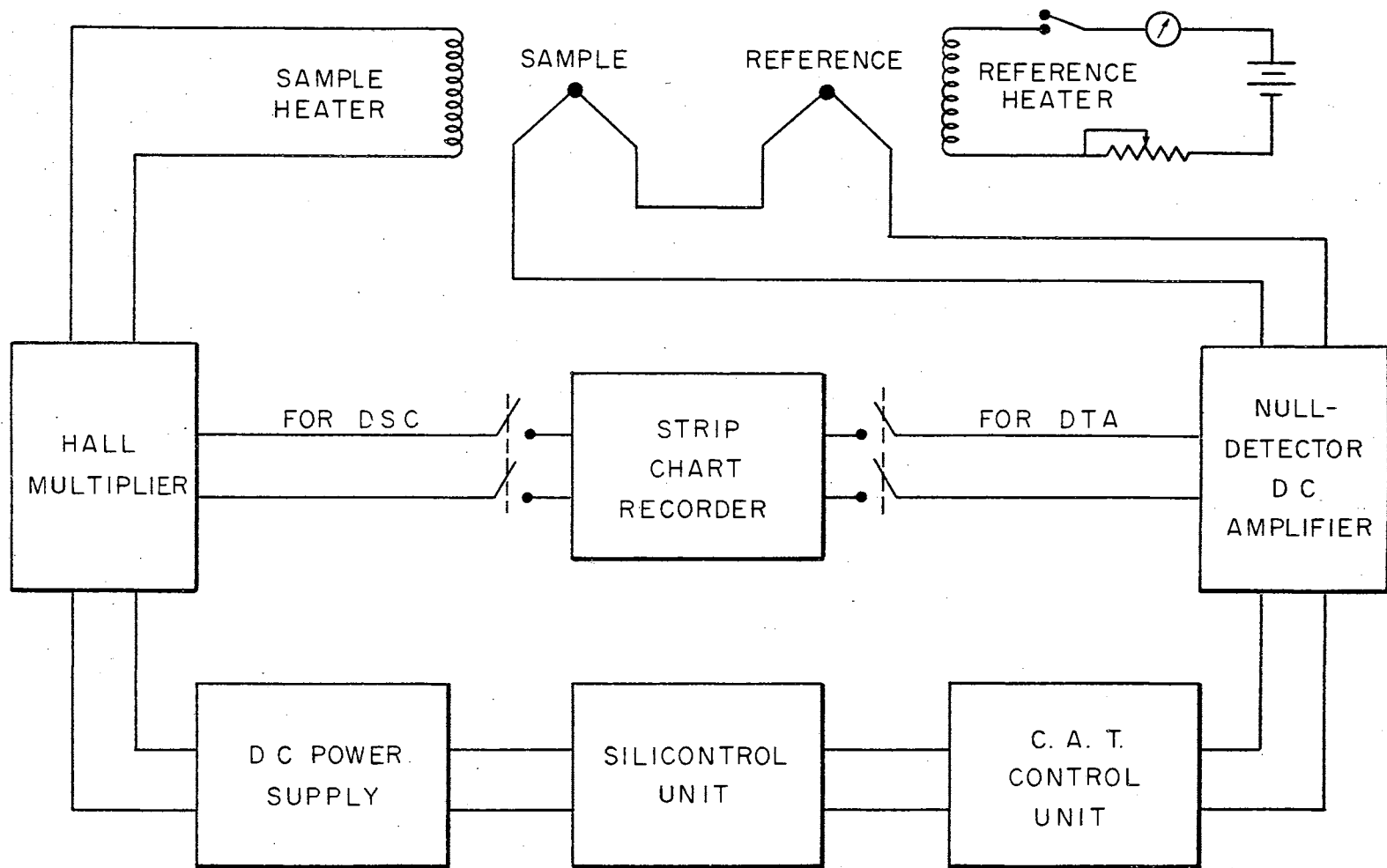
Figure 16. Sample Heater Control System

loop. In this mode of operation the heater is inoperative and the output of the amplifier represents the temperature difference between sample and reference structures as a function of time.

DC Null-Detector

A Leeds and Northrup DC Null-Detector, Model 9834-2, was used to detect any emf across the differential thermocouple arrangement. This amplifier is identical with the amplifier in the furnace control system which was described previously.

C.A.T. Control Unit

A Leeds and Northrup Series 60 Three-Action Current Adjusting Type Control Unit was used to achieve process control. This unit is identical with the C.A.T. unit in the furnace control system and has been described previously. The impedance matching circuit and ac filtering at the input to the Silicontrol is shown in Figure 17.

Silicontrol Unit

A Model VS6431CF Silicontrol unit was used to supply the phase-variable pulse to the SCR's in the dc power supply. This 6400-series unit differs from the 6300-series Silicontrol used in the furnace power supply. The 6400 unit has two sets of output terminals each of which can supply a pulse every 180° of phase angle. The pulse from each set of terminals can be used to "gate on" an SCR during one half of the ac cycle. The SCR's are wired in inverse parallel, i.e., one conducts during the positive half cycle, the other during the negative half cycle, giving control over a complete ac cycle. This more complex
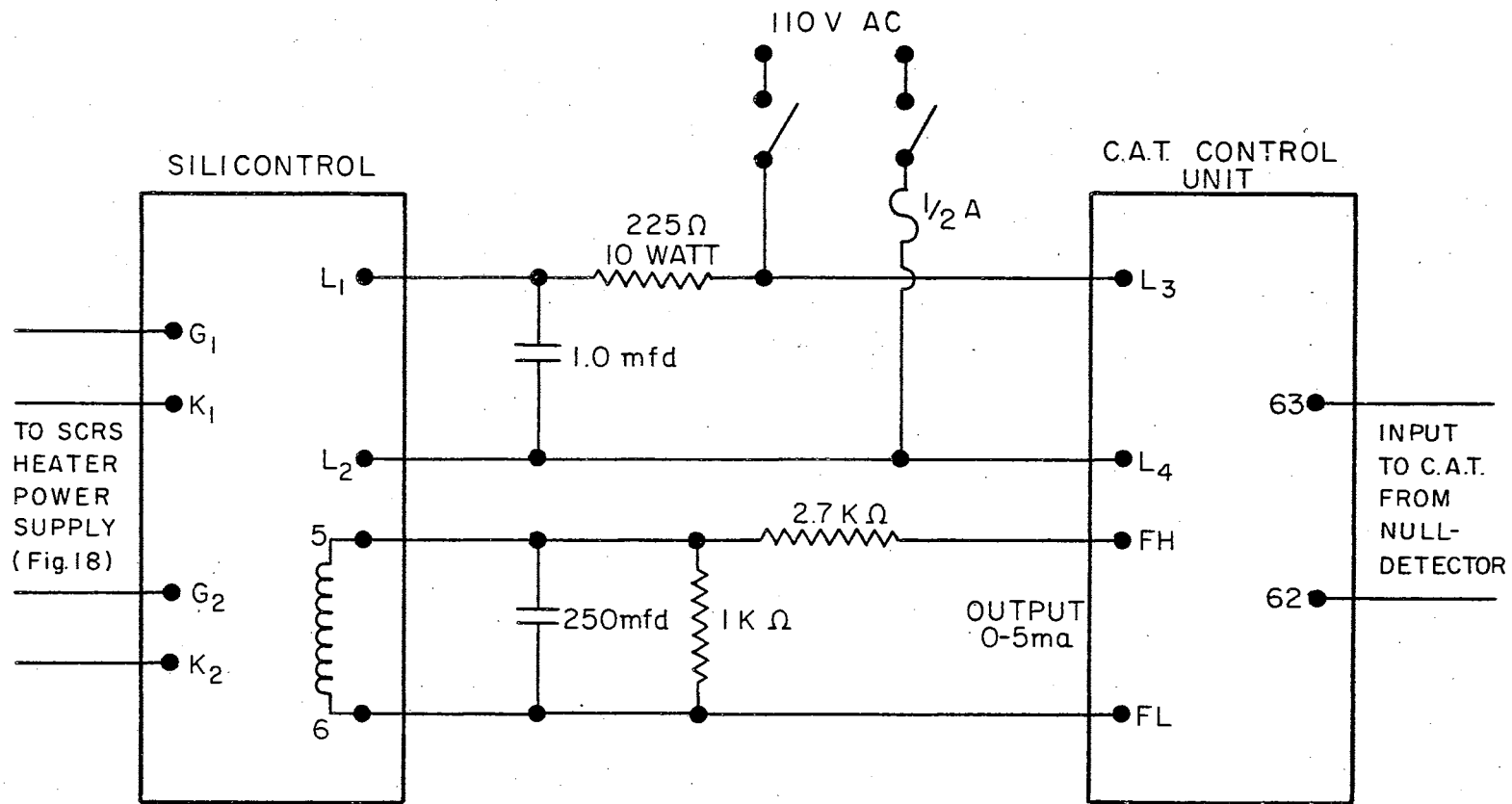
Figure 17. Electrical Connections Between CAT Unit and Silicontrol in
Sample Heater Power Supply

Silicontrol unit is necessary to achieve control from zero power smoothly up to maximum power.

The control of the DSC Heater is different from the furnace control in that when no reaction is occurring there is no heater input. The control system must respond from a zero power level smoothly to the level of power required by the reaction.

It was found that the 6300-series Silicontrol does not control smoothly from zero power, but requires 0.5 mA input to the dc windings of the saturable core reactor to raise the phase variable pulse to an amplitude sufficient to "gate on" the SCR. In the time required for the gate pulse to rise to firing amplitude, the ac across the SCR has risen above zero. When the SCR "gates on" the voltage out is not zero but some small, although significant, value. Thus, it is not possible to control the power smoothly from zero up to maximum. This 0.5 mA "dead band" is still present on the 6400-series but with the separate control over the two SCRs it is possible to use a phase-shifting network at the ac input to the Silicontrol. This network causes the pulse to lag five degrees in phase behind the ac wave impressed across the SCRs. Thus the pulse has time to increase in amplitude sufficiently to "gate on" the SCR at zero potential across the SCR. This is not possible with the simpler 6300-series, since the five degree lag might cause the SCR to "gate full on" on the other half cycle causing full power output. This phase-shifting network is shown in Figure 17.

Heater Power Supply

The dc power supply which provides power for the heater is shown schematically in Figure 18. This power supply is controlled by two
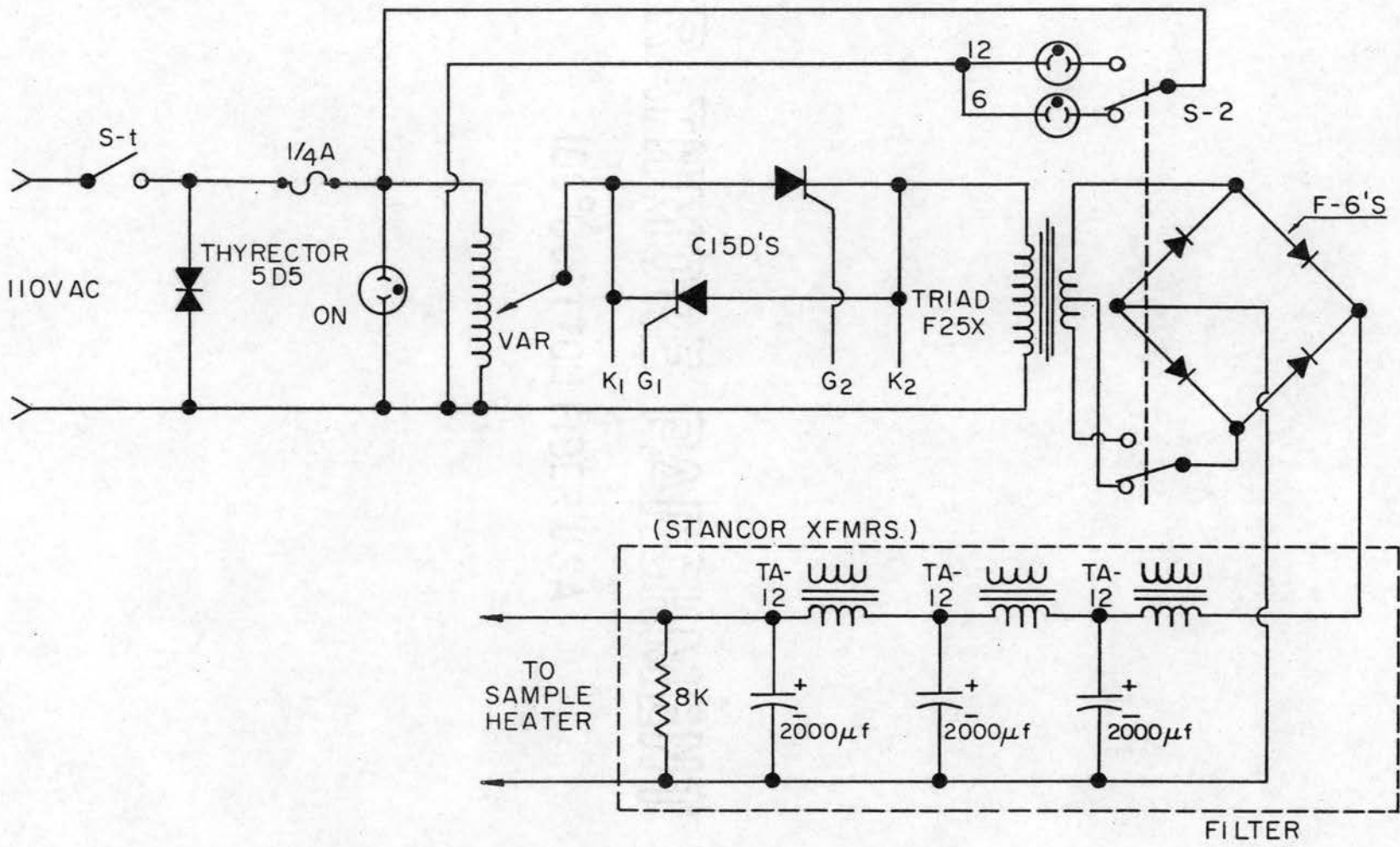
Figure 18. SCR-Controlled DC Power Supply for Sample Heater

C 15-D SCRs wired in inverse parallel. These SCRs are protected
against surges in the circuit by Type 5D5 Thyrectors. The Thyrectors
break over at peak inverse voltages below the rated values for the
C 15-D SCRs. The power supply is equipped with a center tap trans-
former, Triad F 25X, which gives either 6 volt or 12 volt dc output.
Full wave rectification is accomplished by four F-6 diodes in a bridge.
The output of the bridge has three stages of L-C filtering. The im-
pedance of the heater circuit is 7.5 ohms which is low enough to load
the power supply to a level of 2.2 volts on the 6 volt mode with 0.01
volt ac ripple. The 12 volt mode has an output of 5.7 volts with 0.02
volt ac ripple.

The protection circuits for the Silicontrol are identical with
the one shown in Figure 11. This circuit prevents any ac leakage to
the Silicontrol which might damage it or cause oscillation in the con-
trol system.

Hall Device

The power input to the sample heater is measured with a Hall Mul-
tiplier, Type MB 26-EI38-Mu, made by Siemens and Halske. The output
of this device is a voltage, the Hall Voltage, which is proportional
to the heater current through the Hall crystal and to the magnitude of
the magnetic $\underline{B}$ field in the crystal. Symbolically, one writes

$$V_H = K_H I_c B$$

where $\underline{V}_H$ is the Hall voltage, $\underline{K}_H$ the Hall constant, $\underline{I}_c$ the heater cur-
rent, and $\underline{B}$ the magnitude of the magnetic field.

The magnetic field in the crystal is generated by a coil wound

with 1000 turns of No. 36 heavy-Formvar-insulated copper wire. The resistance of the Hall coil is 100 ohms.

The linearity of the Hall Multiplier is dependent upon the terminating resistance of the Hall voltage leads, i.e., the load impedance. The output of the Hall crystal is most nearly linear when the device is operated with a so-called linear terminating resistor. This resistance was chosen by determining the Hall voltage vs. power curve for terminating resistances of 12 to 20 ohms. Figure 21, gives the circuit schematic. Each set of data was fitted to a straight line using the least-squares technique. The computation was done on an IBM 1420 computer. The terminating resistor which gave the least standard deviation of a single $V_H(i)$ about the least-squares line was chosen as the linear terminating resistance. The most nearly linear set of data was for a terminating resistance of 16 ohms. These data are shown in Table I.

Figure 19 shows two possible arrangements for power measurement. In (a) the current through the heater is I_c but the current that establishes the B field, I_B, is dependent upon the potential drop across the Hall crystal as well as the heater. For heaters of low resistance this error can be quite large. In (b) the current through the windings, I_B, is accurately proportional to the potential drop across the heater but now the control current, I_c, is greater than that which goes through the heater by the amount I_B.

These difficulties were circumvented by using a Burr-Brown 1605 operational amplifier to deliver current to the Hall coil in proportion to the potential across the sample heater. The Burr-Brown 1605 responds to the potential across the heater, but leaves the heater

I_B

I_h

FROM
POWER SUPPLY

HALL
COIL

HEATER

HALL
CRYSTAL

I_c

V_H

(a)

I_B

FROM
POWER SUPPLY

HALL
COIL

HEATER

HALL
CRYSTAL

I_c

I_h

V_H

(b)
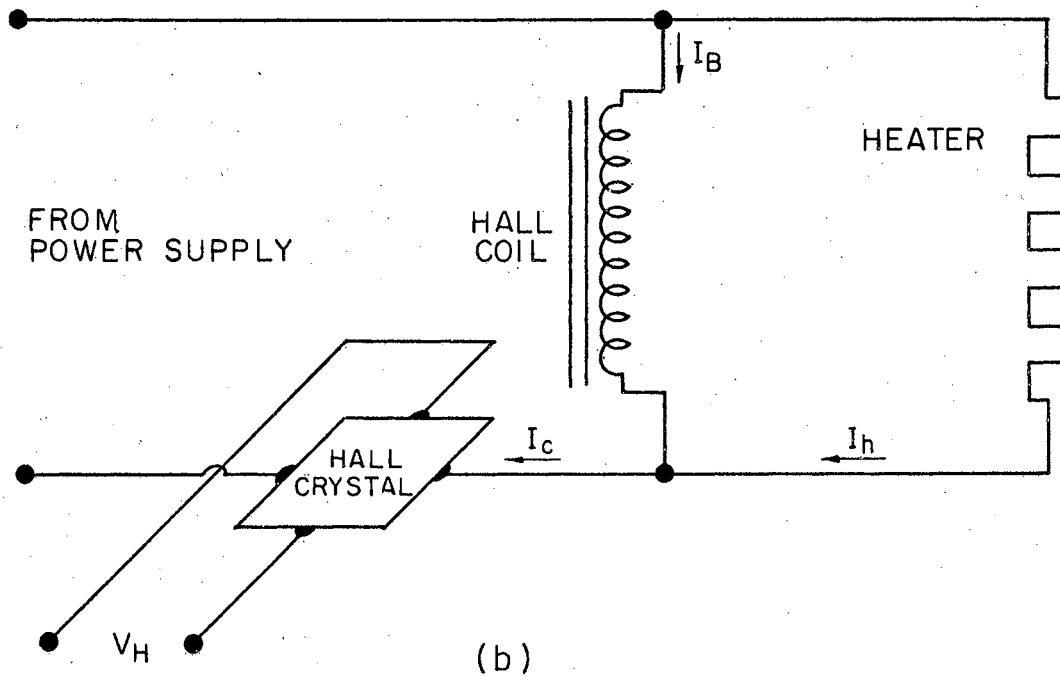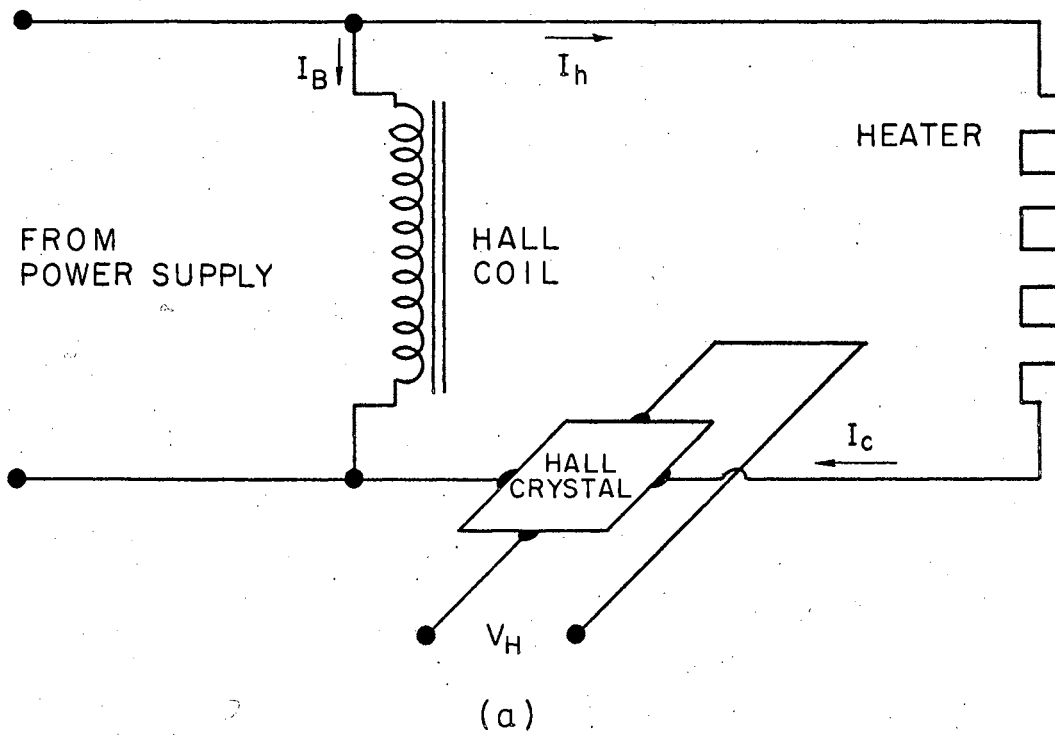
Figure 19. Circuit Arrangements for Power Measurement
with Hall Multiplier

TABLE I

DATA FOR THE DETERMINATION OF THE HALL PROPORTIONALITY CONSTANT

Hall Voltage* Volts	Voltage Across Standard Resistor Volts
0.00024	0.01907
0.00056	0.02984
0.00091	0.03773
0.00123	0.04435
0.00178	0.05388
0.00249	0.06355
0.00312	0.07151
0.00411	0.08209
0.00513	0.09190
0.00668	0.10470
0.00839	0.11759
0.00961	0.12592
0.01057	0.13196
0.01256	0.14408
0.01480	0.15627
0.01736	0.1691
0.01941	0.1789
0.02516	0.2039
0.02778	0.2134
0.03218	0.2306
0.03574	0.2427
0.03767	0.2494
0.04323	0.2671
0.04721	0.2795
0.05095	0.2903
0.05568	0.3041
0.05950	0.3142
0.06419	0.3263
0.06656	0.3322
0.07209	0.3458
0.07695	0.3574
0.08484	0.3756
0.09051	0.3880
0.10184	0.4125
0.10951	0.4281
0.11717	0.4436
0.12664	0.4622
0.13596	0.4803

*With a 16-ohm terminating resistor

circuit essentially undisturbed since the 1605 is in a high input impedance circuit. The $\underline{B}$ field is now effectively isolated from the control current, $\underline{I}_c$, and the Hall voltage is truly proportional to the power input to the heater.

The final Hall circuit is shown schematically in Figure 20. The Hall crystal is in series with the heater and, since the Burr-Brown 1605 in this circuit has an input impedance of about 10-kohms to ground, the current through the heater and $\underline{I}_c$ are essentially identical.

Analysis of the Burr-Brown 1605 Circuit (21)

In operational amplifier circuit analysis two summing point restraints are very important. These are:

(1) No current flows into either input terminal of the ideal operational amplifier.

(2) When negative feedback is applied around the ideal operational amplifier, the differential input voltage approaches zero.

When these restraints apply, Pin J on the 1605 operational amplifier is at virtual ground. Since no current flows into J, Figure 20,

$$\frac{E_h - E_i}{R_1} + \frac{E_{10} - E_i}{R_o} = 0 \qquad (1)$$

where $\underline{E}_h$ is the potential across the heater, $\underline{E}_i$ is the potential at J and $\underline{E}_{10}$ is the potential across the 10-ohm standard resistor. Since Pin J is a virtual ground, $\underline{E}_i$ is essentially zero. Then, from equation (1), we have
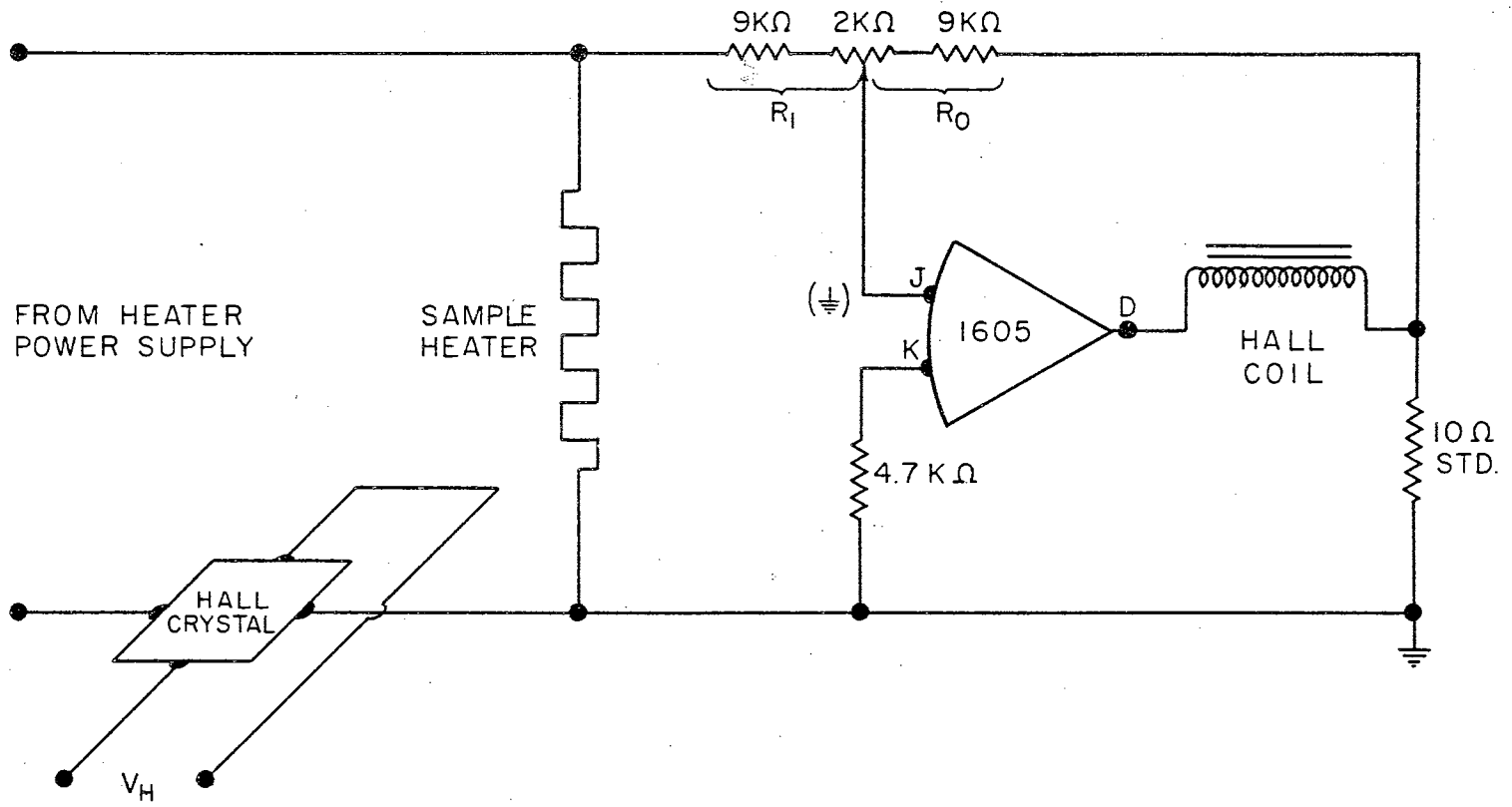
Figure 20. Circuit for Hall Multiplier

$$\frac{E_h}{R_1} + \frac{E_{10}}{R_o} = 0 \tag{2}$$

or,

$$E_h = -\frac{R_1}{R_o} E_{10} . \tag{3}$$

Since I_B also flows through the standard resistor, we may write

$$E_{10} = I_B R_{10} \tag{4}$$

which, when combined with equation (3) gives,

$$E_h = -\frac{R_1 R_{10}}{R_o} I_B . \tag{5}$$

By adjusting the 2-kohm variable resistor until the potential across the heater is equal to the potential across the standard 10-ohm resistor, one makes R_1 equal R_o (see equation (3)). Substitution of this result into equation (5) and subsequent rearrangement give,

$$I_B = -\frac{E_h}{R_{10}} = -0.10 \, E_h . \tag{6}$$

Thus the current I_B that establishes the B field is directly proportional to the voltage across the heater.

From the Hall equation, one writes

$$V_H = K_H I_c B \tag{7}$$

or, since B is proportional to I_B (i.e., $B = kI_B$),

$$V_H = K_H k I_c I_B .$$

From equation (6), $I_B = \dfrac{E_h}{10}$ (neglecting the sign); thus,

$$V_H = K_h k I_c \frac{E_h}{10} = \frac{K_H k}{10} I_c E_h \; . \qquad (8)$$

It is evident from equation (8) that V_H is proportional to power delivered to the heater, since I_c is the current through, and E_h is the voltage across, the heater.

The constant of proportionality was determined by measuring the Hall voltage for various known power inputs to a 1.0000-ohm standard resistor which was substituted for the heater; Figure 21 shows the circuit. The potential across the 1.0000-ohm standard resistor and the Hall voltage were measured with a Leeds and Northrup portable potentiometer (Serial No. 89461). Since the resistance of the standard resistor is 1.0000 ohm, the power is numerically equal to the square of the voltage across the resistor, i.e., $W_s = E^2$. Table I gives the values of the Hall voltage and the voltage across the 1.0000-ohm standard resistor for currents up to 480 milliamps. The maximum rated current of the Hall crystal is 500 milliamps.

A least-squares linear analysis of the Hall voltage vs. the power dissipated in the standard resistor was made using the IBM 1420 computer. The data are represented by the following equation,
$V_H = (0.6019 \pm 0.0003) W_s$ or, in terms of the variables for the heater (see equation 8),

$$V_H = (0.6019 \pm 0.0003) E_h I_c \; . \qquad (9)$$

The energy supplied to the heater during a reaction can be determined by integrating the Hall voltage over the appropriate time interval.
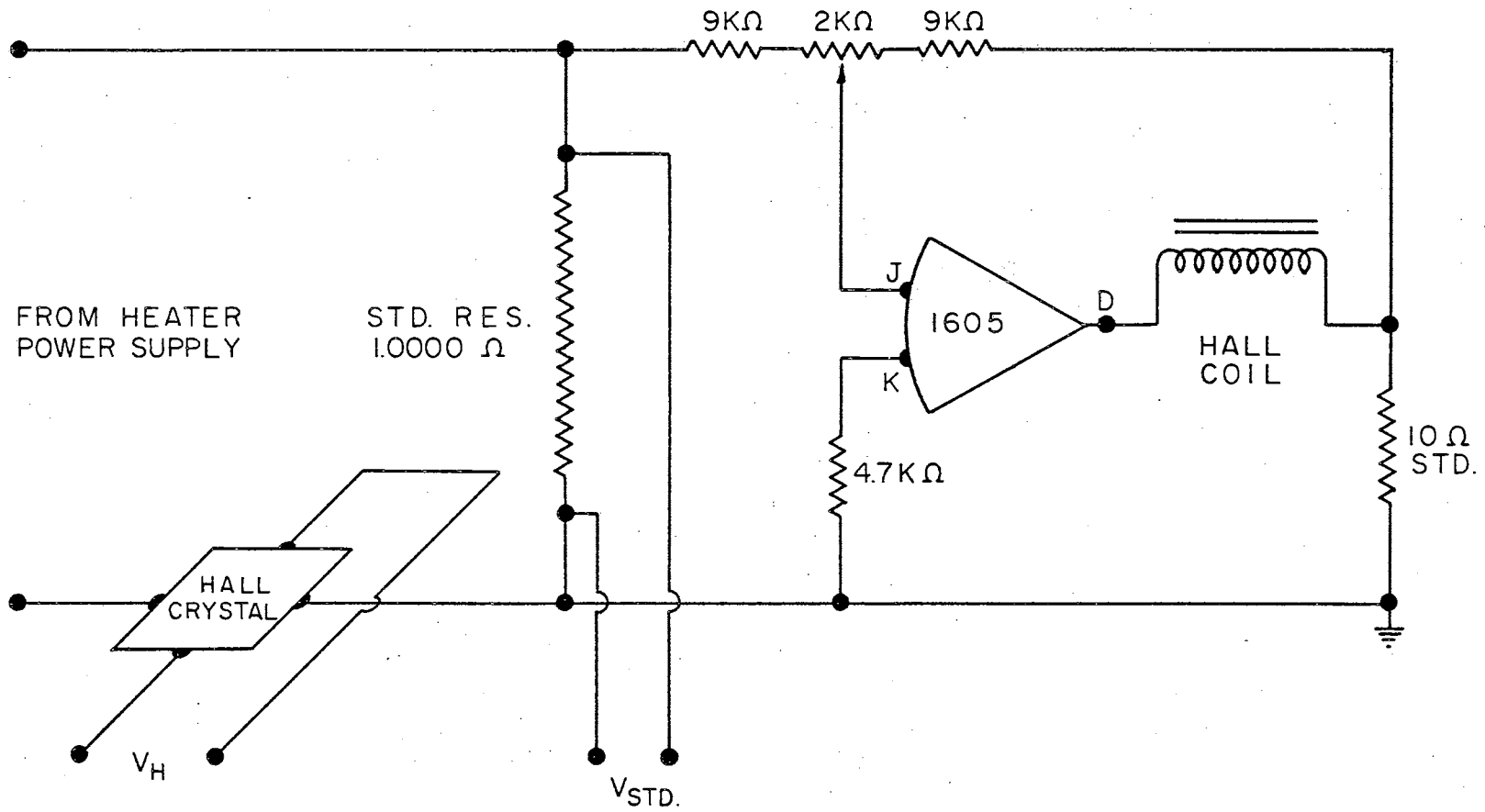
Figure 21. Circuit for Determination of Hall Multiplier Proportionality Constant

Calorimeter System

The calorimeter, Figure 22, consists of two nickel structures each fitted with a heater and thermocouple. The design of the nickel structures follows that of Speros and Woodhouse (10). Each nickel structure is mounted on a ceramic rod which allows the thermocouple leads to be brought out through holes in the rod. Similar ceramic rods insulate the current and potential leads to the heater. These ceramic rods are mounted in machinable ceramic discs which lend strength and rigidity to the assembly as well as thermal and electrical insulation. Figure 23 shows the complete calorimeter mounted on a brass base assembly, fitted with a 55/50 standard taper joint for connection to the Vycor envelope. The feet of the base assembly allow adjustment to position the calorimeter in the furnace. Two stainless steel tubes are fitted with valves to allow the calorimeter to be purged with an inert gas.

The sample and reference structures are identical. The nickel structure and heater shield are shown in Figure 24 (a) and (b). The heater shield was designed to enclose the sample structure and heater, thus reducing heat loss to the surroundings. The grooves in the nickel structure are 0.020 inch deep and 0.040 inch wide. These grooves are filled with Norton RA 1139 High Temperature Cement, using Sauereisen No. P-7 Insu-Lute Hi-Temp Cement as a binder. Before the cement hardens, a groove was made in the cement large enough to hold the heater wire. The cement was then dried for 48 hours at 110°C but never fired. The heater wire, 0.005-inch platinum, was wound in the grooves, while a jig held the sample structure securely and clamped the ends of the heater wire after the winding was completed. About ¼ inch of the
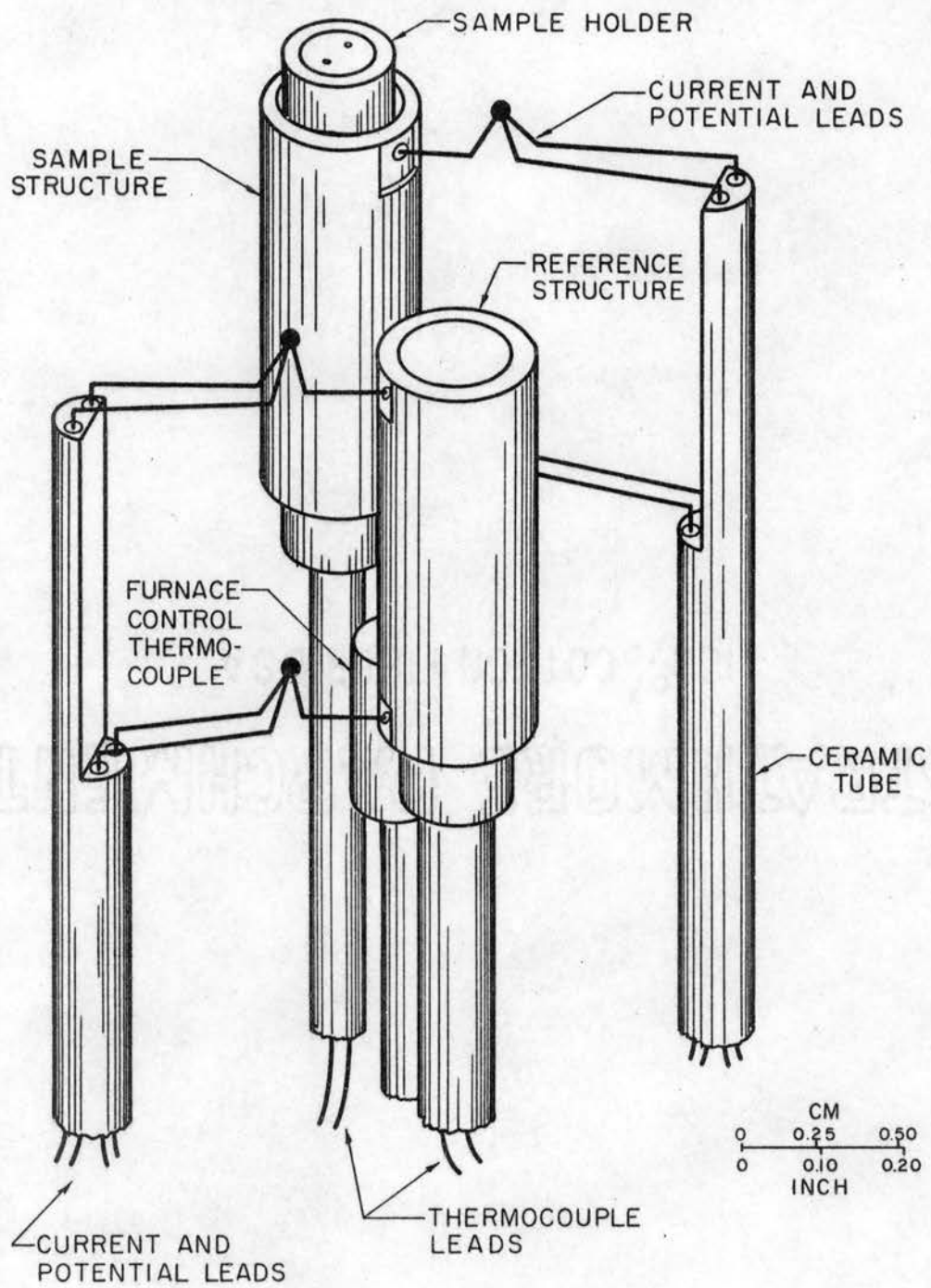
Figure 22.   The Calorimeter

REFERENCE STRUCTURE

SAMPLE STRUCTURE

FURNACE CONTROL THERMOCOUPLE

CERAMIC TUBE

CERAMIC SUPPORTS

CM
0   2.5   5.0
0   2
INCH

BRASS 55/50 STANDARD TAPER

CERAMIC BASE SUPPORT

ADJUSTABLE BASE

GAS PURGE
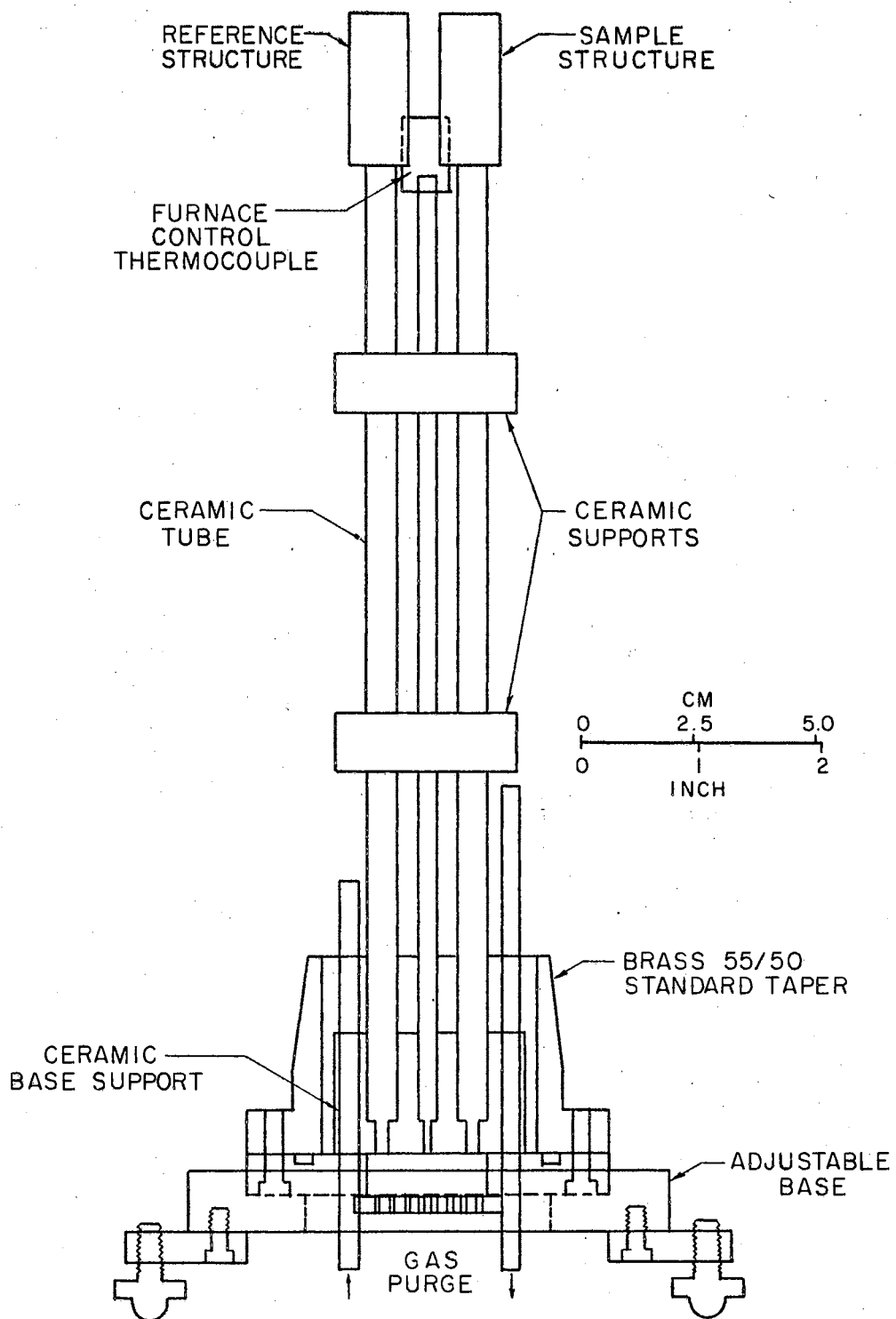
Figure 23. The Calorimeter System

CM
0   0.254   0.508
0   0.10   0.20

SAMPLE STRUCTURE
(a)

HEATER SHIELD
(b)

(c)   (d)   (e)

SAMPLE CONTAINERS
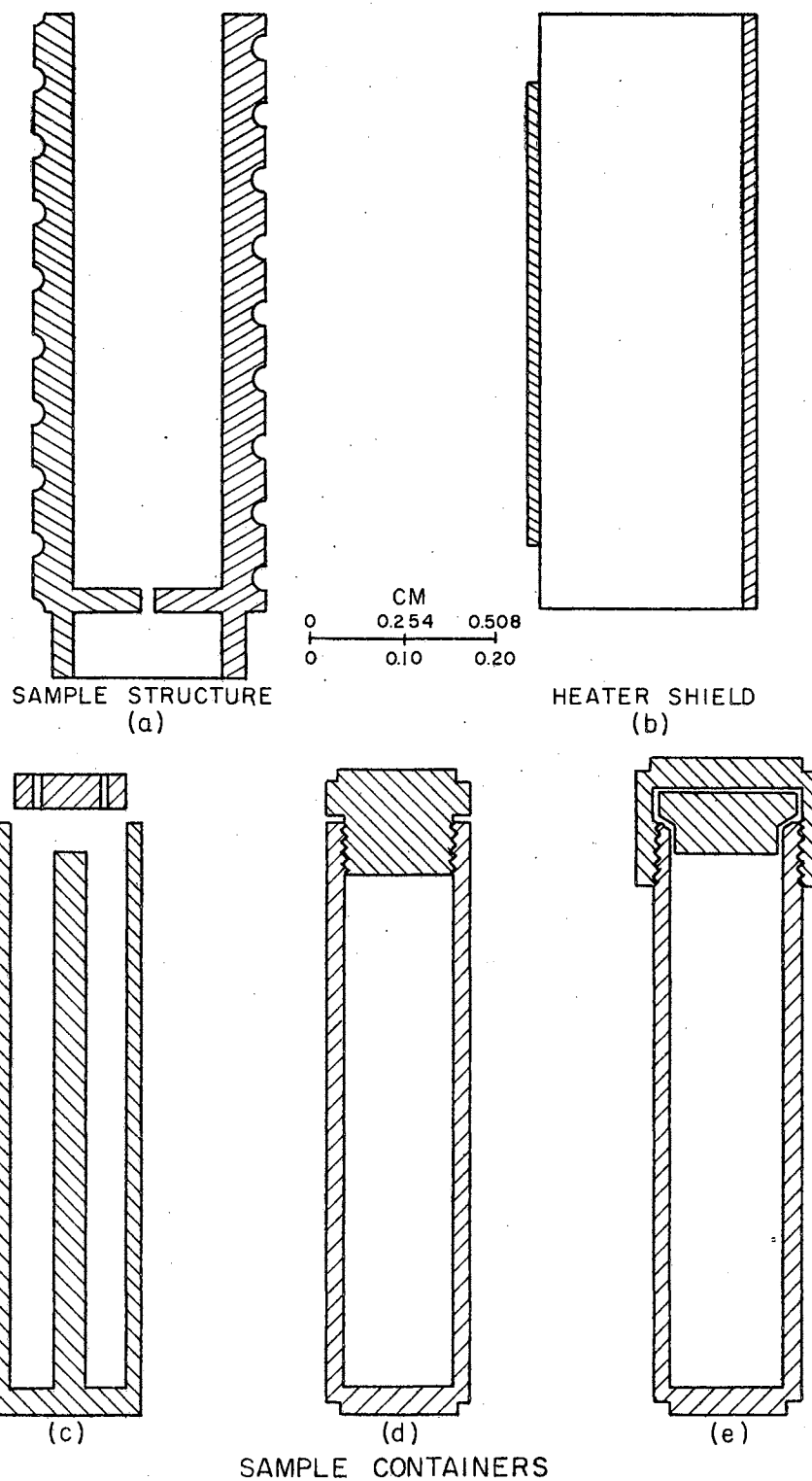
Figure 24.   Sample Holders

groove at the top and bottom of the sample structure was filled with cement; as the cement hardens, the heater wire is held securely in place. The sample structure was again dried at $110^{\circ}C$ for 24 hours, after which the resistance between the heater and sample structure was found to be essentially infinite on the "ohms times 10,000" scale of a Simpson 260 Multi-Meter. The sample structure was then removed from the jig and the heater shield carefully pressed over the sample structure. Care must be exercised at this point to prevent damage to the heater wire. After the shield was in place, it was checked to insure that it was not shorted to the heater.

A Chromel-Alumel thermocouple whose bead was slightly larger than the 0.025-inch hole in the bottom of the sample structure was forced into the 0.025-inch hole. Good thermal contact between the thermocouple junction and the sample structure was thereby assured. The thermocouple leads were then inserted in the ceramic support rod and the structure mounted on the ceramic rod. The assembly was then mounted in the calorimeter and the thermocouple leads brought out to a terminal strip at the base of the calorimeter.

The heater current and potential leads, 0.010-inch platinum wire, were inserted into a ceramic rod. These four leads were brought out to the terminal strip after the rod was inserted in the calorimeter. Two leads are fused to each end of the heater wire with a micro-torch. Between the base of the calorimeter and the terminal strip all electrical leads were insulated with 1/32-inch Teflon spaghetti.

The thermocouple to control the furnace temperature was mounted in a 1/4 by 3/8-inch nickel cylinder which was supported by a 1/8-inch diameter ceramic rod (see Figure 22). The position of this

thermocouple is symmetric with respect to the sample and reference structures and is at the same level as the thermocouples in these structures.

All electrical connections were made on a terminal strip at the base of the calorimeter. The Alumel leads of the sample and reference thermocouples were fused together; the Chromel leads of this differential thermocouple were connected to the input of the sample heater control system using shielded cable. The potential leads from the sample heater were connected to the Hall Device Circuit; the current leads were connected to the dc power supply. The furnace thermocouple was attached to a thermocouple maintained at $0^{o}C$, connection was then made to the input of the furnace control system. A battery power supply was connected to the reference heater; this allows the temperature of the reference structure to be changed, which facilitated adjustment of the sample heater control system.

Three types of sample holders were used in calibrating the calorimeter and in studies of some decomposition reactions. These sample holders are shown in Figure 24 (c), (d), and (e). Sample holder (c) is an open holder made in two parts, the bottom and the barrel which are pressed together. The lid, which has two vent holes, fits rather loosely for easy removal. Sample holders (d) and (e) are closed nickel cells designed to facilitate study of decomposition reactions in self-generated atmospheres. The gaskets for both (d) and (e) were made of platinum or tantalum foil. A special punch was machined to make these gaskets. The tightness of the seal at elevated temperatures was better in sample holder (e).

Balancing Sample Structures

The analysis of Speros and Woodhouse (10) predicts that one should be able to adjust the "distance" between the sample, heater, and thermocouple and thereby change the value of the measured energy input to the heater. If this is indeed true, then it is possible to adjust the "distance", i.e., to balance thermally the structure, such that the measured value of the energy input to the heater is the same as the accepted value for the enthalpy of fusion of some pure substance.

Balancing of the sample structure was effected with the enthalpy of fusion of lead as the standard. The sample, 0.20074 g of Fisher Certified Reagent Grade lead, was placed in a graphite holder and covered with graphite powder to prevent oxidation. The reference structure contained a graphite holder loaded with aluminum oxide.

The energy input to the sample heater during fusion of the lead sample was then measured with quartz discs of varying thickness inserted between the sample holder and the bottom of the sample structure. Table II gives the measured energy input for the different quartz discs. Two determinations were made for each disc and the average value of the energy input was then plotted against the thickness of the quartz disc; this graph is shown in Figure 25. The accepted literature value for the heat of fusion of lead (22) is 1140 cal/mole at 600.6°K. From the smooth curve drawn through the data points (Figure 25), it appeared that a quartz disc 0.009-in. thick should produce a measured energy input equivalent to 1140 cal/mole.

To confirm this, a quartz disc 0.009-in. thick was prepared and inserted between the sample holder and the thermocouple. A new sample

TABLE II

DATA FOR ESTABLISHING THERMALLY BALANCED SAMPLE STRUCTURES

Fusion No.	Quartz Disc Thickness inch	ΔH Fusion* cal/mole
1	0.00	1190
2	0.00	1180
3	0.018	1100
4	0.018	1110
5	0.022	1090
6	0.022	1100
7	0.032	1080
8	0.032	1080

*The same 0.20074-g. sample of Fisher Certified Reagent Grade lead was used for each determination.
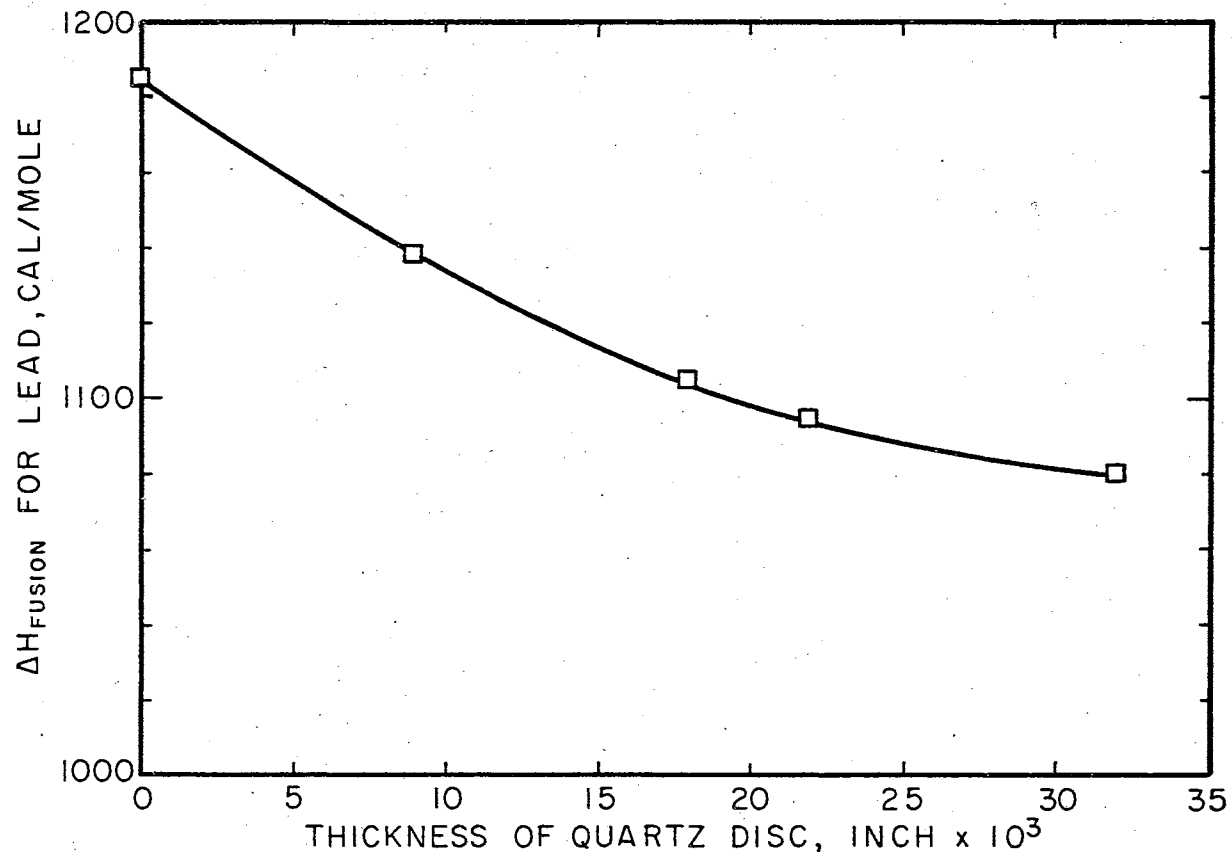
Figure 25. Variation of Measured Energy Input with Thickness of Quartz Disc

of lead, 0.24985 g in a graphite holder, was inserted into the sample structure. Table III shows the data for five fusions of this sample. The average value of the measured energy input corresponds to 1143 cal/mole with a mean deviation of ± 3 cal/mole.

With this confirmation that a 0.009-inch quartz disc would give a measured value in agreement with the literature value, measurements of the heat of fusion of other metals were made to insure that the balancing was not peculiar to lead. The metals chosen were indium, tin, and zinc, which are available in high purity and which span a temperature range that would be of interest later in the study of some decomposition reactions.

The data obtained for indium with the 0.009-inch quartz disc are given in Table IV. The precision of the five measurements is 0.72 per cent; however, the average value for the heat of fusion is 5.8 per cent above the literature value (22). The indium had a stated purity of 99.97 per cent (Indium Corp. of America).

The data for tin are given in Table V. Again the 0.009-inch quartz disc was used as a spacer. The data for tin are in better agreement with the literature value than were the data for indium. The precision of the seven measurements is 1.2 per cent. The average value of 1739 cal/mole is 1.2 per cent above the literature value (22). These data are considered to be in good agreement with the literature value.

The data for zinc are given in Table VI. The 0.009-inch quartz disc again was used. The average value of the heat of fusion for zinc is 1762 cal/mole with a mean deviation of ± 10 cal/mole. This represents a precision of 0.56 per cent and an accuracy of 0.3 per cent (22).

TABLE III

ENTHALPY OF FUSION FOR LEAD

Fusion No.		ΔH Fusion* cal/mole
1		1142
2		1150
3		1142
4		1141
5		1138
	Average	1143 $\pm$ 3

*Using a 0.009-inch quartz disc spacer

TABLE IV

ENTHALPY OF FUSION FOR INDIUM

Fusion No.		ΔH Fusion* cal/mole
1		825
2		816
3		838
4		819
5		827
	Average	825 $\pm$ 6

*Using a 0.009-inch quartz disc spacer

TABLE V

ENTHALPY OF FUSION FOR TIN

Fusion No.	ΔH Fusion* cal/mole
1	1730
2	1720
3	1780
4	1720
5	1760
6	1710
7	1750
Average	1739 $\pm$ 21

*Using a 0.009-inch quartz disc spacer

TABLE VI

ENTHALPY OF FUSION FOR ZINC

Fusion No.		ΔH Fusion* cal/mole
1		1750
2		1780
3		1750
4		1770
5		1760
	Average	1762 $\pm$ 10

*Using a 0.009-inch quartz disc spacer

With the agreement obtained for tin, lead, and zinc with a 0.009-inch quartz disc, it was concluded that the sample structures were indeed thermally balanced.

CHAPTER IV

SYNTHESIS OF ZIRCONIUM

TRICHLORIDE

Several techniques have been used to prepare zirconium trichloride (23-27). Most of these techniques suffer from two disadvantages; the first is the uncertainty of oxidation state of zirconium in the product and the second is the difficulty in separating the trichloride from the unreacted reducing agent and the oxidized form of the reducing agent. Ruff and Wallstein (23) were the first to attempt the reduction of the tetrachloride. These early workers used aluminum as the reducing agent, which remained as an impurity to the extent of a few per cent of the final product. The brown coloration of Ruff and Wallstein's product resulted from the presence of small amounts of water vapor during preparation. Young (24) used the St. Claire-Deville "hot-cold" tube to prepare the tribromide by passing hydrogen and the tetrabromide over a heated aluminum wire and collecting the tribromide in a region not occupied by the aluminum, thus reducing the possibility of contamination by the reducing agent. This technique yielded the tribromide, dibromide and zirconium metal. Similarly, the use of an excess of the tetrachloride with zirconium metal resulted in a mixture of oxidation states (25). This method has the obvious advantage that any unreacted tetrahalide can be sublimed from the desired product. The formation of the trichloride on the surface of the metal forms a

film, however, which makes further reaction of the metal extremely slow; thus, any unreacted metal remains as an impurity which is virtually impossible to remove from the trichloride.

Newnham and Watts (27) investigated the use of hydrogen as a reducing agent, a possibility suggested by the work of Schumb and Sundstrom (28) who prepared titanium trichloride by reducing titanium tetrachloride with molecular hydrogen. This reduction scheme has the very important advantage that both the reducing agent and its oxidized form are gases, which are easily removed from the trichloride. It was discovered, however, that molecular hydrogen would not reduce zirconium tetrachloride. This lead to the use of atomic hydrogen as the reducing agent which has all the advantages that molecular hydrogen affords in that both the reactant and product are gases.

The technique of Newnham and Watts effects the reduction of the tetrachloride with atomic hydrogen produced in a glow discharge. The glow discharge is established between two tungsten electrodes which are connected to a high voltage, high frequency, oscillator circuit. The zirconium tetrachloride is sublimed into the region of the glow discharge where it reacts with the atomic hydrogen. The zirconium trichloride formed adheres to the cool wall of the discharge tube, and the hydrogen chloride gas is removed by a vacuum pump. The increase in thickness of the trichloride on the walls soon causes it to flake away from the walls; it is then collected in a tube which can be separated from the reduction tube using a hand torch. The technique of Newnham and Watts appeared to have all the desirable qualities mentioned above as well as an ease in excluding trace amounts of moisture from the reaction zone.

The apparatus described by Newnham and Watts was closely dupli-
cated in order to insure all the advantages of the technique for our
application. Several difficulties with our apparatus soon became
apparent, however. The small heater used to sublime the zirconium
tetrachloride into the glow discharge also heated the standard taper
joints making contamination of the product with joint grease a very
real possibility. The use of standard taper joints precludes the
possibility of outgassing the tube, at elevated temperatures, to re-
move the moisture from the inner surface of the tube where the zirco-
nium trichloride is condensed. The glow discharge tube was not
maintained at a temperature near the temperature of the sublimation
heater; resulting in the condensation of the zirconium tetrachloride
on the cool portion of the reduction tube before it reached the glow
discharge region. The condensation caused considerably reduced yields,
as well as having a large amount of the tetrachloride mixed with the
trichloride that was formed. Eventually, the accumulation of tetra-
chloride on the cool tungsten electrodes was sufficient to stop the
glow entirely. The flow of hydrogen had to be adjusted to establish
the proper glow and also to entrain the sublimed tetrachloride and
carry it into the region of the glow discharge. These two functions
were not necessarily satisfied by the same flow rate of hydrogen.
When the flow was adjusted to give the proper pressure for a good glow
discharge, back diffusion of the tetrachloride into the hydrogen inlet
was extensive. A flow rate sufficient to carry the tetrachloride into
the region of the glow discharge produced a pressure too high for the
glow discharge. It was difficult to recover the trichloride that was
produced since the flaking from the walls did not occur very

extensively. These difficulties lead to redesign of the reduction apparatus.

Reduction Apparatus Redesigned

The reduction apparatus was redesigned to overcome the difficulties that were encountered with the original apparatus. The reduction tube was enclosed in an isothermal enclosure. The temperature of the enclosure was maintained, by refluxing ethyl benzoate around the reduction tube, at a value that would prevent condensation of the tetrachloride in the region of the glow discharge. The reservoir of zirconium tetrachloride was maintained at the same temperature as the reduction tube. The rate at which zirconium tetrachloride was introduced into the region of the glow discharge was determined by the temperature of the refluxing liquid. The proper glow was established completely independently by adjusting the pressure of hydrogen. At the outlet end of the reduction tube the unreacted tetrachloride was condensed on a cold finger from which it could be removed and used again.

Figure 26 shows the redesigned apparatus. The flask of ethyl benzoate was heated with a heating mantel. The temperature of the refluxing liquid was determined by the pressure on the liquid which could be changed by either admitting nitrogen or reducing the pressure using a mechanical vacuum pump.

Some inherent disadvantages were soon apparent in this design. The temperature of the refluxing liquid was difficult to control even when a ballast was used to increase the volume of the system that was maintained at a reduced pressure. The rate of nitrogen input and the
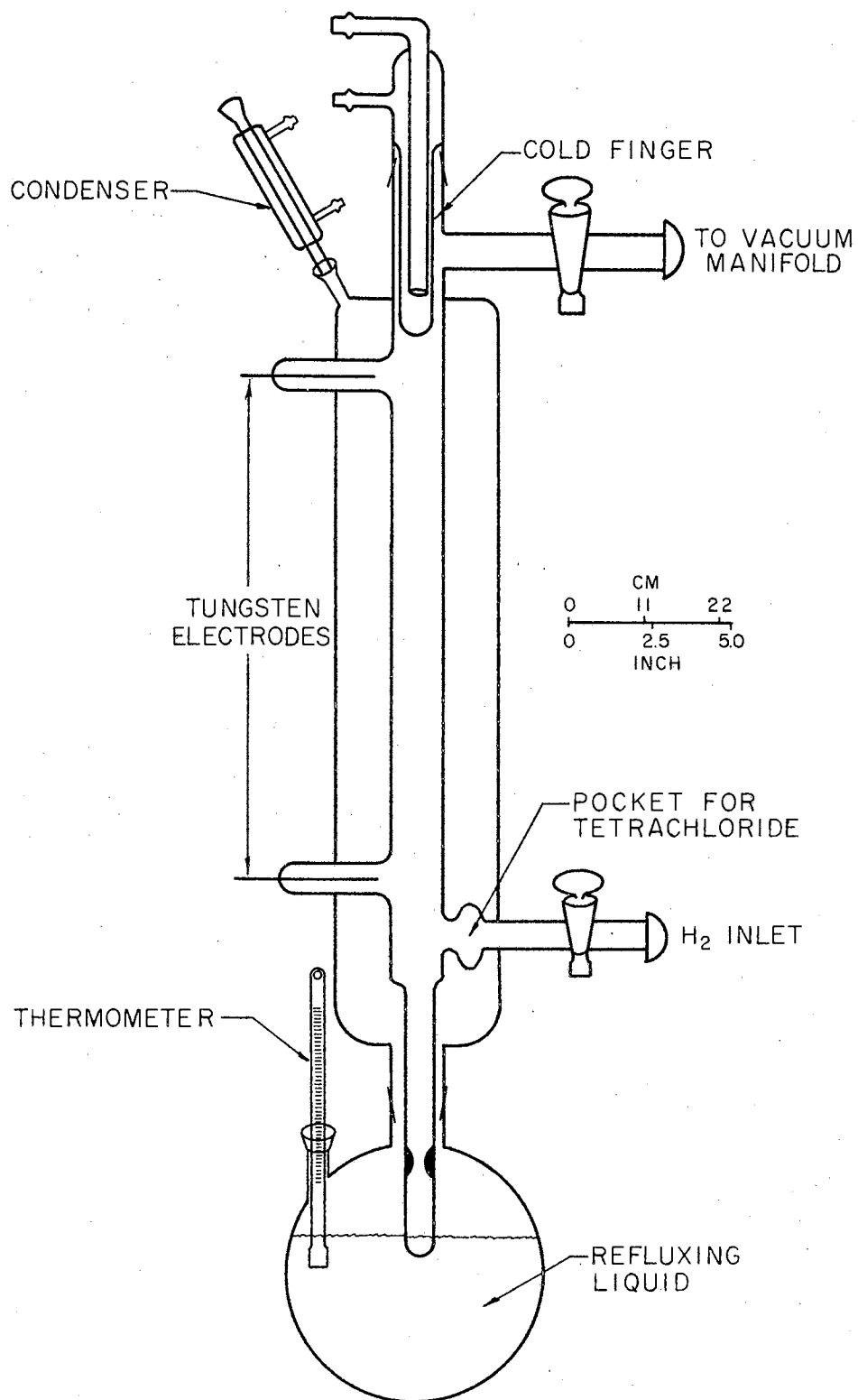
Figure 26. Redesigned Reduction Apparatus with Refluxing-
Liquid Constant Temperature Bath

rate of evacuation were difficult to adjust so as to achieve a constant pressure and thus a constant temperature. The design did not eliminate the condensation of the tetrachloride on the tungsten electrodes; however, the extent of the problem was reduced considerably. The size and fragility of the reduction assembly made it very difficult to handle in the glove box while loading with the tetrachloride. The outer jacket of the reduction apparatus made difficult the vibration of the inner tube sufficiently to cause the zirconium trichloride formed to break away from the glass wall and fall into the collection tube. The apparatus was damaged quite extensively on one occasion while trying to vibrate the trichloride from the walls of the inner reduction tube. With this opportunity to redesign the apparatus, the manner in which the sample was inserted into the reduction tube was changed. The hydrogen inlet tube was redesigned to allow the removal of the side arm and permit access to the sample holder by way of a standard taper joint; this is shown in Figure 27. With this change it was no longer necessary to remove the reduction assembly from the support rack. The sample transfer was then made by use of a dry bag (I^2R Model 3X) which could be closed about the side arm. The plastic glove bag was flushed with pre-purified nitrogen for about an hour before the side arm was removed from the reduction apparatus. The sample of zirconium tetrachloride was then inserted into the sample reservoir, and the side arm replaced. This modification made the reduction assembly much more convenient, but the problems associated with vibrating the trichloride from the walls and maintaining a constant temperature remained.

The low yield from the reaction and the difficulty of recovery prompted the design of another reduction assembly.
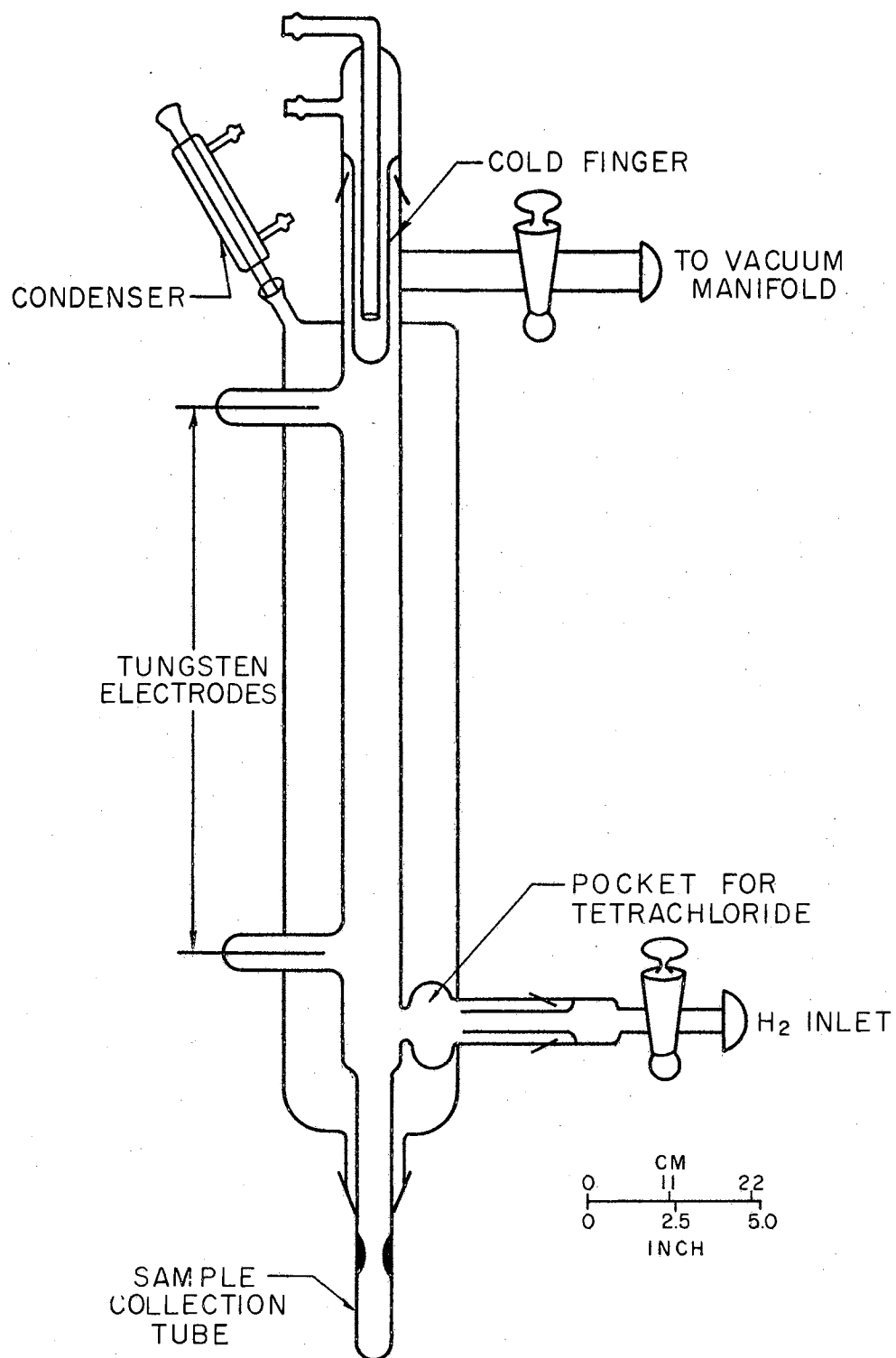
Figure 27. Reduction Apparatus with Improved
Hydrogen Inlet

Reduction Tube For Use In An Air Bath

This simpler design, Figure 28, is in all its essential features the same as the apparatus of Newnham and Watts, but is improved in many important respects. The design allows the portion of the reduction tube that actually comes into contact with the trichloride to be evacuated and heated at 250°C for extended periods of time. The trichloride seemed to be easier to remove from the glass walls after the walls had been heated while the tube was evacuated.

The hydrogen inlet side arm was modified to reduce the back diffusion of the tetrachloride into the cool portions of the inlet assembly. The reduction in back diffusion was accomplished in two ways, first the removable side arm was made long enough to extend up to the sample reservoir and its diameter large enough so that the space between the two tubes was less than a millimeter. The end of the side arm tube was closed, and radial openings for the hydrogen gas were placed up stream from the constriction at the sample reservoir. The hydrogen gas, passing through this constriction at a greatly increased rate, reduced any back diffusion of tetrachloride from the reservoir. The second modification consisted of a heater wrapped around the side arm at the constriction so that the hydrogen passed over the heated glass before entering the sample reservoir. The area of the constriction was at a higher temperature than the sample reservoir, thereby reducing back diffusion and condensation in this region. The tungsten electrodes were maintained at the same temperature as the rest of the reduction tube, which eliminated condensation of tetrachloride on the electrodes. A cold finger was placed at the outlet end of the reduction tube to collect any unreacted tetrachloride.

COLD FINGER

TO VACUUM MANIFOLD

CM
0   5   10
0   2   4
INCH

TUNGSTEN ELECTRODES

POCKET FOR TETRACHLORIDE

H_2 INLET

SAMPLE COLLECTION TUBE
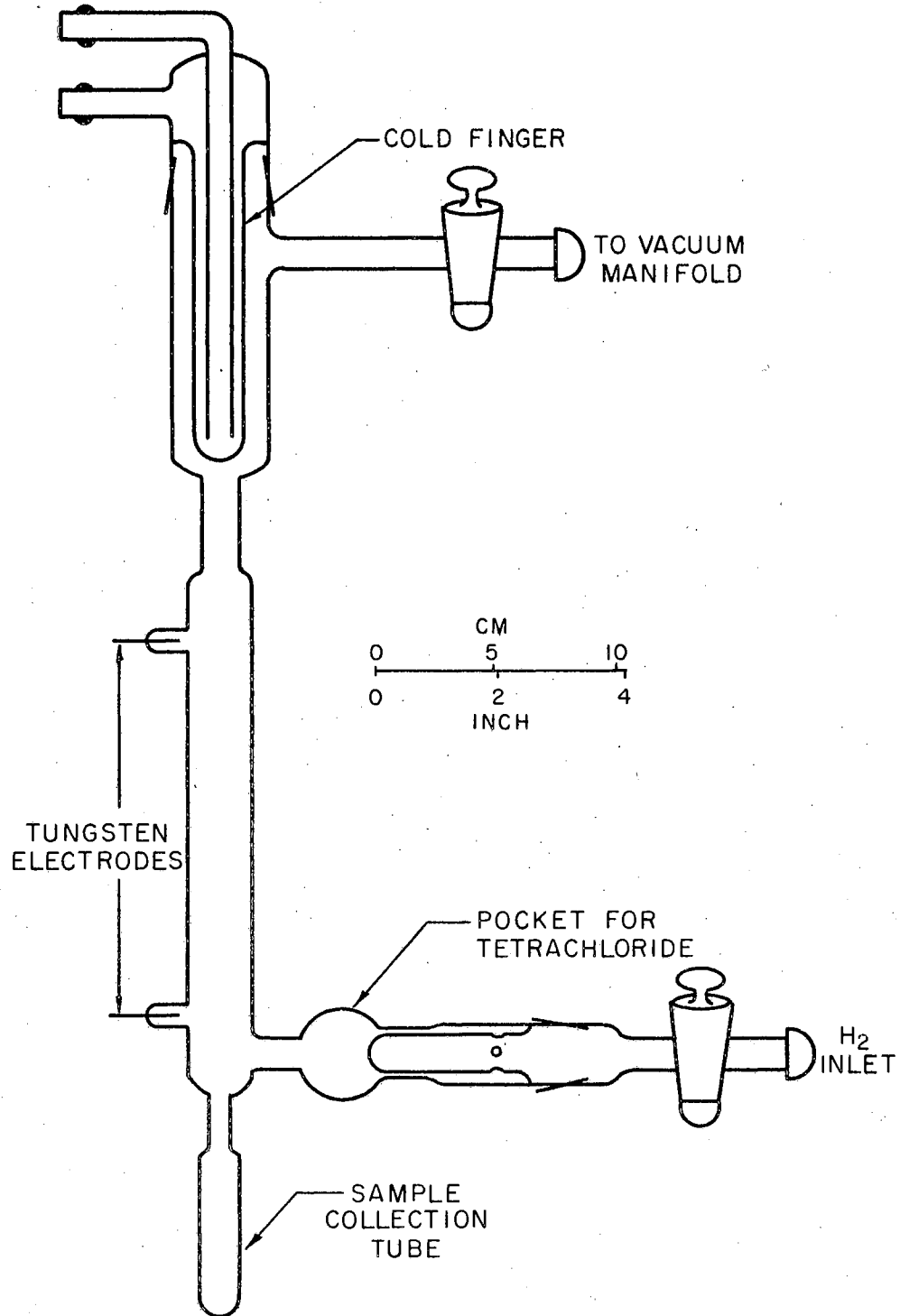
Figure 28.   Improved Reduction Apparatus Used With Hot Air Oven

The reduction tube was designed to be separated from the vacuum manifold while still under vacuum. The side arm could be removed by sealing the tube between the sample reservoir and the reduction tube. This prevented contamination of the trichloride with unused tetra- chloride remaining in the sample reservoir. The main portion of the reduction tube could be sealed, with a hand torch, and separated from the cold finger portion of the assembly. The separated tube, i.e., the portion that contains the electrodes and the trichloride collection tube, was still under vacuum and was very easy to handle. A pyrex scraper was inserted into the assembly before the initial drying of the reduction tube; this scraper was used to remove the trichloride from the inner surface of the reduction tube by sliding the scraper back and forth. The trichloride was then vibrated through the con- striction between the reduction and collection tube. After the tetra- chloride was sublimed from the collection tube, the tube was parted from the remainder of the assembly.

The Hot Air Oven

Figure 29 shows the oven used to maintain the reduction tube at a constant temperature. The oven is made of one-half inch transite held together with wood screws. The heater is 17 feet of bead- insulated Nichrome wire (B&S No. 18) mounted one-half inch from the wall on insulators. A layer of glass wool insulation was placed be- tween the Nichrome heater and the transite wall. It was found that a constant temperature could be attained by use of a Variac, so that no temperature control device was necessary. The temperature of the oven was monitored at the zirconium tetrachloride reservoir with a

OPENINGS FOR
REDUCTION TUBE(Fig.28)

AC TERMINALS

BEADED
NICHROME
HEATER

THERMOCOUPLE
WELL

FIBER GLASS
INSULATION

CM
0   15   30
0   6   12
INCH
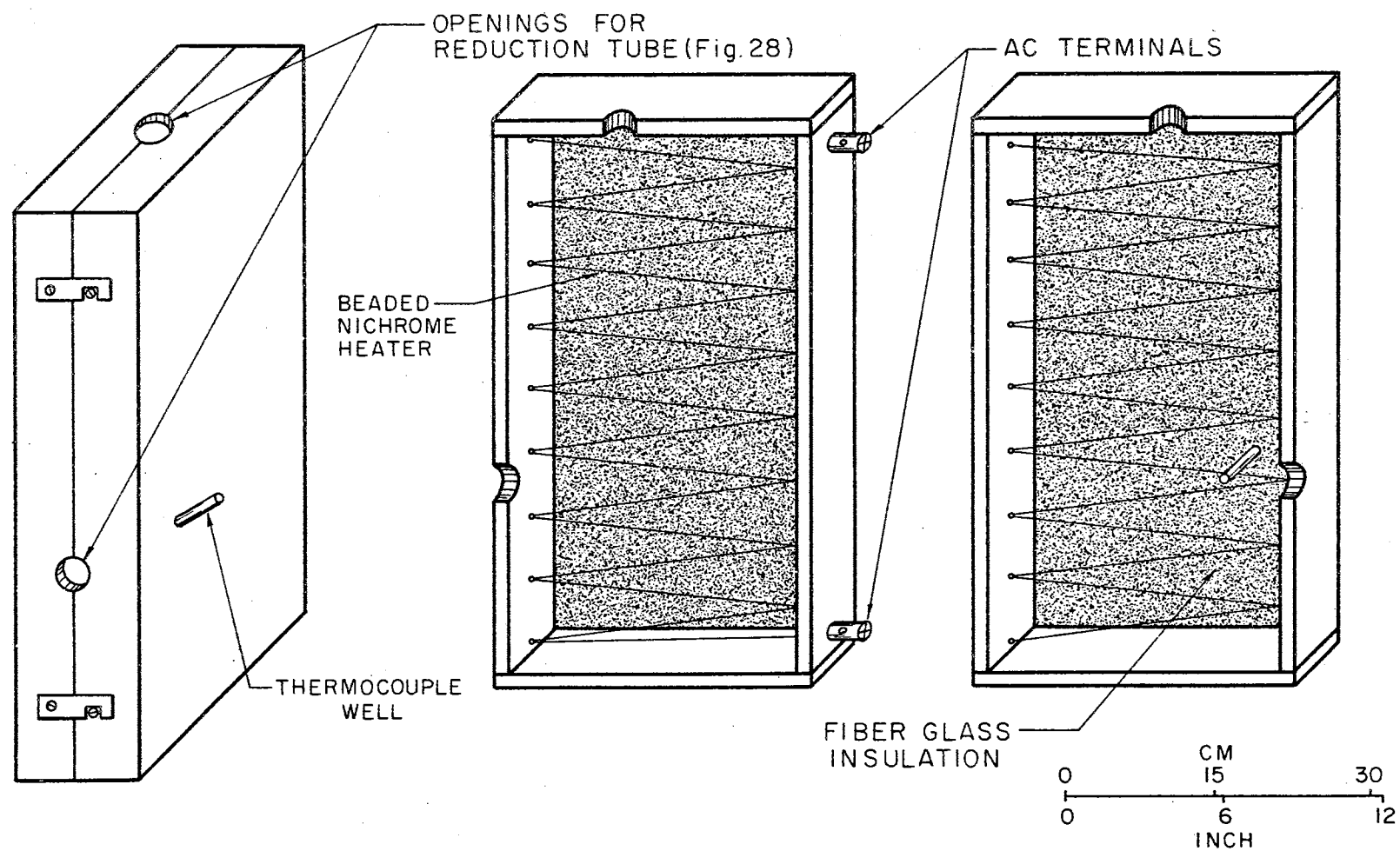
Figure 29. Hot Air Oven

Chromel-Alumel thermocouple referenced at the ice point.

High Voltage Power Supply

Power to sustain the hydrogen glow discharge was provided by a high voltage, high frequency, oscillator circuit. The schematic of the power supply is shown in Figure 30. A 20-amp, 110-volt Variac controls the voltage on the primary of the high voltage transformer between 0 and 130 volts. The high voltage transformer is a Thordarson T21P77, rated at 300 millamperes dc in the secondary windings. The 0.05 microfarad capacitor in series with the oscillator prevents damage to the transformer by limiting the current in the secondary when the spark gap is conducting. The adjustable spark gap consists of two one-half-inch silver discs mounted on brass cooling fins suitably insulated from one another. The distance between the two silver contacts determines the voltage that appears across the 0.05 microfarad capacitor in the oscillator circuit and thus the electrical energy stored. When the voltage across the capacitor, which is the same as the voltage across the spark gap, is sufficient to render the air between the silver contacts conducting, the energy stored in the capacitor is returned to the circuit causing a large current to flow through the primary of the induction coil and a high voltage to appear across the secondary of the coil. This oscillation occurs many times while the spark gap is conducting. The spark gap conducts on each half cycle of the 60 Hz ac, i.e., it conducts 120 times each second.

Figure 31 shows the high frequency induction coil. The Lucite former on which the secondary is wound is stationary. The primary can be moved to change the coupling between the coils to give the best glow discharge.
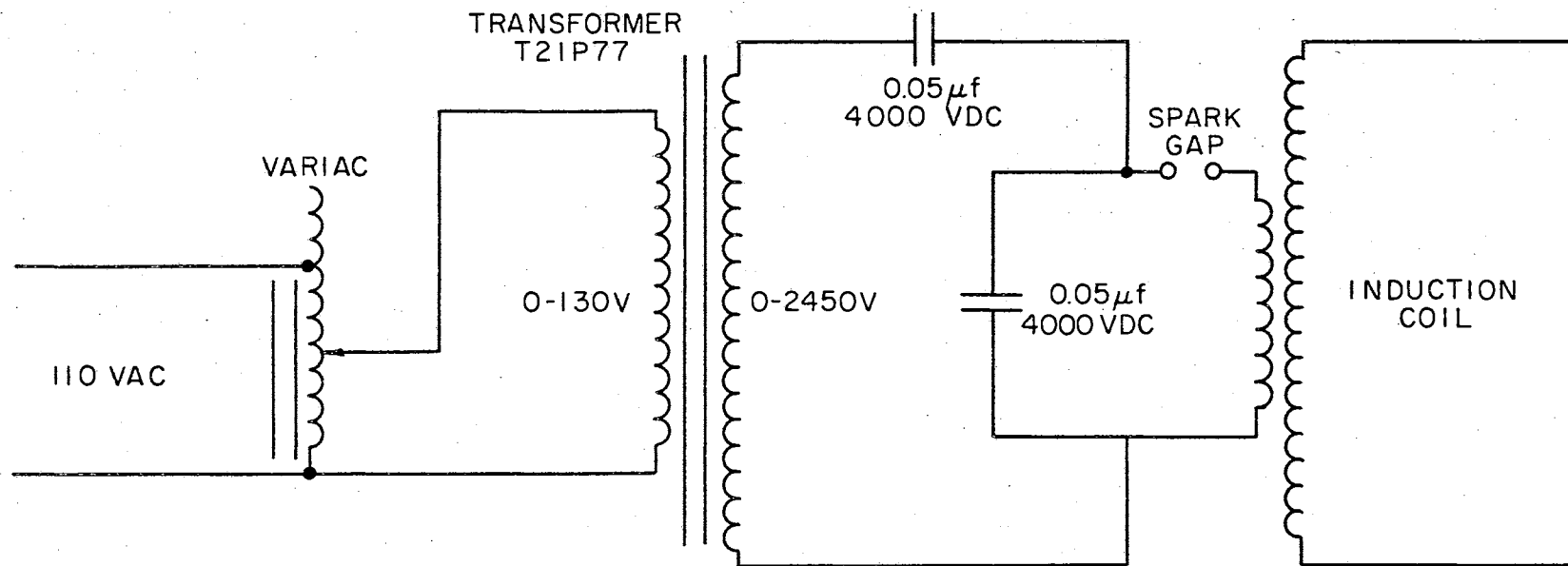
Figure 30. High Voltage Supply for Glow Discharge

HIGH
VOLTAGE
TERMINAL

SECONDARY COIL
FORMER

PRIMARY COIL
FORMER

INPUT
TERMINAL

PRIMARY COIL
SLIDE ADJUSTMENT

CM

0   2.5   5.0

0   I   2
INCH
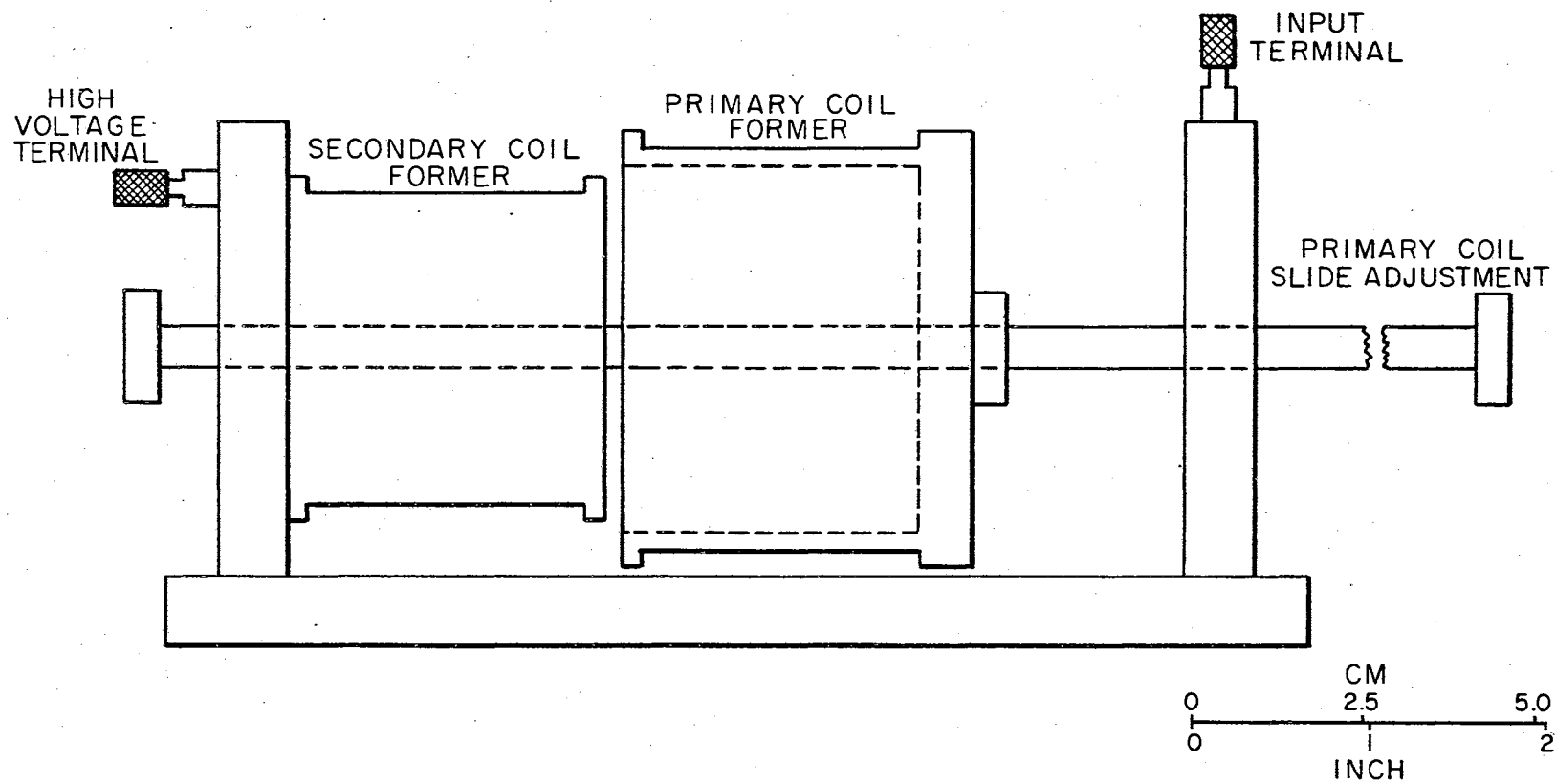
Figure 31. Induction Coil Mount

Considerable difficulty was encountered in providing adequate insulation on the secondary of the induction coil. The difficulties were eliminated by using No. 32 Heavy Formvar insulated magnet wire wound 200 turns to the layer, and using three layers of Permacel-423 Teflon Film Tape between each layer of magnet wire. This Teflon tape is 0.0035 in. thick, has an insulation resistance of two million megohms, and an electric strength of 8,500 volts. Silicone adhesive on one side of the tape facilitates its use in winding coils. The primary of the induction coil consists of 20 turns of No. 18 seven-strand copper wire on a 3-inch diameter former. The secondary consists of ten layers, 200 turns/layer, wound on a 2-inch diameter former. The entire high voltage power supply was housed in a plywood box fitted with high voltage feed-throughs and a cooling fan.

Vacuum Manifold

The vacuum manifold, Figure 32, consists of a series of traps and gauges to measure the pressure at the hydrogen inlet to the reduction tube and at the point where the reduction tube is attached to the manifold. The hydrogen used in the reduction is passed through a molecular sieve trap that has been activated at $300^{\circ}C$ and evacuated. The hydrogen chloride produced in the reaction is removed from the effluent gas by reaction with lead at $100^{\circ}C$ in the first trap on the outlet side. The second trap is molecular sieve which prevents any water vapor from diffusing into the reduction tube where it would react with the zirconium trichloride. The last trap is a Dry Ice-acetone cold trap to prevent oil from the vacuum pump from entering the reduction tube. The vacuum pumps consisted of an MCF-60 oil diffusion pump with a Welch
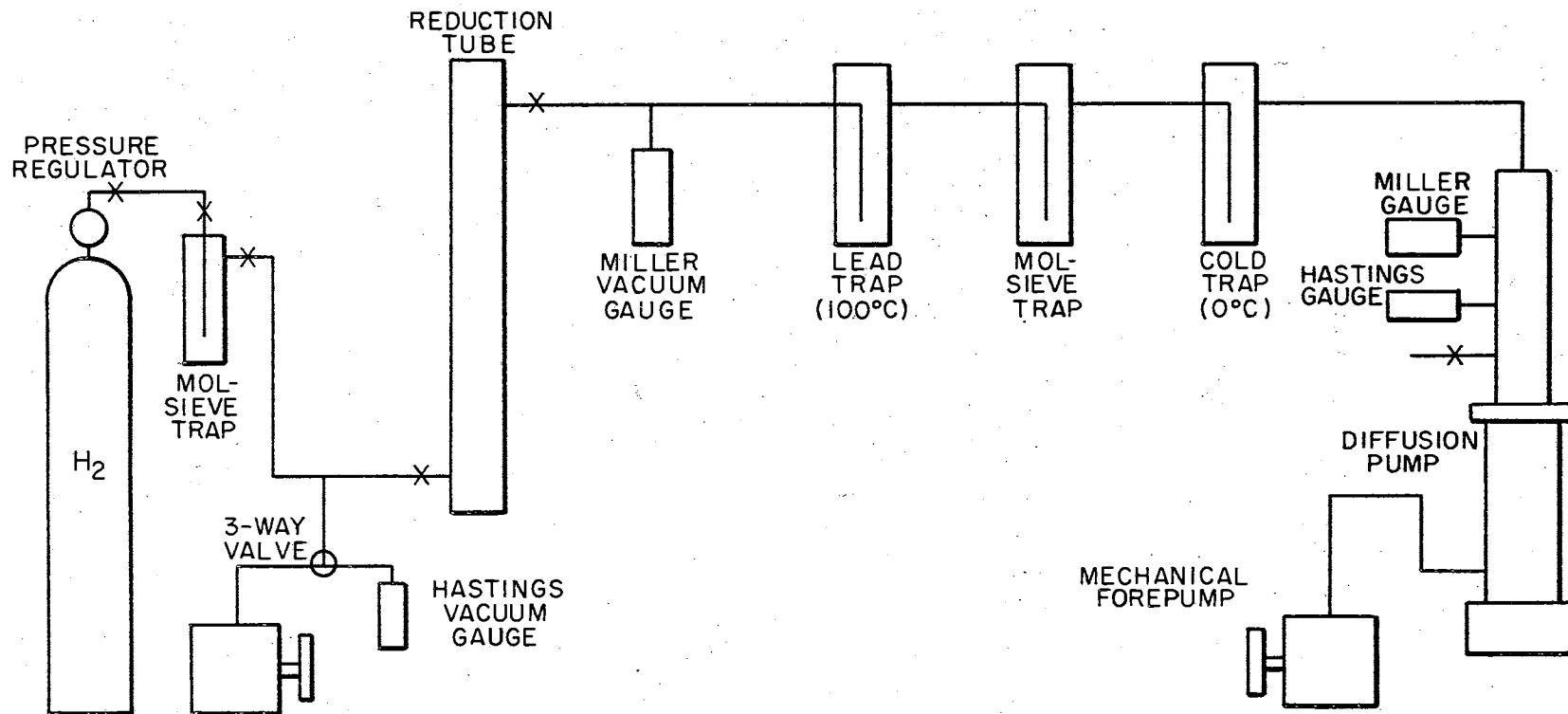
Figure 32. Schematic of Vacuum Manifold

Duo-Seal mechanical fore pump. The pressure of the hydrogen gas at the inlet to the reduction tube was measured with a Hastings DV-6M gauge tube, while at the outlet a Miller cold cathode gauge was used.

Preparation Of Zirconium Trichloride Samples

Reactor Grade zirconium tetrachloride (lot 1802, low hafnium content) was obtained from TAM, a Division of National Lead Company. The tetrachloride was sublimed twice in vacuum before it was used.

In preparation for the synthesis of the trichloride, the reduction tube was cleaned thoroughly with detergent. The tungsten electrodes were cleaned by emersing both electrodes in 20% sodium hydroxide solution and connecting the electrodes to a 10-volt ac source. After the electrodes were brightened, the tube was rinsed with distilled water, then with reagent grade acetone. The Pyrex scraper was inserted into the reduction tube. The tube was then mounted in the oven and attached to the vacuum manifold. All stopcocks and ground glass joints were greased with Apiezon "T". The reduction tube was then evacuated and the temperature of the oven raised to $250^{o}C$. Drying of the reduction tube usually lasted from 12 to 18 hours. After the oven cooled to room temperature, the glove bag, which contained the zirconium tetrachloride, a scoop for loading the sample into the reservoir, a tube of Apiezon "T", a tray, and about a liter of activated molecular sieve in a sealed container, was attached to the hydrogen inlet side arm. The glove bag was flushed, by inflating with pre-purified nitrogen and then deflating, four times before the molecular sieve was poured into the tray. The bag was inflated the fifth time with the gas in contact with the molecular sieve. The valve on the top of the reduction tube

was then closed, and the valve on the hydrogen inlet side arm opened.

Thus, the previously dried and evacuated reduction tube was filled with

dry nitrogen, and the introduction of moisture was eliminated. The

sample reservoir was filled with tetrachloride and the hydrogen inlet

side arm greased and replaced. The reduction tube was then evacuated,

and the hydrogen supply attached to the hydrogen inlet. The hydrogen

pressure at the inlet was adjusted to about one Torr and the glow dis-

charge initiated. The pressure was then more carefully adjusted to

give the "best glow." The correct pressure for "best glow" is more

easily found with a Tesla coil. A Tesla coil held close to the hydro-

gen inlet side arm produces a distinct red glow when the pressure is

in the proper range. This red glow is characteristic of atomic hydro-

gen. The discharge is stopped while the remaining adjustments are

made.

The side arm heater, which prevents back diffusion of the tetra-

chloride into the hydrogen inlet, and the oven are then raised to

operating temperature. With the pressure previously adjusted, the

temperature of the oven is adjusted until the rate of deposition of

the tetrachloride on the cold finger appears to be about equal to the

rate at which it can be reduced in the glow discharge. The discharge

is then re-started in the reduction tube. Reaction time is usually

10 to 12 hours or until all the tetrachloride has sublimed.

After completion of the reaction, the hydrogen inlet side arm is

disconnected from the hydrogen source. The oven is opened and the

high voltage leads removed from the reduction tube. With a hand torch

the hydrogen inlet side arm is parted between the tube and the tetra-

chloride reservoir. Closing the upper stopcock on the reduction tube

then seals the reduction tube from the atmosphere and it can be removed
from the vacuum manifold. At this point the cold finger portion of
the reduction tube could be parted to prevent the condensed tetra-
chloride from falling into the collection tube and contaminating the
trichloride; however, the cold finger was usually covered with the
black trichloride in such qauntities that it seemed best to try to re-
cover as much of it as possible. As much of the trichloride as possi-
ble was dislodged from the walls and cold finger and vibrated into the
collection tube; the reduction tube was then parted just below the cold
finger. The collection tube was placed in the oven with the remainder
of the reduction tube exposed to room temperature. The oven tempera-
ture was then raised to $170^{O}C$ and held for 12 to 18 hours, or until all
the tetrachloride sublimed out of the collection tube. This is checked
by exposing a previously heated portion of the reduction tube to room
temperature; if no tetrachloride condensed thereon, it was assumed that
no more tetrachloride was mixed with the trichloride. The collection
tube was then parted from the reduction tube.

Ten samples of zirconium trichloride, varying in amount from about
0.5 g to 3.0 g, were prepared by this technique. The deep black color
of the samples indicates the absence of hydrolysis which produces a
brown compound (27).

Chemical Analysis

Because of the extreme sensitivity of zirconium trichloride to
trace amounts of moisture, it did not seem advisable to analyse each
sample prepared. Even samples exposed to "dry" N_2 in a glove box in
which the dew point was ~ $-35^{O}C$, hydrolysed rather rapidly as was

evident from formation of a brown color. It appeared that opening the sample tubes for analysis and transferring the remainder to another container for later use would introduce an unknown amount of hydrolysis and possibly cause loss of the entire sample. For these reasons two samples that appeared to be representative were chosen for analysis.

Zirconium analysis was performed by precipitating the metal as the mandelate, then firing and weighing as the oxide (29). The chlorine content of the samples was determined by Volhard's method (78).

Analysis of zirconium tetrachloride which has been vacuum-sublimed twice indicated the following, expressed as per cent of theoretical for $ZrCl_4$:

(a) First experiment Zr - 100.7% ; Cl - 99.8%

(b) Second experiment Zr - 99.8% ; Cl - 99.7%.

The two samples of zirconium trichloride chosen for analysis were vials 1 and 10. The samples for analysis were handled in a glove box, whose atmosphere had a dew point of ~ -45°C. The analysis of the two samples produced the following results, expressed as per cent of theoretical for $ZrCl_3$:

(a) Vial 1   Zr - 100.0%; Cl - 99.6%

(b) Vial 10   Zr - 100.3%; Cl - 99.7%.

X-Ray Diffraction Data

An x-ray diffraction powder pattern was obtained for the $ZrCl_3$ from each vial analysed above. The x-ray capillary was loaded with $ZrCl_3$, broken to the proper length, and sealed with hot Apiezon W wax in the dry box (dew point ~ -45°C). Photographs of the diffraction patterns were taken with Ni-filtered Cu Kα radiation in a 114.6-mm

diameter powder camera. The film was measured with a film-measuring instrument and line intensities were estimated visually.

Calculated values of $\sin^2\theta$ and estimated line intensities are given in Table VII along with similar x-ray data from the work of Swaroop and Flengas (30) and Dahl and Larsen (31). Examination of these data indicate that there is good agreement between the $\sin^2\theta$ values of Dahl et. al. and those for our sample, both of which are in poor agreement with the data of Swaroop and Flengas.

Swaroop and Flengas reported that their $ZrCl_3$ was black, but turned brown upon exposure to atmospheric moisture. The synthesis of the $ZrCl_3$ used by Dahl and Larsen was reported by Larsen and Leddy (25). It was stated by Larsen and Leddy (25) that the $ZrCl_3$ prepared by them was brown in color. However, Dahl and Larsen (31) do not mention the color of the $ZrCl_3$ used by them in their x-ray studies. Our samples of $ZrCl_3$ were black, but when exposed to atmospheric moisture they turned brown. Our x-ray data are for the black compound. The sealed x-ray capillaries remained black for several weeks after the x-ray photographs were made. Photographs of the same capillary made two days apart were essentially identical.

Both workers prepared their samples of the trichloride by reacting the tetrachloride with zirconium metal at elevated temperatures. Swaroop and Flengas performed their syntheses at $700 - 750^\circ C$ and one atmosphere tetrachloride pressure. Larsen and Leddy conducted their synthesis reactions at $500^\circ C$ and 5 to 15 atmospheres of tetrachloride pressure. Analysis of the product in both instances indicated zirconium and chlorine present to greater than 99% of theoretical for $ZrCl_3$.

TABLE VII

COMPARISON OF X-RAY POWDER DIFFRACTION DATA FOR ZIRCONIUM TRICHLORIDE

Line No.	Data of Swaroop and Flengas (30)		This Work		Data of Dahl and Larsen (31)	
	$Sin^2 \theta$	I_c^a	$Sin^2 \theta$	I^b	$Sin^2 \theta$	I_c^c
1	–	–	0.0194	100	0.0199	99
2	0.0286	13.4	–	–	–	–
3	0.0587	9.2	–	–	0.0602	4.2
4	0.0667	70.9	–	–	–	–
5	0.0732	4.1	0.0742	20	0.0749	30.5
6	0.0788	100.0	0.0781	5	0.0781	11.1
7	–	–	0.0828	20	0.0833	25.0
8	0.1028	12.8	–	–	–	–
9	0.1140	41.2	–	–	–	–
10	–	–	0.1213	40	0.1226	33.3
11	–	–	0.1356	10	0.1373	11.1
12	–	–	0.1407	10	0.1419	13.9
13	0.1465	2.0	–	–	–	–
14	–	–	0.1746	10	0.1766	15.3
15	0.1820	18.7	–	–	–	–
16	0.1920	2.7	–	–	–	–
17	0.2013	12.7	0.1991	20	0.2009	17.2
18	0.2242	3.8	–	–	–	–
19	–	–	0.2517	5	0.2542	14.7
20	0.2582	5.0	–	–	–	–
21	0.2724	5.4	0.2705	2	0.2723	3.6
22	–	–	0.2948	5	0.2982	5.6
23	0.3107	0.7	–	–	0.3116	5.8
24	0.3565	0.6	–	–	–	–
25	0.3737	1.5	–	–	–	–
26	–	–	–	–	0.3775	3.3
27	–	–	0.3854	5	–	–
28	–	–	–	–	0.3906	2.8
29	–	–	–	–	0.4114	0.6
30	–	–	0.4284	5	0.4279	1.7
31	0.4581	0.9	–	–	–	–
32	0.4687	6.4	–	–	–	–
33	–	–	–	–	0.4738	1.6

[a,c]Calculated relative intensities

[b]Intensities estimated visually

The differences between the x-ray data could be due to the formation of a different crystalline modification or the presence of $ZrCl_2$. Newnham (79) reports the formation of a greenish-black substance that was analysed to be $ZrCl_3$. The greenish-black substance was formed from zirconium metal and the tetrachloride in the range of reaction temperatures from 330 to 460°C. From the data of Turnbull and Watts (80) on the disproportionation of $ZrCl_3$, one might expect $ZrCl_2$ to be also formed with the reaction conditions used by Swaroop and Flengas. Turnbull and Watts studied the disproportionation of $ZrCl_3$ quantitatively and found the equilibrium pressure of $ZrCl_4$ above $ZrCl_3$ to be 1020 Torr at 450°C. Swaroop and Flengas used only 760 Torr $ZrCl_4$ pressure at 700 - 750°C. One atmosphere $ZrCl_4$ pressure would not be sufficient to prevent the $ZrCl_3$ from disproportionating to $ZrCl_2$ at 700 - 750°C.

Differences in x-ray data due to hydrolysis of this reactive compound are also quite possible.

CHAPTER V

SOME DECOMPOSITION REACTIONS

Several decomposition reactions were studied to determine how well

the balanced differential scanning calorimeter would reproduce enthalpy

and kinetic data obtained by other techniques. The types of reactions

chosen were solid decompositions producing another solid phase and a

gas, or a gas phase only. The particular reactions studied were chosen

more for the availability of the substance, ease of producing controlled

atmospheres, and accessibility of decomposition temperatures, than for

their fundamental nature.

Decomposition of Lead Carbonate

The decomposition of lead carbonate has been the object of many

studies (32-45). The interest is partly due to the ease with which

carbonate decompositions can be studied, but primarily because lead

carbonate decomposes to form stable intermediate solid phases. The num-

ber of these solid phases occurring in the course of the decomposition

of $PbCO_3$ to PbO has been, and to some extent still is, in doubt.

In an early investigation of lead carbonate, Centnerswer (41) re-

ported the existence of three intermediate phases. These phases are

described by the following reactions:

Sequence A

$$8PbCO_3 \longrightarrow [3PbO \cdot 5PbCO_3] + 3CO_2 \qquad (274°C)$$

$$[3PbO \cdot 5PbCO_3] \longrightarrow 4[PbO \cdot PbCO_3] + CO_2 \qquad (285°C)$$

$$3[PbO \cdot PbCO_3] \longrightarrow 2[2PbO \cdot PbCO_3] + CO_2 \qquad (360°C)$$

$$[2PbO \cdot PbCO_3] \longrightarrow 3PbO + CO_2 \qquad (412°C)$$
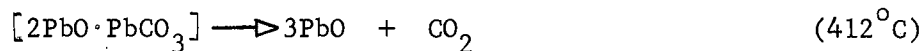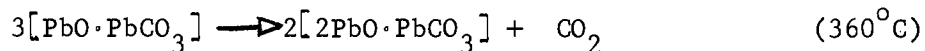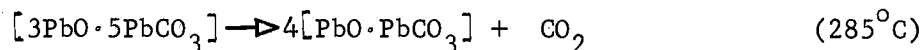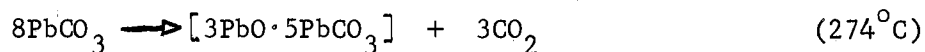
Bruzs (44) found no evidence for $[3PbO \cdot 5PbCO_3]$ nor for $[2PbO \cdot PbCO_3]$; His decomposition scheme would be described by only two equations:

Sequence B

$$2PbCO_3 \longrightarrow [PbO \cdot PbCO_3] + CO_2$$

$$[PbO \cdot PbCO_3] \longrightarrow 2PbO + CO_2$$
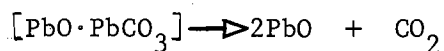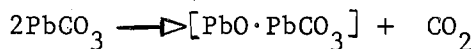
From the International Critical Tables (46), and the work of Lamure (37) and Peretti (36), two intermediate solid phases and, therefore three equations in the decomposition sequence are indicated:

Sequence C

$$2PbCO_3 \longrightarrow PbO \cdot PbCO_3 + CO_2 \qquad (263°C)$$

$$3[PbO \cdot PbCO_3] \longrightarrow 2[2PbO \cdot PbCO_3] + CO_2 \qquad (389°C)$$

$$[2PbO \cdot PbCO_3] \longrightarrow 3PbO + CO_2 \qquad (438°C)$$
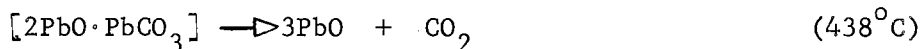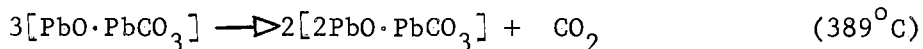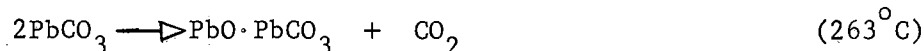
It would seem that the number of intermediate oxy-carbonates could be resolved from the number of DTA peaks that occur during the decomposition. However, the DTA studies of Cuthbert and Rowland (40), Kauffman and Dilling (43), Beck (38), Gruver (45), and Collins and Swan (42) still leave the number of peaks in doubt.

Warne and Bayliss (33) made a systematic study of the effects of heating rate, particle size and uniformity, dilution with inert material, and composition of furnace atmosphere on the DTA peaks observed. They demonstrated that suitable combinations of variables would produce

The DTA curves previously reported. The optimum conditions, which pro-
duced the best separation of the three endothermic peaks at $340^{\circ}C$,
$390^{\circ}C$, and $440^{\circ}C$, were a heating rate of 2 deg per minute, an atmosphere
of carbon dioxide, and sample from the -100 + 150 mesh fraction
(British Standard Sieves). The three peaks indicate the existence of
only two intermediate solid phases at one atmosphere of carbon dioxide.

Glasner and Hodara (35) studied the decomposition of lead carbon-
ate, and found $[2PbO \cdot 3PbCO_3]$, $[5PbO \cdot 6PbCO_3]$, and $[3PbO \cdot 2PbCO_3]$. The
phase $[PbO \cdot PbCO_3]$ was found only in an atmosphere of air.

Grisafe and White (32) used equilibrium methods to study the
$PbO - CO_2$ system over the range of 200 to $900^{\circ}C$ and 15 to 1400 bars CO_2
pressure. Four oxy-carbonates were found, two of which were identical
with those found by Lamure (37) and Paretti (36); one phase $3PbO \cdot 4PbCO$
$[3PbO \cdot 4PbCO_3]$ was stable only at high pressure-temperature conditions,
and the fourth phase $[PbO \cdot 2PbCO_3]$ had not been reported previously.
Their results extrapolated to one atmosphere CO_2, suggest the following
reactions would occur at the indicated temperatures:

Sequence D

$$3PbCO_3 \longrightarrow [PbO \cdot 2PbCO_3] + CO_2 \qquad (204^{\circ}C)$$

$$2[PbO \cdot 2PbCO_3] \longrightarrow [3\ PbO \cdot PbCO_3] + CO_2 \qquad (283^{\circ}C)$$

$$3[PbO \cdot PbCO_3] \longrightarrow 2[2PbO \cdot PbCO_3] + CO_2 \qquad (373^{\circ}C)$$

$$[2PbO \cdot PbCO_3] \longrightarrow 3PbO + CO_2 \qquad (435^{\circ}C)$$
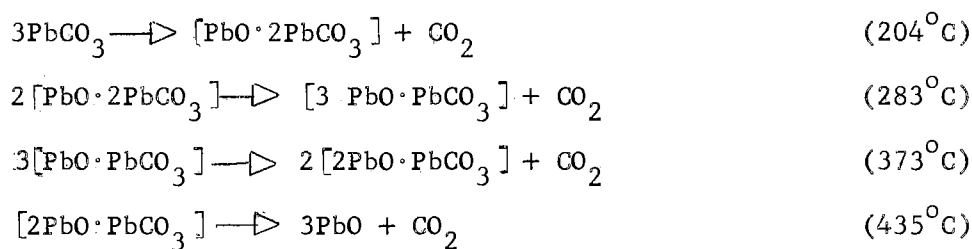
The authors indicate the first reaction to be sluggish, and sug-
gest that the first two reactions overlap one another and appear as one
reaction under the dynamic conditions of DTA or TGA.

The decomposition of lead carbonate in one atmosphere of CO_2 was studied using the DSC. Lead carbonate was contained in a graphite sample holder (C), Figure 24, and the temperature scanning rate was 3 deg per minute. A typical decomposition curve is shown in Figure 33 with the reaction temperatures and the range of stability of the intermediate phases indicated. Figure 33 shows that under the above conditions the DSC is able to separate the three peaks quite well.

The appearance of only three peaks in the decomposition of $PbCO_3$ would tend to confirm the reactions in "Sequence C." If the three peaks are assumed to represent the three reactions in "Sequence C," the enthalpy changes for these reactions may be calculated from peak areas:

$$PbCO_3 \longrightarrow 1/2[PbO \cdot PbCO_3] + 1/2CO_2 \quad \Delta H_{599} = 9.26 \text{ KCal/mole}$$
$$1/2[PbO \cdot PbCO_3] \longrightarrow 1/3[2PbO \cdot PbCO_3] + 1/6CO_2 \quad \Delta H_{662} = 4.48 \text{ KCal/mole}$$
$$1/3[2PbO \cdot PbCO_3] \longrightarrow PbO + 1/3CO_2 \quad \Delta H_{729} = 7.40 \text{ KCal/mole}$$
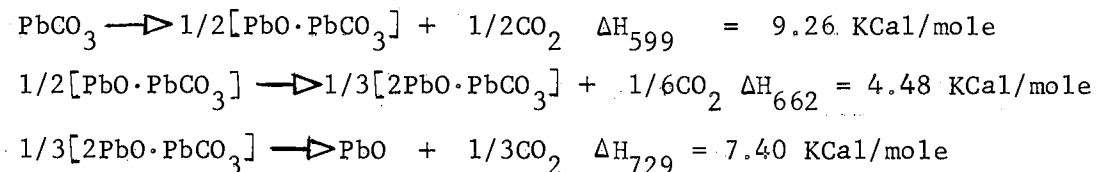
The sum of the enthalpies for the three reactions of "Sequence C" gives the enthalpy change for the decomposition of one mole of $PbCO_3$ at an average temperature of $658^{\circ}K$,

$$PbCO_3 \longrightarrow PbO + CO_2, \quad \Delta H_{658} = 21.1 \text{ KCal/mole.}$$

The value thus obtained may be compared with 20.4 KCal/mole which was calculated from enthalpies of formation and heat capacities (47,22).

Again assuming the three DSC peaks represent the reactions in "Sequence C," one can compare the enthalpy values per mole of CO_2 with those reported in the literature (32, 36, 41). The values of Centnerswer, Falk, and Averbuch (41) are the values obtained from measurements of CO_2 pressure over $PbCO_3$, $[PbO \cdot PbCO_3]$, and $[2PbO \cdot PbCO_3]$.
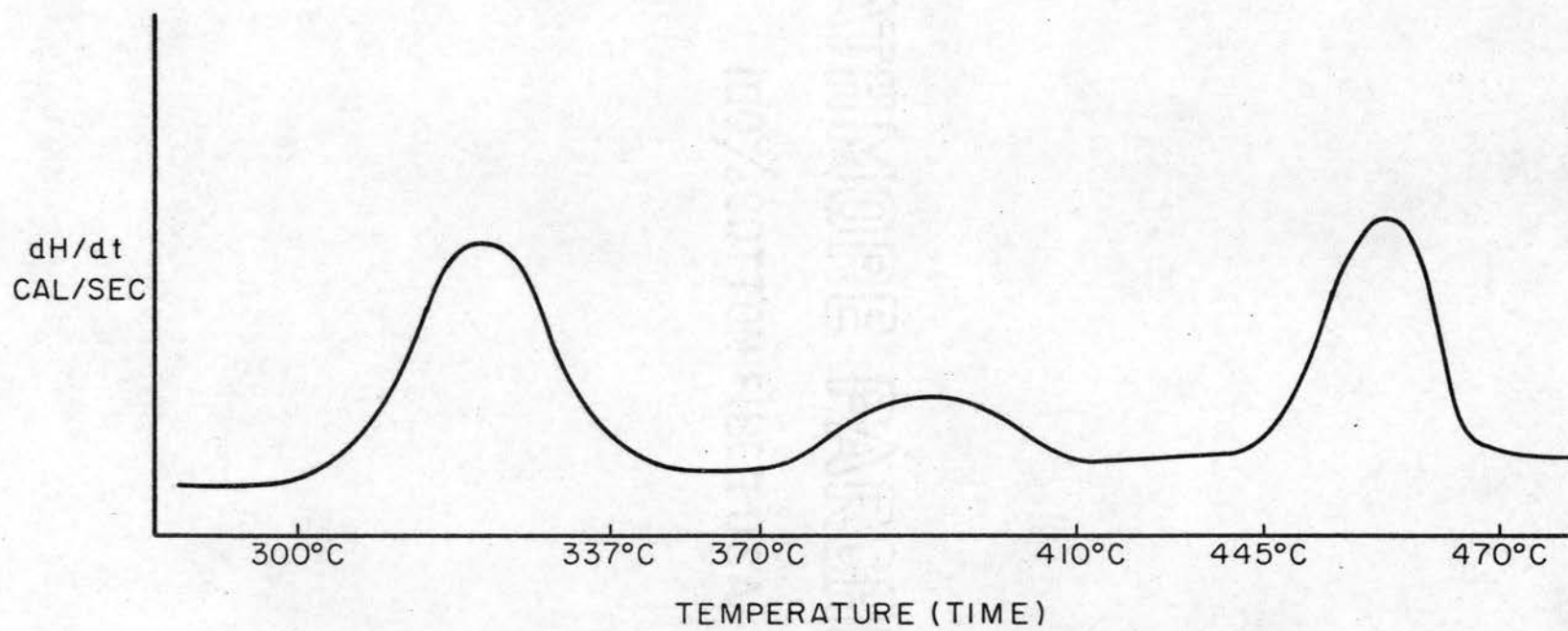
Figure 33. DSC Thermogram of Thermal Decomposition of Lead Carbonate

Grisafe and White (32) have extrapolated their equilibrium data at 100

bars to one bar for comparison purposes. Their extrapolations of log

P vs. 1/T curves indicate the enthalpy values for reactions one and

three of "Sequence C" to be about the same at 1 bar as at 100 bars; re-

action two, however, would have a higher enthalpy value at one bar than

at 100 bars. The values Peretti (36) reported are for reaction

"Sequence C" directly.

Comparisons are made in Table VIII. The enthalpy values from this

work compare quite favorably with the equilibrium values of Grisafe and

White (32); the higher temperature for the first reaction is due to the

dynamic nature of the DSC.

Decomposition Kinetics For Lead Carbonate

Studies of the kinetics of decomposition of lead carbonate have

been few in number, and limited to the initial decomposition reaction

(44, 48-50). The decomposition in one atmosphere of CO_2 was studied

by Bruzs (44) who found the activation energy to be 69.6 kcal/mole.

Kadlec and Dubinin (48) followed the decomposition in vacuum by weigh-

ing with time the carbon dioxide adsorbed on cooled charcoal, and ob-

tained an activation energy of 41.5 kcal/mole. Samal (49) studied the

decomposition in vacuum manometrically and found an activation energy

of 40.2 kcal/mole. Tuccarbasi (50) followed the rate of evolution of

gas in a nitrogen atmosphere, and obtained an activation energy of

11.5 kcal/mole.

With differential scanning calorimetry the decomposition kinetics

of all three peaks can be determined. The discussion in Chapter II on

obtaining kinetic data from DSC peaks was followed except that a more

TABLE VIII

DECOMPOSITION OF LEAD CARBONATE: COMPARISON OF ENTHALPY VALUES

Investigation	Number of Reaction in "Sequence C"					
	1		2		3	
	Reaction Temp, $^{\circ}$C	ΔH Kcal/mole	Reaction Temp, $^{\circ}$C	ΔH Kcal/mole	Reaction Temp, $^{\circ}$C	ΔH Kcal/mole
This Work	300	18.5	370	26.9	445	22.2
Peretti (36)	263	24.4	389	21.3	438	28.2
Centnerswer (41)	280	19.8	360	23.0	412	25.0
Grisafe (32)*	250	17.1	373	26.6	435	23.8

*These enthalpy values are at 100 bars CO_2. Grisafe's extrapolations of log P vs. 1/T indicate, however, that at one bar only the second enthalpy value would be appreciably changed, and it should be higher.

general rate equation was chosen to represent the data. The equation

has been used by Erofeev (51) to describe several decomposition re-

actions which involve an initial solid phase and a product solid phase.

The equation

$$\frac{dx}{dt} = kx^{\alpha}(1-x)^{\beta} \qquad\qquad (5\text{-}1)$$

has also been used by Lewis (52), with $\alpha = \beta = 1$, to describe the de-

composition of silver oxide. With $\alpha = 0$ equation (5-1) reduces to the

equation considered in Chapter II.

The data were treated as outlined in Chapter II, except that values

for both $\underline{\alpha}$ and $\underline{\beta}$ must be assumed before $\underline{k}$ at the end of each interval

can be calculated. The values of $\underline{\alpha}$ and $\underline{\beta}$ in the ranges, $0 \leq \alpha \leq 2$ and

$0 \leq \underline{\beta} \leq 2$, that resulted in the least scatter of the data about the

least-squares line were determined using the computer program given in

Appendix A. The program in Appendix A is written in Fortran IV for an

IBM 7040 computer.

Figure 34 presents the fraction of product $\underline{x}$ formed as a function

of temperature for the first decomposition peak. The data in the

intermediate region in Figure 34 were best represented by equation (5-1)

with $\underline{\alpha} = 0.4$ and $\underline{\beta} = 0.6$. For these values of $\underline{\alpha}$ and $\underline{\beta}$ an activation

energy of 67.2 kcal/mole was determined from the slope of the ln $\underline{k}$ vs.

$1/\underline{T}$ line, Figure 35. This value for the activation energy compares

quite well with 69.6 kcal/mole determined in CO_2 by Bruzs (44).

For the second peak, $\underline{x}$ as a function of temperature is given in

Figure 36. The best fit of equation (5-1) to the data resulted when

$\underline{\alpha} = 0.2$ and $\underline{\beta} = 1.6$. Figure 37 gives the graph of ln $\underline{k}$ vs. $1/\underline{T}$ for the

data, from which an activation energy of 73.4 kcal/mole was determined.
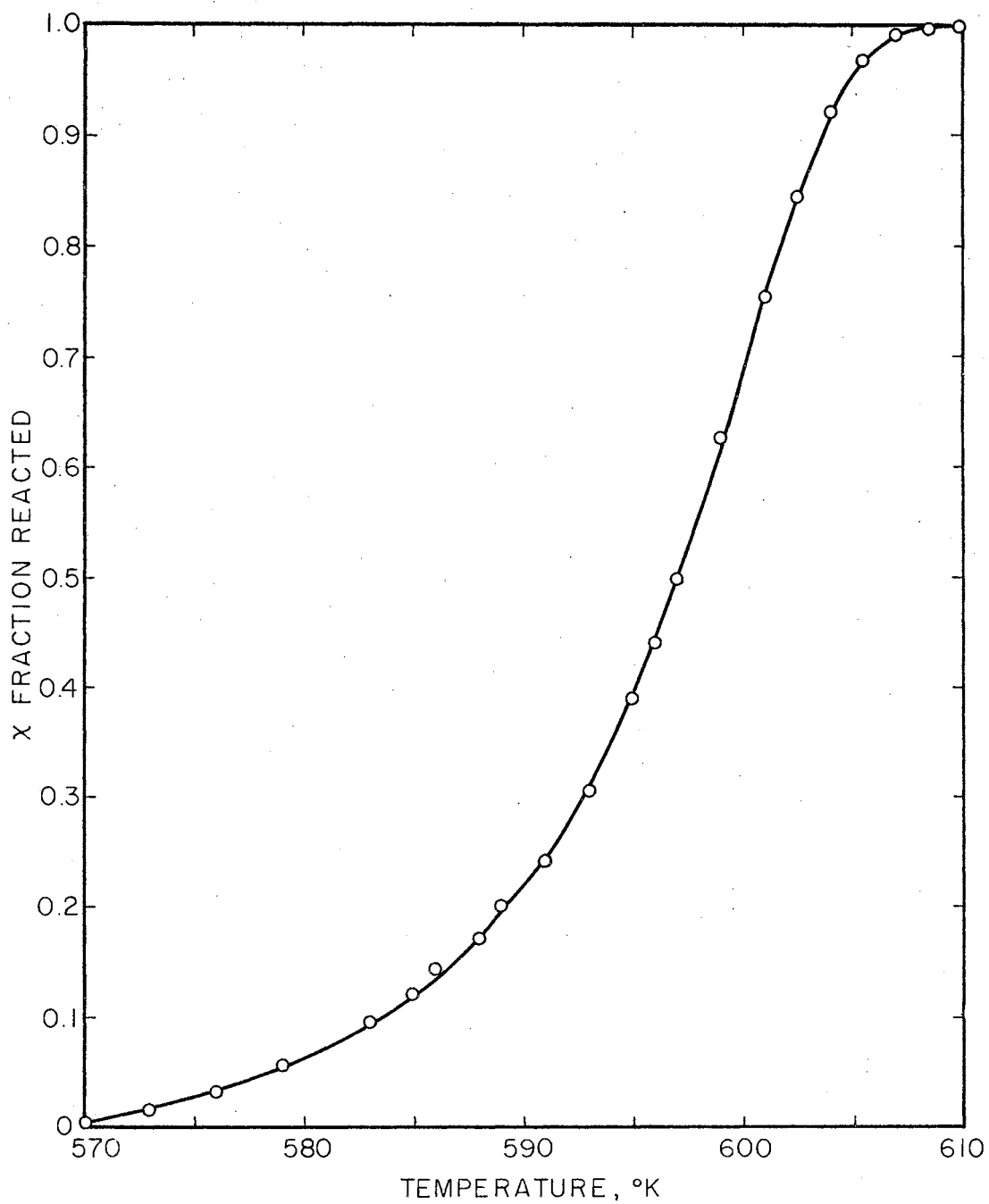
Figure 34. Lead Carbonate, First Peak. Fraction Reacted vs. Temperature
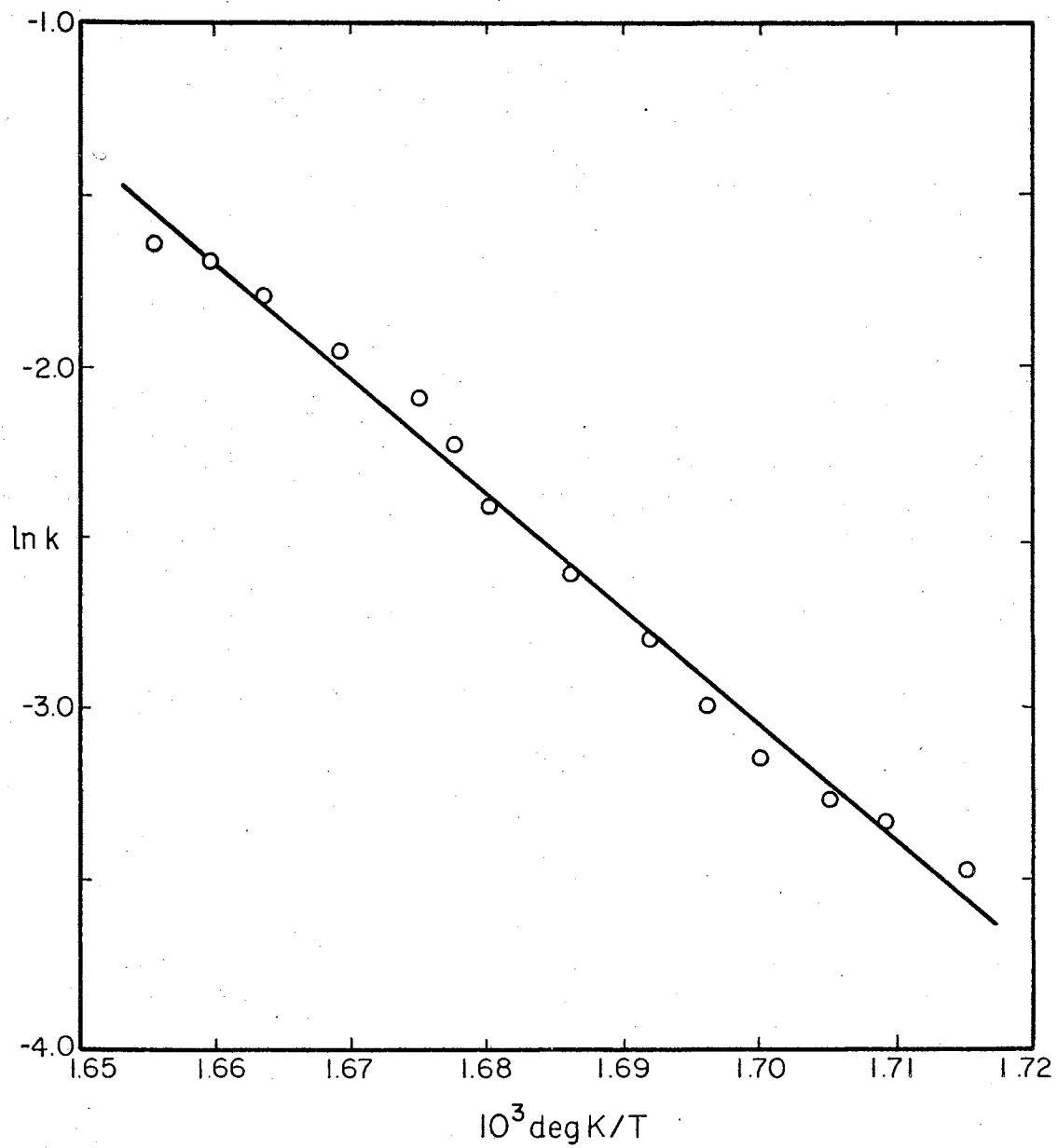
Figure 35.   Lead Carbonate, First Peak.   Arrhenius Activation
Energy Plot
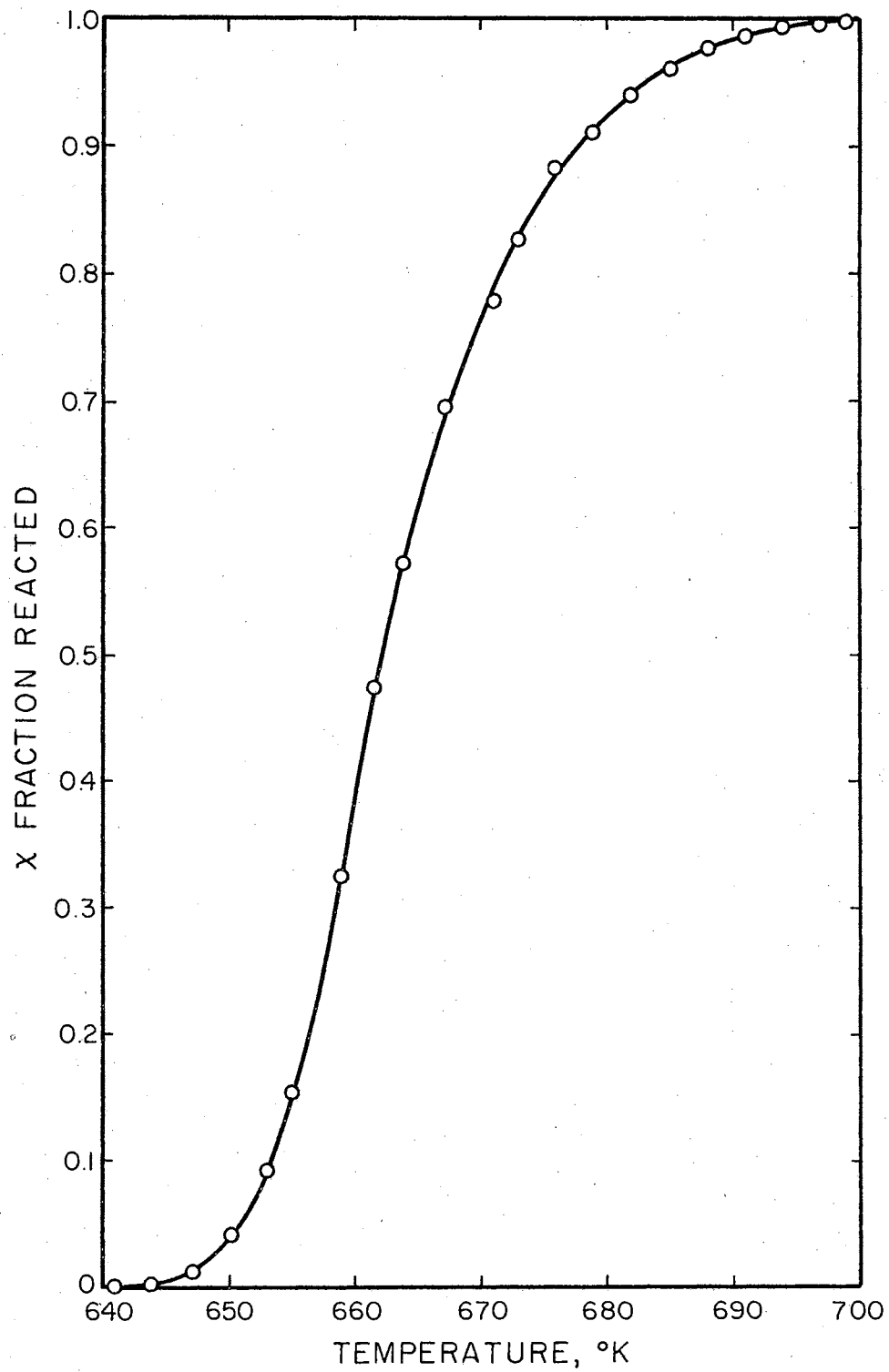
Figure 36. Lead Carbonate, Second Peak. Fraction
Reacted vs. Temperature
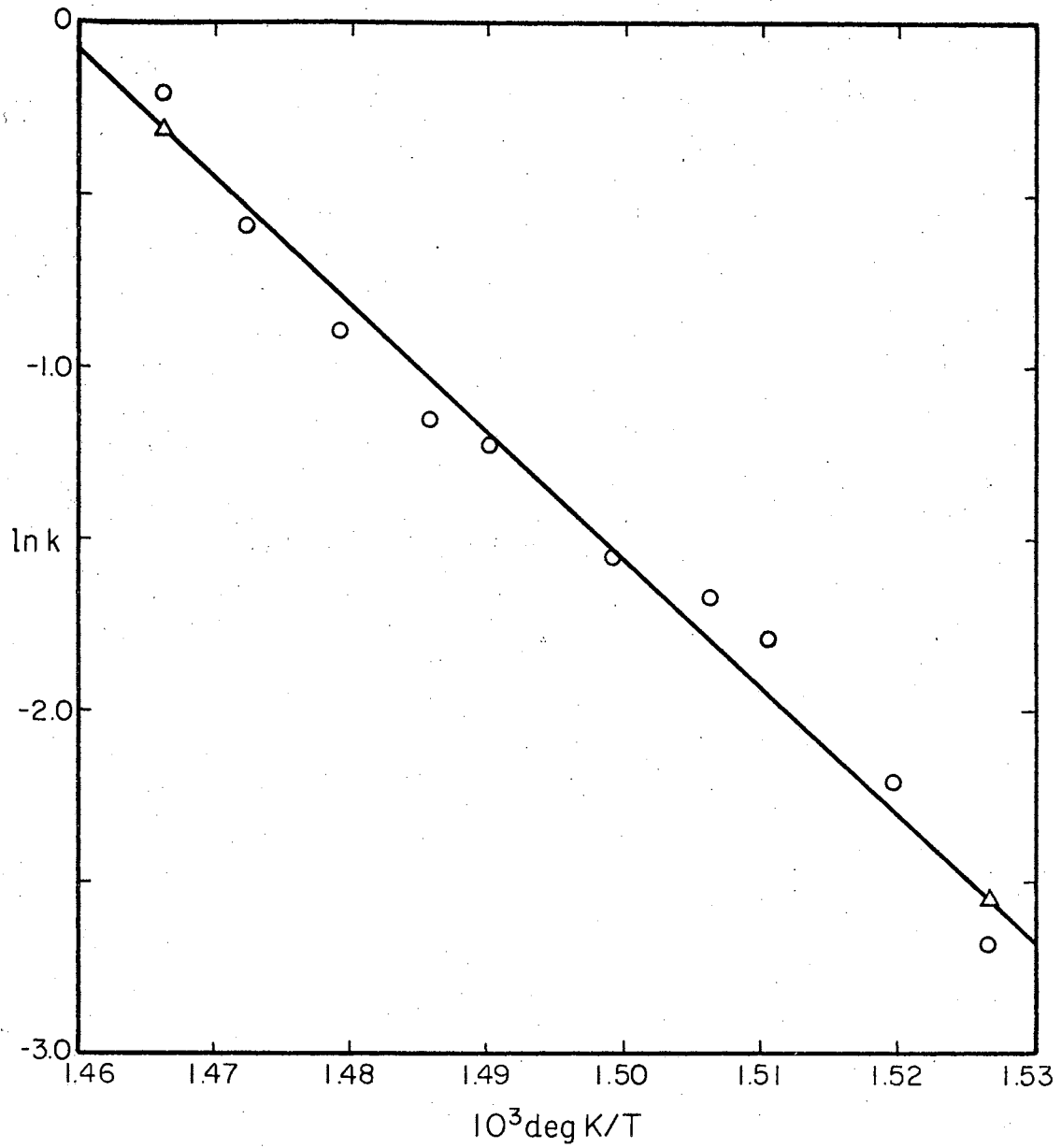
Figure 37. Lead Carbonate, Second Peak. Arrhenius Activation
Energy Plot

Data for the third peak are given in Figures 38 and 39. The best representation of the data was with $\underline{\alpha}$ = 0.6 and $\underline{\beta}$ = 1.0. The activation energy from the slope of the line in Figure 39 was found to be 79.4 kcal/mole.

These values for the activation energies are in reasonable agreement with those reported for the first peak of lead carbonate and the value of 80 kcal/mole suggested by Bruzs (44) to be characteristic of the carbonate ion in the crystal.

Decomposition Of Zinc Carbonate

The decomposition of zinc carbonate was studied in an atmosphere of carbon dioxide with a heating rate of 2 deg/min. Only one very sharp peak was found for this decomposition reaction. The average enthalpy for four determinations was 16.2 $\pm$ 0.7 kcal/mole at 541°K. Thus one can write

$$ZnCO_3 \longrightarrow ZnO + CO_2 \quad \Delta H_{541} = 16.2 \pm 0.7 \text{ kcal/mole}$$
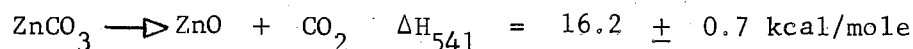
The observed enthalpy change may be compared with 17.1 kcal/mole obtained from enthalpies of formation and heat capacities (22, 53).

Decomposition Kinetics For Zinc Carbonate

All attempts to represent the data for the decomposition of zinc carbonate in carbon dioxide with equation (5-1) have been unsuccessful. The DSC peak is quite sharp, much like the peaks for the fusion of the metals. The reaction rate increases from essentially zero to maximum in such a small temperature interval, that the ln $\underline{k}$ vs. 1/$\underline{T}$ graph has an extremely large slope. The value of the activation energy calculated
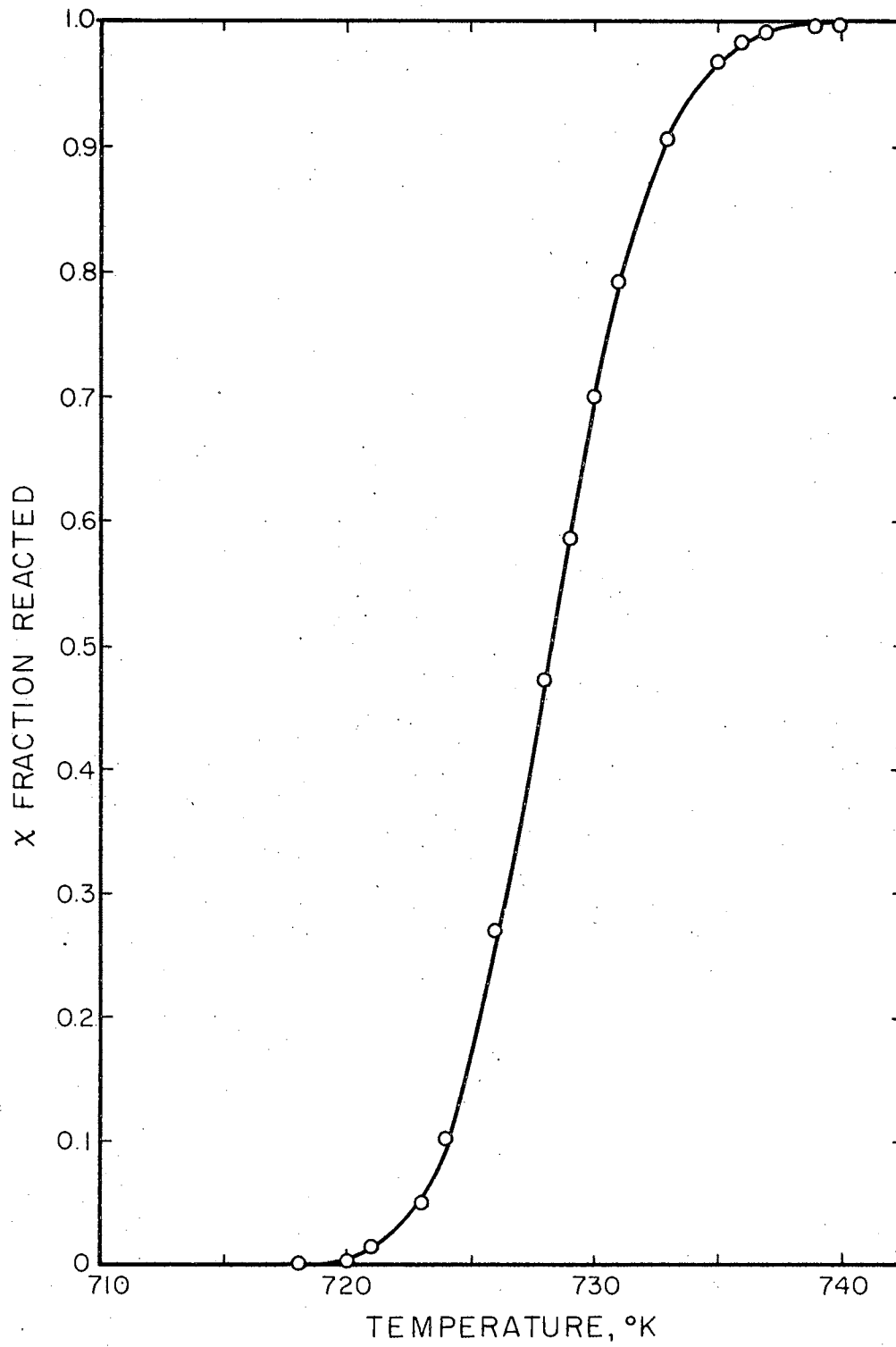
Figure 38. Lead Carbonate, Third Peak. Fraction
Reacted vs. Temperature
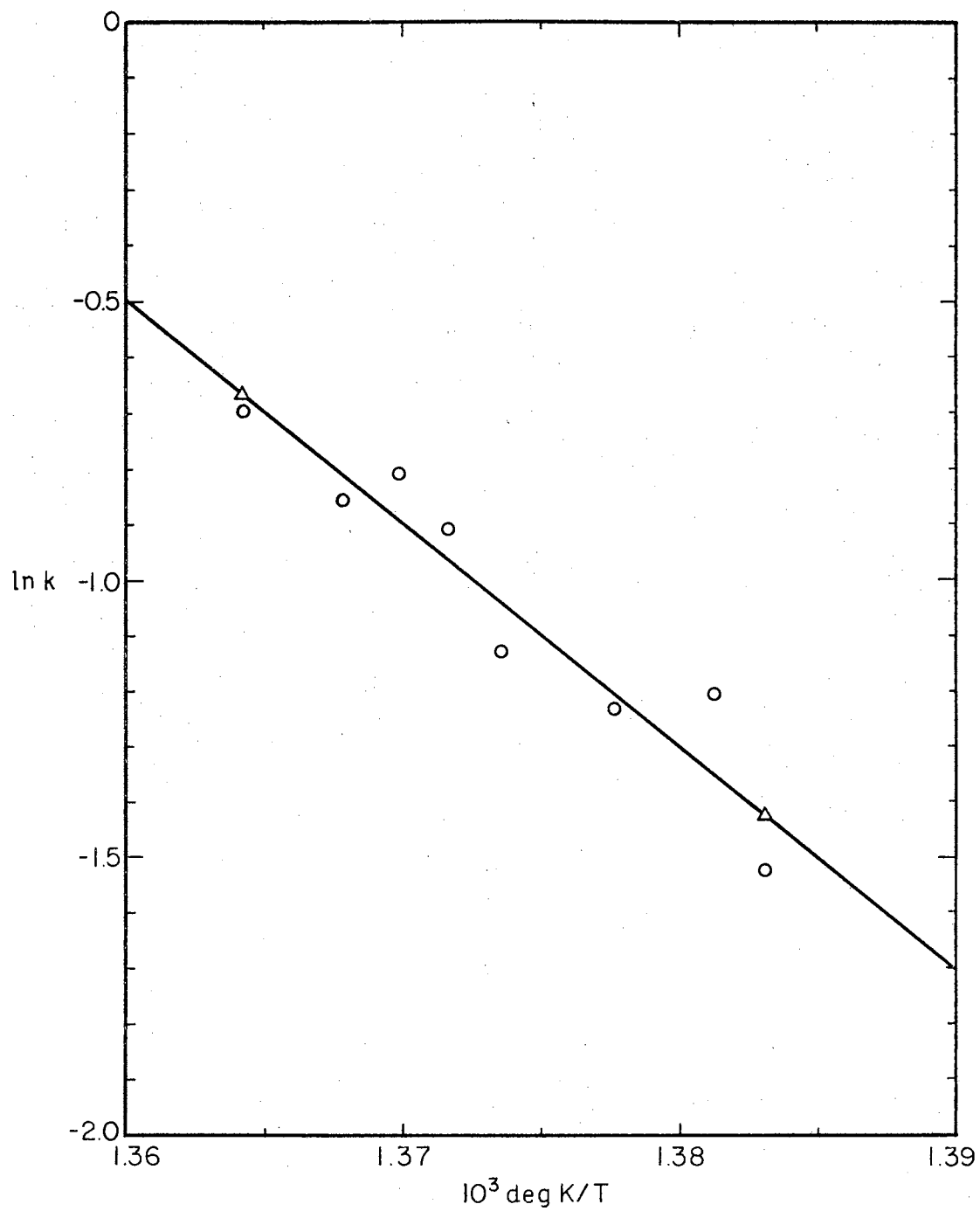
Figure 39. Lead Carbonate, Third Peak. Arrhenius Activation Energy Plot

from this slope is of the order 500-700 kcal/mole, which is completely
unreasonable.

Decomposition of Ammonium Chloride

The decomposition of ammonium chloride was studied because it de-
composes without the formation of a product solid phase. The solid-
solid transition that ammonium chloride undergoes at $186^{\circ}C$ could also be
studied for each decomposition reaction by starting the temperature scan
appreciably below $186^{\circ}C$.

Two decomposition determinations were performed in one atmosphere
of nitrogen; the observed enthalpy of decomposition was $\Delta H_{600^{\circ}K}$ =
29.2 ± 3 kcal/mole. This value is only 74 per cent of the accepted
value, $\Delta H_{600^{\circ}K} = 39.3$ kcal/mole (54). Part of the discrepancy may
be due to the formation between the decomposing particles and the sample
holder of a gas phase which would represent an energy transfer barrier
between the sample, thermocouple, and heater. The result would be a
change in the calibration, i.e., the "distance" between sample and
thermocouple would be increased and the measured energy input would be
lower than expected. Another difficulty was due to the nature of the
decomposition peak. The peak was quite broad making accurate inte-
gration of the area difficult. The broad peaks are quite different
from the DTA curves for the decomposition reported by Markowitz and
Boryta (55). The broad peaks may have been due to the small openings
in the sample holder which prevented the product gas from escaping. The
presence of the product gas would cause decomposition under near-
equilibrium conditions. The kinetics of decomposition (see below) also
indicate that the product gas escaped from the sample holder only with

difficulty.

The solid-solid transition for these two determinations occurred at $188^{\circ}C$, and the enthalpy change was $\Delta H_{Trans} = 982 \pm 14$ cal/mole. This may be compared with 944 cal/mole given in the JANAF Tables (54) and 940 cal/mole from the Bureau of Mines Bulletin 584 (22). Somewhat higher enthalpy values for this transition have been reported, however, e.g., Popov (56) 1059 $\pm$ 8 cal/mole, and Arell (57), 1073 cal/mole.

<div align="center">Kinetics Of Decomposition For Ammonium Chloride</div>

The rate data from the decomposition peak was treated as for lead carbonate; calculations with equation (5-1) were iterated with various values of α and β until the best representation of the data was obtained. The variation with temperature of the fraction reacted is given in Figure 40. The best fit of the data was with $\alpha = 0.2$ and $\beta = 0.2$; the value for the activation energy is 27.5 kcal/mole (Figure 41). It should be pointed out that for $\alpha = 0.2$ the rate of the reaction was dependent upon the reaction products to the same extent as the reactants, $\beta = 0.2$. This dependence of the rate on the product and the high value for the activation energy (the accepted value, in vacuum, is 13.5 kcal/mole) also indicate that decomposition occurred at near-equilibrium conditions (58). Both Chaiken (59) and Schultz (60) have observed that the rate of decomposition of ammonium chloride is much lower, at a given temperature, in an atmosphere than in vacuum. This remains true up to the temperature at which the decomposition pressure equals the external pressure, where the rates become identical with those determined in vacuum. The rate of the decomposition reaction at temperatures for which the decomposition pressure is less than atmospheric seems to
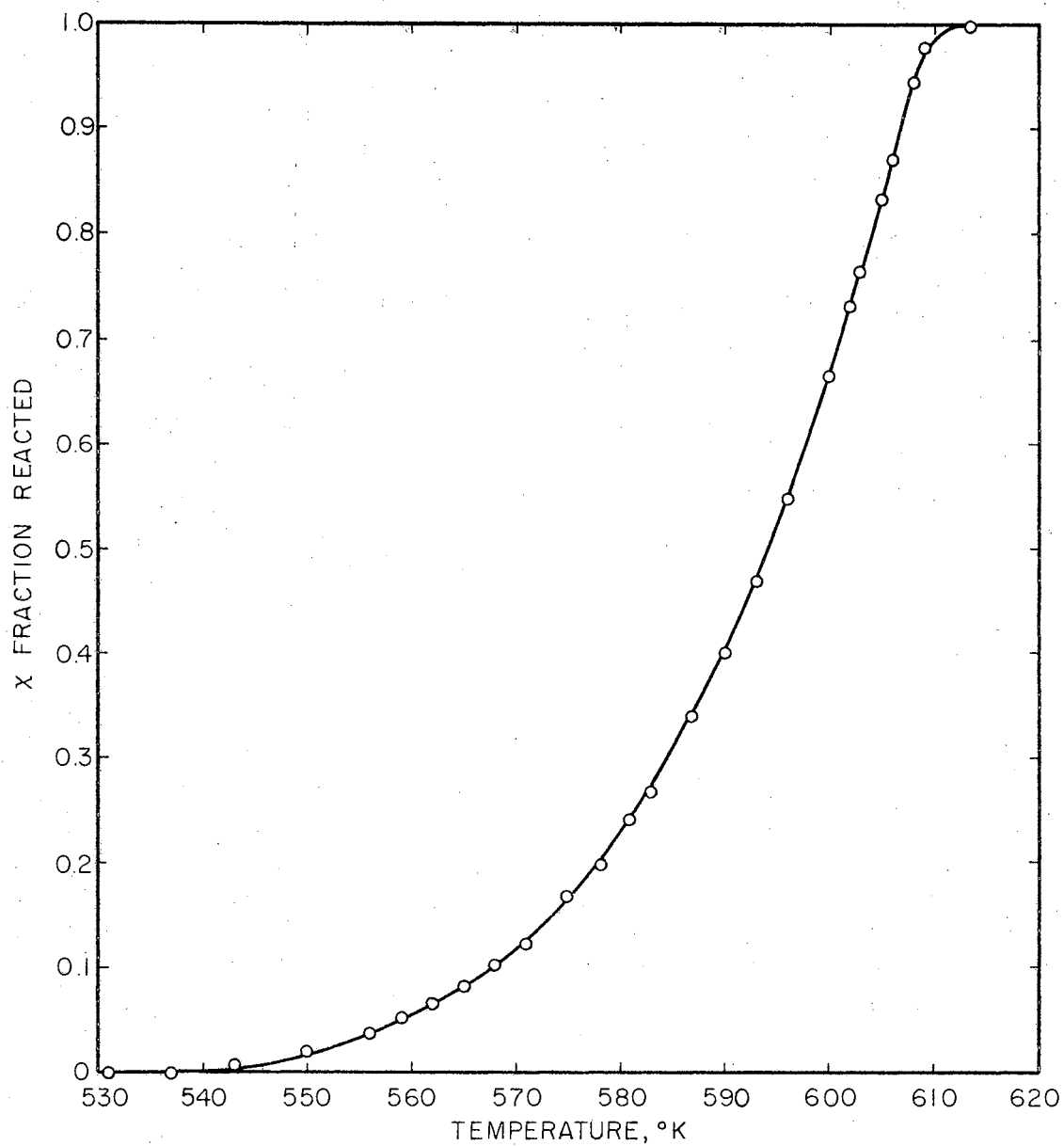
Figure 40. Ammonium Chloride. Fraction Reacted vs.
Temperature
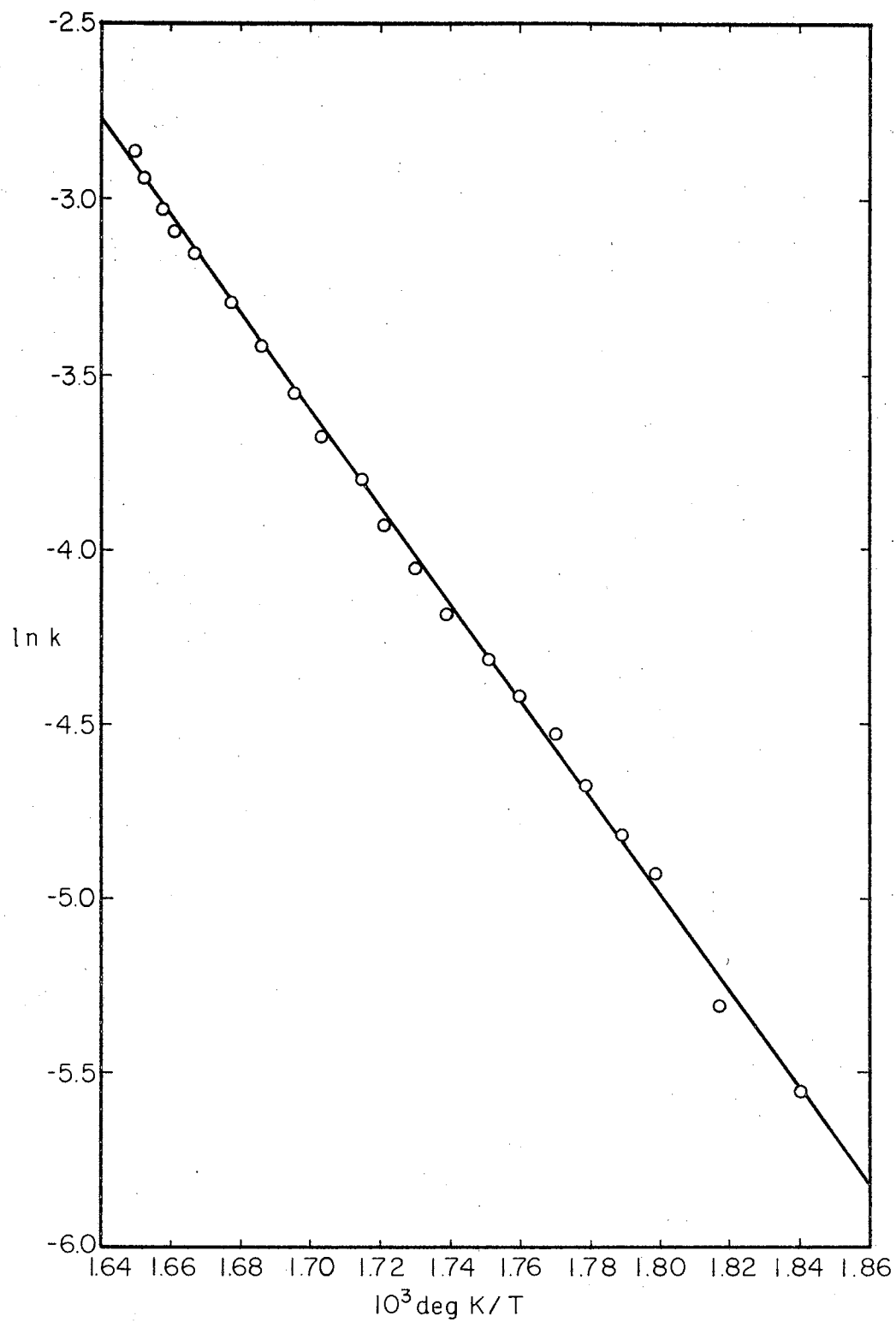
Figure 41. Ammonium Chloride. Arrhenius Activation
Energy Plot

be diffusion controlled. In these determinations the reaction was completed at about 335°C. Markowitz (55) reports the decomposition pressure to be one atmosphere at 338°C; thus the rate was diffusion controlled during the course of the entire reaction. Therefore, the higher value for the activation energy is to be expected and represents the activation energy for the diffusion process.

Disproportionation Of Zirconium Trichloride

Five determinations of the disproportionation of zirconium trichloride were attempted. Closed-nickel cells were used in four determinations to prevent the reaction of the trichloride with atmospheric moisture. One open-cell experiment was conducted in a dry box. The first two determinations were made with tantalum foil as a gasket for the cell shown in (d) Figure 24. The first run was heated at 2 deg/min to a maximum temperature of 566°C. The recorder trace had no excursions that would indicate the occurrence of a reaction. Examination of the cell showed that the gasket had failed, and that a white, low-density material had deposited around the outside of the gasket. The second run was made also with a tantalum gasket; however, the cell body was machined to give a sharper sealing surface, and greater torque was applied when sealing the cell. Nothing occurred on the thermogram between room temperature and 675°C that could possibly be attributed to a chemical reaction. Examination of the cell also showed the same white material around the gasket, which indicated that the seal had failed. The third experiment was performed with a platinum foil gasket, with essentially the same results: failure of the seal and the appearance of the white material, but no indication of any reaction up to 725°C.

A new cell was designed, (e) in Figure 24, which used a platinum foil gasket and an improved seal design. The fourth determination resulted in an endothermic drift in the recorder trace from about 185°C to 354°C. At 354°C the recorder trace returned to near zero, then remained essentially constant up to 730°C, about the maximum of the furnace. Examination of the cell indicated that the new seal performed quite satisfactorily. The contents of the cell were grey in color, and appeared to be stable to atmospheric moisture.

The absence of a thermal effect for the first three determinations may be attributed to hydrolysis of the trichloride. The hydrolysis of the trichloride could occur in the time required for temperature equilibration and instrument adjustment. Hydrolysis occurring prior to beginning a run would not cause an excursion of the recorder trace. Since the disproportionation reaction would not then occur, no excursions of the recorder trace would be noticed as the temperature of the calorimeter is increased. In the fourth determination there may have been a reaction, but it was very slow because of the pressure build-up in the sample holder. The total pressure in the sample holder at the elevated temperatures of an experiment could be as high as 4-8 atmospheres, more than enough to cause the reaction to proceed quite slowly. Even the most conservative integration of the slow endothermic drift from 185°C to 354°C, results in a value for the enthalpy change which is much too large.

One determination was performed in a dry box (Dew Point ~ -35°C) with an open cell, thus eliminating the effect of a pressure increase. The recorder trace was somewhat erratic, but no indication of a thermal effect that could be attributed to the disproportionation reaction.

Examination of the cell revealed the same white, low-density product, which was observed previously for those closed-cell determinations in which the seals failed. A much drier atmosphere (Dew Point ~ -50°C) appears to be necessary before the reaction could be conducted in an open cell without hydrolysis.

CHAPTER VI

ELECTRODYNAMOMETER MOMENTUM DETECTOR

The Electrodynamometer Momentum Detector was originally conceived
as a device with which to measure the momentum of a molecular beam.
Two types of studies were planned: (1) measurement of angular dis-
tribution of momentum in a beam emerging from a non-ideal orifice, as
a function of orifice parameters; and (2) measurement of beam momentum
coupled with weight-loss data for the Knudsen cell-source to give suf-
ficient data for evaluation of the average molecular weight of the
effusing species. The magnitude of the torques generated by a molecu-
lar beam of reasonable cross-sectional area is in the range 10^{-3} to
10^{-1} dyne cm. It was hoped that the Electrodynamometer would provide
a means for making the torque measurements with a precision of ± 0.10-
0.2% and an accuracy of ± 0.2-0.5%, independently of any torsion wire
calibration.

The Electrodynamometer Momentum Detector, Figure 42, consists of
a small movable coil suspended in the center of, and at right angles
with, a larger stationary coil. The small coil is attached to an
assembly which is clamped to the lower end of a fine torsion wire.
This assembly has a cubical mirror to indicate the position of the
movable coil. A cross arm with a target on one end and a counter-
balance on the other is also attached to the lower assembly. In an
experiment, the target would be placed in the beam of molecules

113
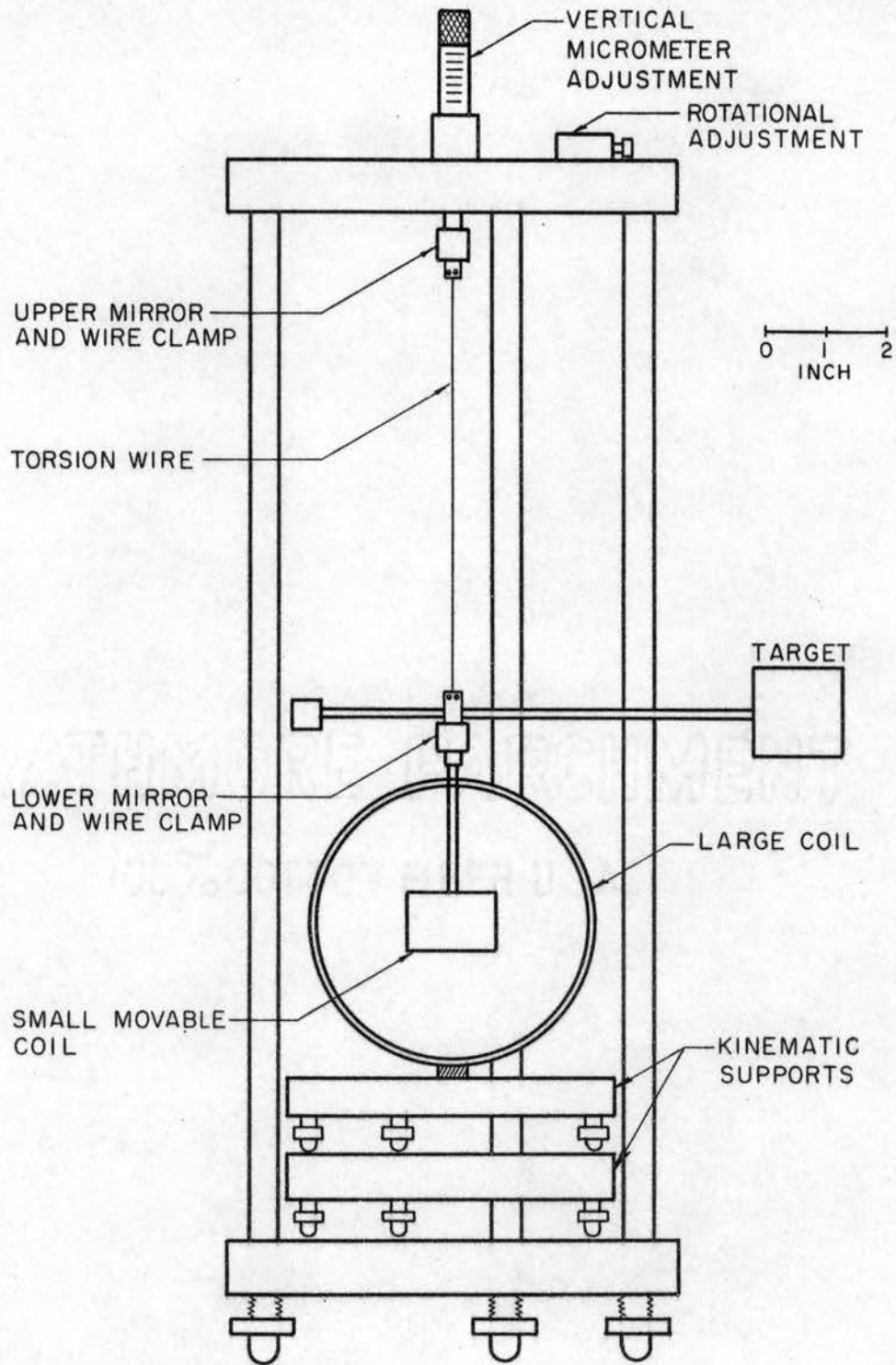
Figure 42. The Electrodynamometer

effusing from a Knudsen cell. The impact of molecules on the target would produce a torque which would cause rotation of the suspension. Passage of electrical currents through the large stationary coil and the small movable coil would generate a counter-torque which would return the target to its initial position. The force of the molecules striking the target could then be determined from the physical dimensions of the coils and target and from the currents through the coils. This force has been related to the pressure in the Knudsen cell by the equation (61).

$$F_{\theta} = (AP/2)(1 - \cos^3 \theta), \tag{1}$$

where

A - is the area of the orifice in the Knudsen cell

P - is the pressure of the substance in the Knudsen cell

θ - the half angle subtended by the target at the orifice.

The Electrodynamometer Momentum Detector provides data sufficient to calculate $\underline{F}_{\theta}$ in equation (1); since $\underline{A}$ and θ are readily measurable, $\underline{P}$ can be calculated.

The most frequently used technique for obtaining vapor pressures of substances at high temperatures is the Knudsen (62) effusion technique. In this technique a cell containing the sample is maintained at a constant temperature in high vacuum. The rate at which the sample effuses through the small orifice of the Knudsen cell is determined from the weight loss; the pressure $\underline{P}$ is then obtained from the Knudsen equation

$$P = \frac{g}{\omega a t} \sqrt{\frac{2\pi RT}{M}} \tag{2}$$

where

    g = weight lost by effusion from the cell

    a = area of the orifice

    t = effusion time

    ω = transmission probability to correct for orifice non-ideality

    R = gas constant

    T = absolute temperature of the cell

    M = molecular weight of the effusing substance.

All of these quantities are experimentally obtainable except the molecular weight of the effusing substance. To use this expression for vapor pressure determinations, one must obtain knowledge of the molecular weight from some other experiment or must assume a value. In many investigations the molecular weight, i.e., the identity of the effusing substance, is the primary interest. If the pressure $\underline{P}$ were known by some other independent measurement, the average molecular weight could be calculated from equation (2). This independent measurement of the vapor pressure of the substance under study can be made (cf. equation 1) with the Electrodynamometer Momentum Detector.

The Electrodynamometer used in this study is a 1/5 scale modification of the one used by Guthe (63) in a determination of the absolute ampere. The electrodynamometer has been constructed and described by Dawson (64).

Description of the Instrument

A detailed description of the design and construction of the electrodynamometer (EDM) has been given by Dawson (64) and also by

Freeman (65). The description of the EDM given here will be brief and will cover only that part of the design and construction necessary for the development that follows.

Both coils of the EDM are cylindrical with the ratio of the length of each coil to its radius being $\sqrt{3}$; both the large stationary coil and the small movable coil have a single layer of wire. When the two coils of an EDM have this particular configuration and their centers coincide, the expression for the torque, which in general is given by a series of terms, is simplified by the disappearance of all terms after the first and up to the seventh. The seventh and succeeding terms are usually extremely small if the suspended coil is small in comparison to the stationary coil (63).

If the axes of the two coils are perpendicular, the torque is expressed by

$$ T = \frac{2\pi^2 r^2 N_1 N_2 I_1 I_2}{C} = G I_1 A I_2 \tag{3} $$

in which r is the radius of the suspended coil, and N_1 and N_2 are the whole number of turns of wire on the fixed and suspended coils respectively. I_1 and I_2 are the currents, in electromagnetic units, passing through the fixed and suspended coils respectively; they may or may not be identically the same current (63). C is one-half the diagonal of the fixed coil, $\sqrt{a^2 + b^2}$; a is the radius of the fixed coil and $2b$, its length. $G = 2\pi N_1 / C$ is the magnetic force at the center of the stationary coil when unit current flows through it, and $A = \pi r^2 N_2$ is the sum of the areas of the several turns of the suspended coil.

Stationary Coil

The large coil was machined from a four-inch tube of Lucite, with a wall thickness of 0.25 inch, which had previously been cured at $100^{\circ}C$ for three hours. The form was threaded, 44 threads per inch, to allow the winding to be as even as possible. Windings on the coil consisted of 150 turns of 0.0221-inch diameter, "Nyclad"-insulated, copper magnet wire. Coil diameters were measured with a precision micrometer, which could be read accurately to 0.0001 inch. One thickness of wire was subtracted from the average outside diameter to give the pitch diameter. The pitch diameter was found to be 9.9931 ± 0.0010 cm.

The length of the coil was measured using a toolmakers' microscope which was accurate to ± 0.0001 inch. The average coil length is 8.6545 ± 0.0010 cm.

It was necessary to displace several windings on the large coil to allow suspension and alignment of the small movable coil. The movable coil was suspended by a fine wire which passed through a 0.125-inch hole in the top of the stationary coil. The hole was located in the exact center of the winding with the aid of a centering microscope, and its axis was coincident with a diameter of the coil. To facilitate alignment of the two coils with their axes perpendicular, two 0.062-inch holes were drilled in the stationary coil, one at each end of the diameter which passes through the center of the stationary coil and which is perpendicular to the axis of the opening for the suspension wire. The 0.062-inch holes were plugged with Lucite sighting tubes which had an internal diameter of 0.010 inch.

The constant $\underline{G}$ in equation (3) may be evaluated from the length

and pitch diameter of the large coil:

$$G = \frac{2\pi N_1}{C} = \frac{2\pi N_1}{\sqrt{a^2 + b^2}} = 142.58. \qquad (4)$$

The effect on $\underline{G}$ of displacing the windings of the coil was found to be negligible (<u>64</u>).

Movable Coil

The movable coil was machined from a one-inch Lucite rod, which had been cured at $100^{o}C$ for three hours. The small coil was also threaded, 44 threads per inch. The windings consisted of 30 turns of 0.0221-inch diameter, "Nyclad"-insulated, copper magnet wire. The pitch diameter and the length of the small coil were determined in the same manner as they were for the stationary coil and were found to be 1.9964 $\pm$ 0.0010 and 1.7287 $\pm$ 0.0010 cm, respectively.

The constant $\underline{A}$ in equation (3) is found to be

$$A = \pi r^2 N_2 = 93.91. \qquad (5)$$

The value for $\underline{G}$ from equation (4) and $\underline{A}$ from equation (5) can be substituted into equation (3); the result is

$$T = GI_1 AI_2 = 13,389 I_1 I_2 = 133.89 i_1 i_2$$

where $\underline{i}_1$ and $\underline{i}_2$ are the currents in amperes.

Suspension System

The stationary coil, Figure 42, is mounted on a brass plate which sits on a kinematic support, the superstructure of which carries a

micrometer screw for precise and reproducible adjustment of the verti-

cal position of the suspended coil, and a worm-gear device for precise

adjustment of the angular orientation of the axis of the suspended coil

in the horizontal plane. Leveling bulbs are incorporated in the plate

on which the large coil is mounted and in the superstructure.

The suspension wire is typically 21 cm in length and for most of

the measurements has been 0.00079-inch diameter tungsten wire.

Fourteen-karat gold ribbon, 0.0035 x 0.00026 inch, has also been used.

The wire is clamped between small brass plates; assembly of the wire

and mounting clamps, etc., is accomplished in a jig which permits

alignment within ±0.001 inch of the wire with the axis of its support.

A small cubical mirror is mounted on the upper suspension as-

sembly. This mirror allows the upper end of the suspension system to

be precisely positioned via the worm-gear device. The angles between

the faces of this mirror were measured by the method described by

Guthe (63); all four angles were found to be 90.00 ± 0.02 degrees. The

upper end of the torsion wire may be rotated through a known angle,

measured with the mirror and a telescope and scale; thereby introducing

a known torque in the wire. On the lower suspension assembly is also

mounted a small cubical mirror, which, with a telescope and scale,

allows one to follow the motion of the small coil as well as to es-

tablish a null position.

In the ends of both the movable and stationary coil were placed

plugs with 0.010-inch holes located precisely on the axis of the coil.

Alignment of the two coils with axes perpendicular and in the same

plane, was accomplished by sighting through the "side" holes in the

stationary coil with a telescope. The vertical position of the

suspended coil was adjusted with the micrometer until the far "side"
hole of the stationary coil could be seen while looking through the
"end" holes of the small coil. The worm-gear device was then adjusted
until the axis of the small coil was aligned with the "side" holes of
the stationary coil. Measurement on a spectrometer table indicated
that the angle between the longitudinal axis of the stationary coil,
defined by the end-plug holes, and a diameter, defined by the "side"
holes, is 90.00 $\pm$ 0.04 degrees.

Electrical Control Circuit

Supplying an electrical current to the small coil presented a
difficult problem, since the leads to the movable coil must hinder
its rotation as little as possible. Several lead arrangements have
been tried; the only successful one has been to connect electrically
the ends of the suspended coil to immediately adjacent binding posts
through two freely-suspended, catenary loops of 0.002 x 0.0002-inch
copper ribbon. Similar arrangements have been used at the National
Bureau of Standards in high precision current measuring devices (66).

The control circuit for the coil currents is shown schematically
in Figure 43. The output voltage of the transistorized voltage regu-
lator varies less than $\pm$0.1 per cent over a several-hour period; the
ripple voltage is 1 millivolt or less in the 12 volt output. Switches
S-1,2, and 3 are massive knife switches which reverse the direction of
current in the coils and connect the potentiometer to the appropriate
standard resistor.
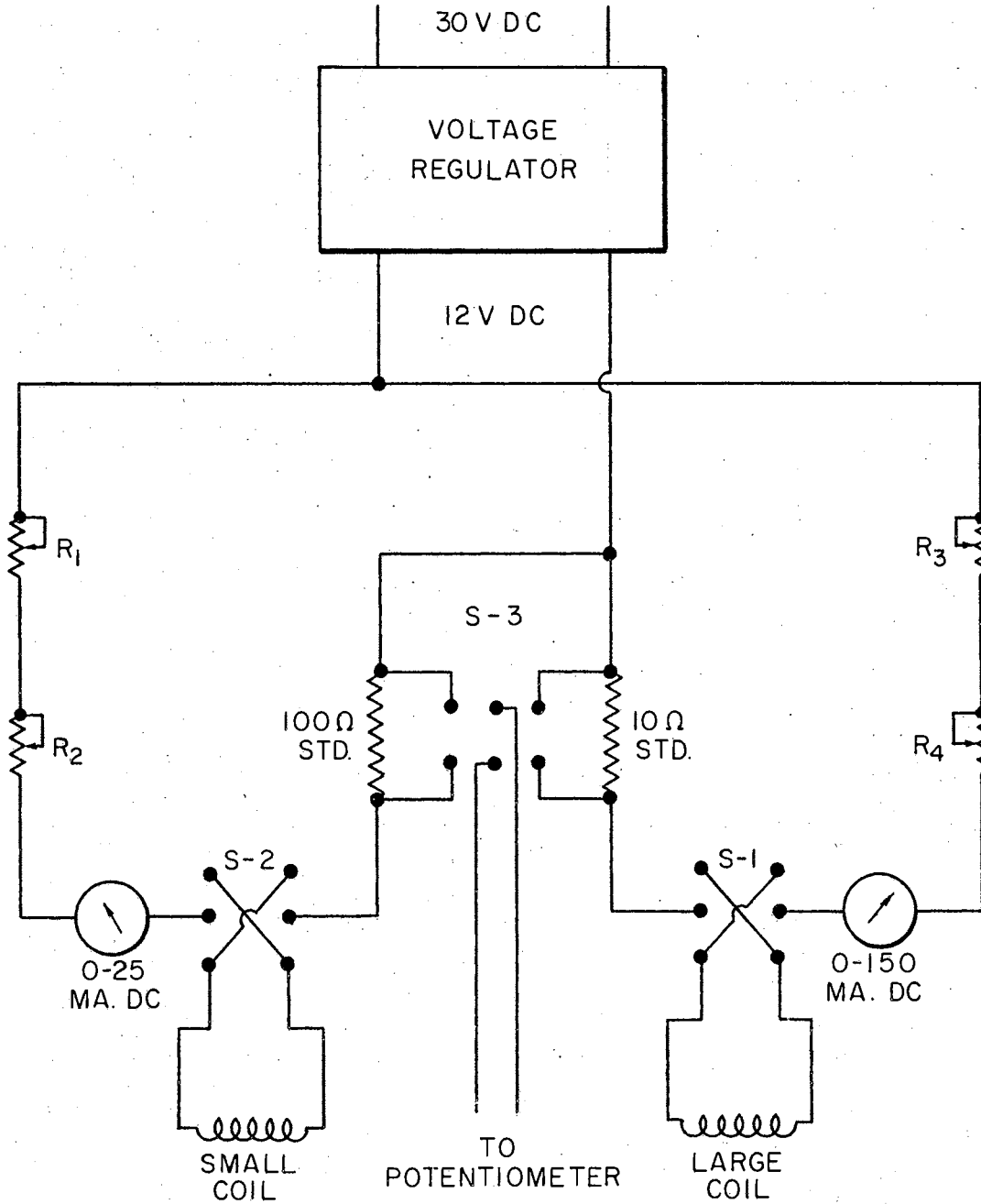
Figure 43. Electrodynamometer Control Circuit

Correction for Magnetic Fields
of the Earth and of Lead Wires (65)

In Guthe's (63) work the two coils were connected in series and
identically the same current passed through both. Early in our work
it became apparent that the current through the two coils have to be
controlled independently, because the currents required when the coils
are in series (typically 8 to 20 milliamperes) can produce ambiguous
results which arise from the comparable magnitude of the field of the
large coil and the earth's field, and which are eliminated if the
current in the fixed coil is sufficient to make the field of the fixed
coil larger than the earth's field by a factor of at least 5.

For convenience equation (3) is written

$$T = GI_1AI_2 = giai' = Kii' \tag{6}$$

with $\underline{G} = (2\pi\underline{N}_1/\underline{C}) = 10\underline{g}$; $\underline{A} = \pi\underline{r}^2\underline{N}_2 = 10\underline{a}$; $\underline{K} = \underline{ga}$; $\underline{I}_1$ and $\underline{I}_2$ are in
electromagnetic cgs units; and $\underline{i}$ and $\underline{i}'$ are in amperes. The field
strength $\underline{H}$ at the center of the large coil is $\underline{H} = \underline{G}\,\underline{I}_1 = \underline{gi}$. The local
horizontal component of the earth's field is represented by $\underline{H}_e$; the
effective horizontal component in (oersted/10) units for combination
with currents expressed in amperes is $\underline{h}_e$, and $\underline{h}_e = (\underline{H}_e \sin \theta)/10$,
with θ designating the angle between $\underline{H}_e$ and the axis of the suspended
coil. The direction of $\underline{h}_e$ is chosen as positive; $\underline{H}$ may be parallel
(+) or antiparallel(−) to $\underline{h}_e$. The four possible combinations of flow
of current in the coils are designated by $j = 1,2,3,$ and 4; the posi-
tive direction of flow is arbitrarily chosen so that with both $\underline{i}_j$ and
$\underline{i}'_j$ positive, $\underline{H}$ is positive and the resultant torque $\underline{T}_j$ is positive,
i.e., upward by the right-hand rule. Table IX gives these various

relations in detail.

Table IX

RELATIONSHIPS FOR THE FOUR POSSIBLE
COMBINATIONS OF CURRENT FLOW

Direction* of Current, j	i_j	i'_j	H	T_j	Relative Magnitude of i'_j for Fixed T and i_j
1	+	+	+	+	low
2	-	-	-	+	high
3	+	-	+	-	low
4	-	+	-	-	high

*Corresponds to the four possible combinations of positions of the reversing switches S-1 and S-2 of Figure 43.

Suppose that a negative torque is produced on the suspended coil by rotation of the upper end of the torsion wire and that this torque is exactly counterbalanced by a positive torque T_1 produced by coil currents for $j = 1$, i.e., i_1 and i'_1. If the currents are now reversed, $j = 2$, and the (same) negative torque again counterbalanced by positive torque T_2, the currents required, i_2 and i'_2, will be appreciably different from i_1 and i'_1. This difference may be attributed to the reversal of H with respect to the earth's field. Fields surrounding lead wires to the coil cannot contribute to this difference since the effect of these fields is the same in both magnitude and direction for $j = 1$ and $j = 2$. A similar argument is valid for the difference in currents, at constant torque, for $j = 3$ and $j = 4$. However, the currents measured for $j = 1$ and $j = 3$ differ in magnitude as well as

direction, not because of the influence of the earth's field which is the same for both, but because any contribution to the torque from fields around lead wires is reversed in direction when the current in only one coil is reversed. This is also the case for $j = 2$ and $j = 4$. The contribution to the torque by lead wires is proportional to the product of the currents in the two coils and may be expressed as $\pm \delta i_j i'_j$; δ is the unknown, and hopefully small, positive proportionally constant.

Equations may now be written which describe the equilibrium counterbalance situations discussed above and which explicitly describe the contribution from the earth's field and the lead wires,

$$T_j = K i_j i'_j \pm \delta i_j i'_j + h_e a i'_j \qquad (7)$$

the negative sign being appropriate for $j = 3$ and $j = 4$ only. If equation (7) for $j = 1$ is multiplied by $-i'_2$, and that for $j = 2$ by i'_1, the resulting equations added and solved for $T_{12} = T_1 = T_2$, one obtains

$$T_{12} = (K+\delta) i^2_{12} = (K+\delta) i'_1 i'_2 (i_2 - i_1)/(i'_1 - i'_2). \qquad (8)$$

Similarly, from equation (7) for $j = 3$ and $j = 4$, one obtains

$$T_{34} = (K-\delta) i^2_{34} = (K-\delta) i'_3 i'_4 (i_3 - i_4)/(i'_4 - i'_3). \qquad (9)$$

It should be noted that this procedure has produced equations, (8) and (9), in which the contribution from the earth's field does not appear.

Equations (8) and (9) may be combined in two ways to eliminate the contribution δ from the lead wires. First, if equations (8) and (9) are multiplied, and T_{12} and $-T_{34}$ $(=T_{12})$ are replaced by T_x, one

may obtain

$$T_x = K(1-\delta^2/K^2)^{\frac{1}{2}}(-i_{12}^2 i_{34}^2)^{1/2} . \tag{10}$$

Guthe (63) reported that δ/K = 1/12000 for his apparatus; hence, the factor $(1-\delta^2/K^2)^{1/2}$ contributed about 1 part in 3 x 10^8 and was dropped. Even if δ/K were as large as 1/10, the error introduced by omitting the factor $(1-\delta^2/K^2)^{1/2}$ would be no greater than 0.5 per cent; accordingly, this factor may be dropped and we have

$$T_x' = K(-i_{12}^2 i_{34}^2)^{1/2} . \tag{11}$$

Second, the contribution δ can be _eliminated_, rather than incorporated into a presumably negligible term, by multiplying equation (8) by i_{34}^2, equation (9) by i_{12}^2, and adding the resulting equations to obtain

$$T_z = T_{12} = -T_{34} = 2Ki_{12}^2 i_{34}^2/(i_{34}^2 - i_{12}^2) . \tag{12}$$

A convenient check on the self-consistency of data resulting from the various directions of current flow may be obtained by equating equation (7) with j = 1 to (7) with j = 2 (T_1 and T_2 are required to be identical), from which one may obtain

$$\frac{h_e}{g} = (1+\delta/K)(i_2 i_2' - i_1 i_1')/(i_1' - i_2') . \tag{13}$$

Since h_e and g are constants determined by the earth's field and by the geometry and orientation of the fixed coil, the ratio h_e/g is an apparatus constant and the right side of equation (13) should be a constant regardless of individual values of i_j and i_j' or of the

value of the torque being measured. The constant $\underline{h}_e/g$ is designated by $\underline{\rho}$, and

$$\rho_{12} = (1+\delta/K)(i_2 i_2' - i_1 i_1')/(i_1' - i_2') = (1+\delta/K)R_{12} . \qquad (14)$$

An analogous equation may be obtained from equation (7) for $j = 3$ and $j = 4$:

$$\rho_{34} = (1-\delta/K)(i_3 i_3' - i_4 i_4')/(i_4' - i_3') = (1-\delta/K)R_{34} . \qquad (15)$$

It is convenient to write and use equations (8) through (15) in a form which considers only the magnitude of the torque and the currents; this transformation is easily made with use of Table IX and yields;

$$T_{12} = (K+\delta)i_{12}^2 \equiv (K+\delta)i_1' i_2'(i_1+i_2)/(i_1'+i_2') \qquad (16)$$

$$T_{34} = (K-\delta)i_{34}^2 \equiv (K-\delta)i_3' i_4'(i_3+i_4)/(i_3'+i_4') \qquad (17)$$

$$T_x = K(1-\delta^2/K^2)^{1/2}(i_{12}^2 i_{34}^2)^{1/2} \equiv K(1-\delta^2/K^2)^{1/}i_x^2 \qquad (18)$$

$$T_x' = K(i_{12}^2 i_{34}^2)^{1/2} \equiv Ki_x^2 \qquad (19)$$

$$i_x^2 \equiv (i_{12}^2 i_{34}^2)^{1/2} = i_1' i_2' i_3' i_4'(i_1+i_2)(i_3+i_4)/(i_1'+i_2')(i_3'+i_4') \qquad (20)$$

$$T_z = 2Ki_{12}^2 i_{34}^2/(i_{12}^2+i_{34}^2) \equiv Ki_z^2 \qquad (21)$$

$$\rho_{12} = (1+\delta/K)(i_2 i_2' - i_1 i_1')/(i_1'+i_2') \equiv (1+\delta/K)R_{12} \qquad (22)$$

$$\rho_{34} = (1-\delta/K)(i_4 i_4' - i_3 i_3')/(i_3'+i_4') \equiv (1-\delta/K)R_{34} \qquad (23)$$

From equations (18) and (21), if $\underline{T}_x = \underline{T}_z$, we have

$$(\delta/K)^2 = 1 - (i_z^2/i_x^2)^2 \tag{24}$$

and from equations (21) and (22), if $\underline{\rho}_{12}$ and $\underline{\rho}_{34}$ are required to be equal, as they theoretically should,

$$\delta/K = (R_{34} - R_{12})/(R_{12} + R_{34}) . \tag{25}$$

Torque Comparison Measurements

To check the combined accuracy of construction of the coils and of alignment procedures, the torque produced by rotation through $\pi/2$ radians of a calibrated suspension wire was measured with the electro-dynamometer. After the coils had been aligned and the suspension calibrated as described below, the upper end of the torsion wire was rotated through $90.00 \pm 0.02^{\circ}$, as measured by the upper cubical mirror; the resulting torque on the small coil was exactly counterbalanced by the torque produced by currents through the two coils. The currents were measured by standard resistors and potentiometer as indicated in Figure 43. The currents were then reversed, the torque again counterbalanced, and the currents measured. These two sets of measurements are for directions $j = 1$ and $j = 2$. The upper end of the torsion wire was then rotated back through the null position, which was checked for constancy, to a position $-90.00 \pm 0.02^{\circ}$ from null so as to produce on the small coil a torque equal in magnitude but opposite in direction to that produced by the initial rotation. This torque was then counterbalanced by currents flowing in the two possible directions, $j = 3$ and $j = 4$.

The torsion constant, $\underline{D}$, of a wire can be obtained by measuring the period of oscillation, $\underline{t}$, when a mass of known moment of inertia, $\underline{I}$, is suspended by the wire: $\underline{D} = 4\pi^2\underline{I}/\underline{t}^2$. In the electrodynamometer suspension system, the lower wire clamps and mirror assembly remain in place for both calibration and measurement, and represent a moment of inertia, $\underline{I}_x$, which is difficult to calculate precisely. This difficulty is eliminated by measuring the periods of oscillation, $\underline{t}_a$ and $\underline{t}_b$, when masses with moments of inertia $\underline{I}_a$ and $\underline{I}_b$ are suspended; the torsion constant is then obtained by combining equations

$$D = 4\pi^2(I_i + I_x)/t_i^2 \; ; \; i = a,b$$

to obtain

$$D = 4\pi^2(I_a - I_b)/(t_a^2 - t_b^2) \; . \tag{26}$$

Determination of a period of oscillation is typically accomplished by timing ten periods with an electronic scaler set to count the pulses of 60 Hz line current or with a suitable electric stop clock.

The first torque comparison measurements, Series A, were made with wire No. 1, 0.00079-inch tungsten. This wire was taken directly from the spool and used without further treatment. The torsion constant of wire No. 1 was determined by using the three cylinders indicated in Table X. The value of the torsion constant calculated from the data for cylinders 3 and 5 is high and given zero weight because the periods are so nearly the same that the denominator of (26) is imprecisely determined. Cylinder No. 1 was machined to have a moment of inertia and a period appreciably different from that of cylinders 3 and 5. The

TABLE X

TORQUE COMPARISON MEASUREMENTS SERIES A DETERMINATION
OF TORSION CONSTANT
WIRE NO. 1

<u>A</u>

PERIODS OF OSCILLATION

Cylinder No.	I g cm^2	No. of Sets of 10 Periods Measured	Period, t sec
1	2.7561	6	$32.61^{+}_{-}0.01$
3	5.8460	6	$46.77^{+}_{-}0.01$
5	7.1859	6	$51.66^{+}_{-}0.01$

<u>B</u>

TORSION CONSTANT FOR VARIOUS PAIRS OF CYLINDERS

Cylinder a	Cylinder b	Torsion Constant D dyne-cm/radian
1	3	0.1085
1	5	0.1089
3	5	(0.1099)
	Selected average	$0.1087^{+}_{-}0.0002$

torsion constant for wire No. 1 was taken as 0.1087 dyne cm/radian.

Table XI gives the currents which were necessary to counterbalance the torque produced by rotation of wire No. 1 through $\pm\pi/2$ radians. From these data $\underline{R}_{12}$ and $\underline{R}_{34}$, equations (22) and (23) were calculated; from them $\underline{\delta}/\underline{K}$ was calculated by equation (24). This method of calculating $\underline{\delta}/\underline{K}$ assumes the $\underline{\rho}_{12} = \underline{\rho}_{34}$ for a given set of measurements; therefore, the agreement between values of $\underline{\rho}_{12}$ and $\underline{\rho}_{34}$ for each measurement, Table XII, is expected and redundant. However, these quantities should have constant value for each set of measurements. As Table XII shows, the values of $\underline{\rho}_{12} = \underline{\rho}_{34}$ are indeed constant within ±0.2 per cent for the five measurements.

Table XII also gives the values for the torque produced by interaction of the coils and calculated from equations (18), (19), and (21). The values of $\underline{T}_x$ and $\underline{T}'_x$ are essentially identical, which demonstrates the validity of the simplifying assumption used in obtaining equation (19). This is also evident from the smallness of $\underline{\delta}/\underline{K}$. The torque $\underline{T}_w$ calculated from the torsion constant of the wire is $(0.1087)(1.5708) =$ 0.1707 dyne cm, which is 1.2% greater than that calculated from the coil currents.

In an effort to determine the cause of the discrepancy between the measured torques $\underline{T}_w$ and $\underline{T}_z$, the electrical circuit and the torsion wire calibration procedure were carefully checked. The standard resistors in the coil circuits, Figure 43, were compared with another standard, 10.000 ± 0.001 ohm at 25°C. The 10-ohm resistor was $\pm0.04\%$, and the 100-ohm resistor $\pm0.06\%$ from their nominal values. The potentiometer standard cell was compared with an auxiliary cell and found to be 0.05% low. Since none of these errors could account for the

TABLE XI

TORQUE COMPARISON MEASUREMENTS SERIES A
CURRENTS THROUGH ELECTRODYNAMOMETER
COILS TO COUNTERBALANCE TORQUE
OF $(0.1087\pi/2)$ DYNE CM
WIRE NO. 1

| Expt. No. | Coil Current | Milliamperes | | | |
| | | Current Direction, j | | | |
		1	2	3	4
I	i	101.41	101.37	101.39	101.34
	i'	11.276	14.038	11.151	13.902
II	i	101.37	101.34	101.38	101.36
	i'	11.276	14.038	11.070	13.794
III	i	101.29	101.27	101.26	101.24
	i'	11.315	14.096	11.112	13.838
IV	i	101.22	101.18	101.25	101.22
	i'	11.391	14.194	11.086	13.821
V	i	101.19	101.18	101.22	101.20
	i'	11.392	14.191	11.096	13.844

TABLE XII

TORQUE COMPARISON MEASUREMENTS SERIES A
TORQUE PRODUCED BY ELECTRODYNAMOMETER*
WITH CURRENTS GIVEN BY TABLE XI
WIRE NO. 1

| Expt. | δ/K | milliampere | | $(\text{milliampere})^2$ | | Torque, dyne cm | | |
		ρ_{12}	ρ_{34}	i_x^2	i_z^2	T_x'	T_x	T_z
I	0.0041	11.05	11.07	1261.21	1261.19	0.16886	0.16886	0.16886
II	0.0027	11.07	11.07	1256.28	1256.24	0.16820	0.16820	0.16820
III	0.0010	11.08	11.04	1259.66	1259.60	0.16866	0.16865	0.16865
IV	0.0001	11.10	11.10	1262.18	1262.07	0.16899	0.16899	0.16898
V	0.0032	11.11	11.10	1262.65	1262.55	0.16906	0.16905	0.16904
Average	0.0022	11.08	11.08			0.16875	0.16875	0.16875

*Torque from torsion constant: $T_w = 0.1087\pi/2 = 0.1707$ dyne cm.

differences in the measured torques, attention was directed to the wire calibration.

The three masses used in the calibration of wire No. 1 were weighed and their moments of inertia recalculated. No important differences were found in the moments of inertia of these masses. Two new masses were machined and their moments of inertia determined. With periods for these five masses, ten values for the torsion constant may be calculated; the average should represent an improved value for $\underline{D}$.

The second torque comparison measurement, Series B, was made with wire No. 2, also taken directly from the spool and used without further treatment. Table XIII gives the data from the calibration of wire No. 2. If the values for $\underline{D}$ from cylinder pairs (2,1), (4,3), and (5,4) are rejected on the basis of similarities in their periods and moments of inertia, the selected average torsion constant for wire No. 2 is 0.1052 dyne cm/radian.

The electrodynamometer was leveled, the coils aligned, and the torque comparison measurements made exactly as in the first comparison. Table XIV indicates the values of the currents in the large and small coils necessary to counterbalance the torque produced by rotation of the torsion wire through $\pm 90.00 \pm 0.02$ degrees. The values for the torque, Table XV, calculated from the currents through the coils in this set of measurements is 0.9% above the value for the torque, 0.1652 dyne cm, from the torsion constant.

The improvement in the agreement between torques $\underline{T}_z$ and $\underline{T}_w$ from Series A to Series B indicated that the calibration of the torsion wire was the area in which improvements could be made. A third wire was mounted in the electrodynamometer, and the aluminum cylinder with

TABLE XIII

TORQUE COMPARISON MEASUREMENTS SERIES B
DETERMINATION OF TORSION CONSTANT
WIRE NO. 2

A

PERIODS OF OSCILLATION

Cylinder No.	I g cm^2	No. of sets of 10 Periods Measured	Period, t sec
1	2.7561	6	33.10±0.01
2	3.1899	6	35.41±0.01
3	5.8460	6	47.43±0.01
4	7.0645	6	52.12±0.02
5	7.1859	6	52.46±0.02

B

TORSION CONSTANT FOR VARIOUS PAIRS OF CYLINDERS

Cylinder a	Cylinder b	Torsion Constant D dyne cm/radian
2	1	(0.1082)
3	1	0.1057
4	1	0.1049
5	1	0.1056
3	2	0.1053
4	2	0.1046
5	2	0.1053
4	3	(0.1030)
5	3	0.1053
5	4	(0.1348)
	Selected average	0.1052

TABLE XIV

TORQUE COMPARISON MEASUREMENTS SERIES B
CURRENTS THROUGH ELECTRODYNAMOMETER
COILS TO COUNTERBALANCE TORQUE
OF (0.1052π/2) DYNE CM
WIRE NO. 2

Expt. No.	Coil Current	Milliamperes Current Direction, j			
		1	2	3	4
I	i	100.97	100.99	101.05	100.96
	i'	11.044	13.812	11.081	13.886
II	i	100.78	100.76	100.80	100.78
	i'	11.100	13.887	11.181	14.000
III	i	100.76	100.74	100.82	100.72
	i'	11.126	13.928	11.102	13.913
IV	i	100.70	100.78	100.78	100.72
	i'	11.166	13.990	11.058	13.860

TABLE XV

TORQUE COMPARISON MEASUREMENTS SERIES B
TORQUE PRODUCED BY ELECTRODYNAMOMETER*
WITH CURRENTS GIVEN BY TABLE XIV
WIRE NO. 2

Expt.	δ/K	milliampere		$(milliampere)^2$		Torque, dyne cm		
		ρ_{12}	ρ_{34}	i_x^2	i_z^2	$T_x{}'$	T_x	T_z
I	0.0018	11.28	11.28	1242.2	1242.2	0.16632	0.16632	0.16632
II	0.0018	11.25	11.25	1248.4	1248.4	0.16715	0.16715	0.16715
III	0.0004	11.26	11.27	1245.4	1245.4	0.16675	0.16675	0.16675
IV	0.0008	11.29	11.29	1244.8	1244.8	0.16667	0.16667	0.16667
Average	0.0012	11.27	11.27			0.16672 $\pm$ 0.00023	0.16672 $\pm$ 0.00023	0.16672 $\pm$ 0.00023

*Torque from torsion constant: $T_w = 0.1052\pi/2 = 0.1652$ dyne cm.

a mass of 14.3230 g (the largest of five cylinders), was suspended from the wire. This mass remained suspended for two days before the torsion constant was measured.

A third torque comparison measurement, Series C, was then made with wire number 3. Table XVI gives the periods of oscillation for the set of five weights, and the torsion constants calculated from the various pairs. Again because of the small differences in periods and moments of inertia, the pairs (2,1), (4,3), and (5,4) can be eliminated from consideration. The selected average torsion constant for wire No. 3 is 0.1150 ± 0.0002 dyne cm/radian. The electrodynamometer was aligned and balanced exactly as in the two previous torque comparison measurements. Table XVII gives the values of the currents through the coils necessary to balance the torque introduced by rotating the wire ±90.00 ± 0.02 degrees. The various calculated values of importance are presented in Table XVIII. The average value for the torque, T_z, is 0.18127 dyne cm which is 0.4% above the value from the torsion constant, $T_w = (0.1150)(\pi/2) = 0.1806$ dyne cm.

These three torque comparison measurements were encouraging in that they indicated a relative agreement within 1% between the torques T_z and T_w. However, to achieve agreement within 0.1-0.2% appeared to require refinement of every detail of the torque comparison measurements. For example, the stability of the zero point for wires No. 1 and 2 was ±0.006 radian; wire No. 3 had a much more stable zero point, ±0.0013 radian, but further improvement seemed desirable. Vibrations from the building were a problem in all three measurements even though many different antivibration mountings had been tried.

TABLE XVI

TORQUE COMPARISON MEASUREMENTS SERIES C
DETERMINATION OF TORSION CONSTANT
WIRE NO. 3

<u>A</u>

PERIODS OF OSCILLATION

Cylinder No.	I $g\ cm^2$	No. of Sets of 10 Periods Measured	Period, t sec
1	2.7561	6	31.73±0.01
2	3.1899	6	33.95±0.02
3	5.8460	6	45.44±0.01
4	7.0645	6	49.89±0.01
5	7.1859	6	50.24±0.01

<u>B</u>

TORSION CONSTANT FOR VARIOUS PAIRS OF CYLINDERS

Cylinder a	Cylinder b	Torsion Constant D dyne cm/radian
2	1	(0.1175)
3	1	0.1153
4	1	0.1148
5	1	0.1153
3	2	0.1150
4	2	0.1145
5	2	0.1150
4	3	(0.1134)
5	3	0.1152
5	4	(0.1365)
	Selected average	0.1150

TABLE XVII

TORQUE COMPARISON MEASUREMENTS SERIES C
CURRENTS THROUGH ELECTRODYNAMOMETER
COILS TO COUNTERBALANCE TORQUE
OF $(0.1150\pi/2)$ DYNE CM
WIRE NO. 3

Expt. No.	Coil Current	Milliamperes			
		Current Direction, j			
		1	2	3	4
I	i	100.74	100.66	100.98	100.90
	i'	12.107	15.190	12.038	15.111
II	i	100.93	100.83	100.83	100.76
	i'	12.095	15.166	12.041	15.122
III	i	100.62	100.51	100.66	100.56
	i'	12.121	15.215	12.055	15.146
IV	i	100.63	100.50	100.49	100.45
	i'	12.113	15.202	12.075	15.164
V	i	100.64	100.58	100.71	100.64
	i'	12.131	15.225	12.029	15.108
VI	i	100.64	100.56	100.54	100.48
	i'	12.149	15.240	12.038	15.114

TABLE XVIII

TORQUE COMPARISON MEASUREMENTS SERIES C
TORQUE PRODUCED BY ELECTRODYNAMOMETER*
WITH CURRENTS GIVEN BY TABLE XVII
WIRE NO. 3

Expt.	δ/K	milliampere		$(milliampere)^2$		Torque, dyne cm		
		ρ_{12}	ρ_{34}	i_x^2	i_z^2	$T_x{}'$	T_x	T_z
I	0.0024	11.36	11.36	1354.7	1354.7	0.18138	0.18138	0.18138
II	0.0036	11.36	11.36	1354.4	1354.4	0.18134	0.18134	0.18134
III	0.0026	11.36	11.36	1353.7	1353.7	0.18125	0.18125	0.18125
IV	0.0028	11.34	11.34	1353.3	1353.3	0.18119	0.18119	0.18119
V	0.0019	11.37	11.37	1353.4	1353.4	0.18121	0.18121	0.18121
VI	0.0019	11.33	11.33	1353.6	1353.6	0.18123	0.18123	0.18123
Average	0.0025	11.35	11.35			0.18127 $\pm$ 0.00006	0.18127 $\pm$ 0.00006	0.18127 $\pm$ 0.00006

*Torque from torsion constant: $T_w = 0.1150\pi/2 = 0.1806$ dyne cm.

Pretreatment of Torsion Wires

Several 0.00079-inch tungsten torsion wires were annealed in an atmosphere of hydrogen in an effort to improve their zero-point stability and torsional properties (67,68). These wires were annealed at 800-1000°C in a reduced-pressure (500 millitorr) hydrogen atmosphere. Heating was effected by passing an alternating current through the wires for 5-20 minutes. Each wire was loaded with a 20 to 30 gram load during the annealing process, then stored to age while supporting the same weight. Figure 44 is a diagram of the annealing tube, and wire clamps which held the wires while heating and aging.

Whether the annealing process itself improved the behavior of the wire is not known. However, when the wires were being annealed, it was noted that some were very uniformly incandescent, while others exhibited small areas of incandescence with emissivities less than that of most of the surface. On the assumption that non-uniform incandescence is indicative of non-uniform surface characteristics and perhaps of non-uniform crystal structure, wires which exhibited uniform incandescence were chosen for use in further torque comparison measurements.

The fourth set of torque comparison measurements was made using wire No. 4. This wire showed uniform incandescence during annealing, and was aged for three weeks supporting a 35-g mass. The torsion constant of wire No. 4 was determined before and after the torque comparison measurements to check the stability of the torsion constant. Table XIX presents the calibration data obtained before, series 1, and after, series 2, the torque comparison measurements. The periods
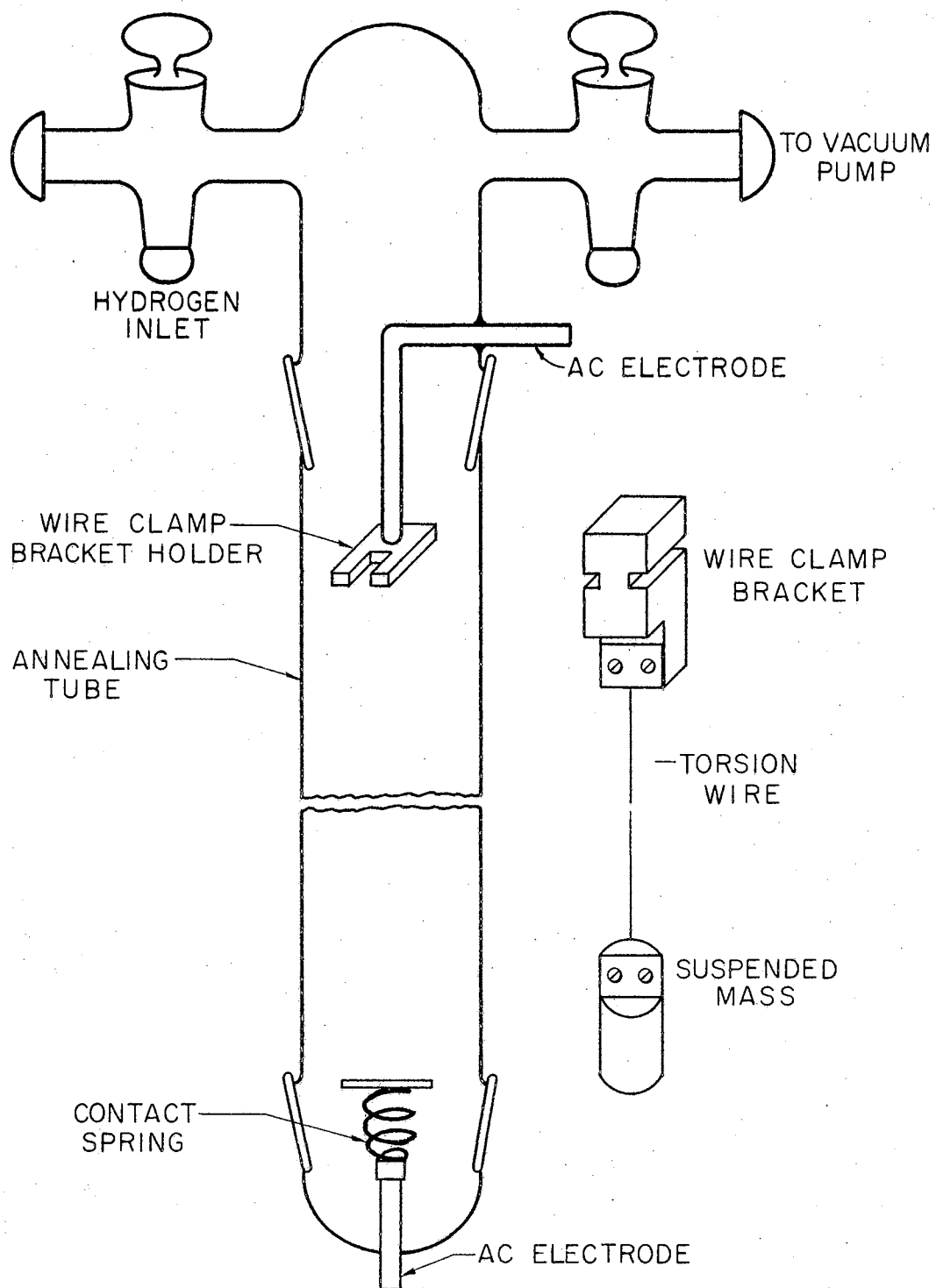
Figure 44. Apparatus for Annealing Torsion Wires

TABLE XIX

TORQUE COMPARISON MEASUREMENTS SERIES D
DETERMINATION OF TORSION CONSTANT
WIRE NO. 4

A

PERIODS OF OSCILLATION

Cylinder	Mass, g	Moment of Inertia, I, g cm^2	Period: t, sec Series 1	Series 2
1	13.94	2.7561	31.452 ± 0.023	31.436 ± 0.016
2	13.93	3.1899	33.663 ± 0.008	33.632 ± 0.025
3	12.91	5.8460	45.101 ± 0.044	45.069 ± 0.030
4	14.32	7.0645	49.504 ± 0.030	49.525 ± 0.054
5	14.00	7.1859	49.791 ± 0.009	49.854 ± 0.012

B

TORSION CONSTANT FOR VARIOUS PAIRS OF CYLINDERS

Cylinder a	Cylinder b	Torsion Constant D, dyne cm/radian Series 1	Series 2
1	2	(0.1195)	(0.1199)
1	3	0.1168	0.1170
1	4	0.1164	0.1162
1	5	0.1174	0.1168
2	3	0.1164	0.1165
2	4	0.1161	0.1158
2	5	0.1172	0.1165
3	4	0.1155	(0.1141)
3	5	(0.1189)	0.1165
4	5	(0.1681)	(0.1466)

Average excluding (1,2), (3,5), and (4,5) 0.1165 ± 0.0005

Average excluding (1,2), (3,4), and (4,5) 0.1165 ± 0.0003

listed represent the average result from 10 measurements in each of which 10 periods were timed. An electric "Standard Timer" accurate to 0.01 second was used for the period measurements.

Table XIXB gives the torsion constants, $\underline{D}$(a,b), calculated from the two series of data by equation (26) for various pairs of the five cylinders. The results exhibit much more inconsistency than can be explained in terms of the precision with which the moment of inertia and the period of each cylinder can be determined; however, some of the inconsistency can be removed by consideration of each result. For example, $\underline{D}$(1,2) is calculated from data for cylinders for which the difference in moments of inertia, and hence in the periods, is small compared to the difference for other pairs. This considerably smaller difference results in loss of precision. Therefore, the result $\underline{D}$(1,2) should either be disregarded or be given low weight in the calculation of an average value. Similar arguments can be made for $\underline{D}$(3,4) and $\underline{D}$(3,5), although the evidence is not quite as convincing. Further examination of the $\underline{D}_1$(a,b)s reveals that those involving cylinder $\underline{5}$ are consistently high, but the $\underline{D}$(a,5)s of series 2 are in excellent agreement with other values of that series. $\underline{D}$(3,4) presents another problem: $\underline{D}_1$(3,4) appears to be somewhat low but cannot reasonably be excluded, while a very good case can be made for excluding $\underline{D}_2$(3,4) on the basis that it deviates from the average of series 2 by 2.5 standard deviations if it is given equal weight in the averaging and by 7 standard deviations if it is given no weight. These same pairs have also produced values in the previous wire calibrations that were significantly discordant. That cylinder pairs (1,2) and (4,5) might not produce reasonable values for $\underline{D}$ is obvious from their moments of

inertia. These two pairs have always been excluded from each wire calibration. Usually, $\underline{D}(4,5)$ is not even calculated. It is possible that the moments of inertia, and therefore the periods, of cylinders 3,4, and 5 are close enough that a loss of precision can occur when the difference of the squares of their periods is taken. Also, building vibration, which is observed in all of these measurements, might couple with the oscillations of these masses to cause the period of one to be low and one high or $\underline{vice}$ $\underline{versa}$. In such cases loss of precision would occur, and in a random manner as is observed. When no coupling with building vibration occurs for either mass, the value for $\underline{D}$ would agree with the other calculated values.

The electrodynamometer was aligned and leveled in the usual manner. Table XX lists the currents through the coils necessary to balance the torque produced when wire No. 4 was rotated $\pm 90.00 \pm 0.02$ degrees. It should be noted that there was a much greater variation in the currents through the large coil in these measurements than in previous ones. The large coil current was adjusted initially to a value near 100 milliamperes, and then was not disturbed during the remainder of the measurements. Therefore, the variation in this series (D) was probably due to the power supply or the electrical control circuit. The torque from the torsion constant is $\underline{T}_w = (0.1165)(\pi/2) = 0.18300$ dyne cm which is 0.7% above the torque from the currents in the electrodynamometer (Table XXI). Table XXI shows that $\underline{\rho}_{12}$, $\underline{\rho}_{34}$, and $\underline{\delta}/\underline{K}$ are different from the values of the previous series. Before the measurements of Series D were conducted, the electrodynamometer was moved into a laboratory which contained more electrical equipment than was present in the previous location. The values of $\underline{\rho}_{12}$ and $\underline{\rho}_{34}$ depend

TABLE XX

TORQUE COMPARISON MEASUREMENTS SERIES D
CURRENTS THROUGH ELECTRODYNAMOMETER
COILS TO COUNTERBALANCE TORQUE
OF (0.1165π/2) DYNE CM
WIRE NO. 4

Expt. No.	Coil Current	Milliamperes Current Direction, j			
		1	2	3	4
I	i	100.90	101.03	102.03	102.24
	i'	14.190	13.173	14.070	13.011
II	i	101.34	101.34	101.45	101.24
	i'	13.727	12.688	13.694	12.698
III	i	101.47	101.28	102.05	102.24
	i'	14.136	13.069	14.043	13.008
IV	i	101.98	101.85	101.86	101.87
	i'	13.632	12.619	13.643	12.605
V	i	100.97	100.82	101.43	101.68
	i'	14.249	13.117	14.195	13.063
VI	i	102.41	102.79	102.00	102.56
	i'	13.594	12.496	13.598	12.514
VII	i	102.23	102.41	102.16	102.41
	i'	14.071	12.943	14.080	12.973
VIII	i	101.97	102.50	102.46	102.76
	i'	13.642	12.514	13.583	12.461
IX	i	101.22	102.52	102.52	102.41
	i'	14.263	12.834	14.071	12.841
X	i	102.52	102.50	103.11	103.06
	i'	13.734	12.531	13.644	12.461

TABLE XXI

TORQUE COMPARISON MEASUREMENTS SERIES D
TORQUE PRODUCED BY ELECTRODYNAMOMETER*
WITH CURRENTS GIVEN BY TABLE XX
WIRE NO. 4

Expt.	δ/K	milliamperes		(milliamperes)^2		Torque, dyne cm		
		ρ_{12}	ρ_{34}	i_x^2	i_z^2	$T_x{}'$	T_x	T_z
I	0.0121	3.73	3.96	1357.7	1357.6	0.18178	0.18173	0.18177
II	0.0172	3.94	3.86	1357.7	1357.5	0.18178	0.18167	0.18176
III	0.0172	4.14	3.88	1356.1	1355.9	0.18157	0.18146	0.18154
IV	0.0172	4.07	3.95	1357.0	1356.8	0.18169	0.18158	0.18166
V	0.0172	4.31	4.16	1355.8	1355.6	0.18153	0.18142	0.18150
VI	0.0172	4.06	3.90	1357.2	1357.0	0.18172	0.18161	0.18169
VII	0.0172	4.26	4.07	1356.9	1356.7	0.18168	0.18157	0.18165
VIII	0.0172	4.13	4.20	1357.2	1357.0	0.18172	0.18161	0.18169
IX	0.0172	4.80	4.80	1359.8	1359.6	0.18206	0.18196	0.18204
X	0.0121	4.64	4.71	1359.2	1359.1	0.18198	0.18193	0.18197
Average	0.0162	4.21	4.15			0.18179 ± 0.00013	0.18171 ± 0.00015	0.18177 ± 0.00013

*Torque from torsion constant: $T_w = 0.1165\pi/2 = 0.18300$ dyne cm.

theoretically on the earth's magnetic field, but in actuality it is the field that exists where the electrodynamometer is located that determines their values. The lead wire arrangement was also changed, causing the values of $\underline{\delta}/\underline{K}$ to be different than previously.

The precision (<0.1%) of these measurements with the electrodynamometer and the good reproducibility of the torsion constant of wire No. 4 indicates the presence of a small systematic error which produces the 0.7% discrepancy. This small error may be involved in the alignment procedures, the electrodynamometer itself, or in the calibration of the torsion wire.

In determining the torsion constant there remains the problem of deciding what weight to assign in averaging the various values of $\underline{D}$ obtained in a given calibration. It would, of course, be preferable to bypass this problem by eliminating the inconsistencies. If equation (26) is rewritten in the form

$$D = 4\pi^2 (I_i + I_x)/t_i^2 \tag{27}$$

and solved for t_i^2 ,

$$t_i^2 = \left(\frac{4\pi^2}{D}\right)I_i + \left(\frac{4\pi^2}{D}\right)I_x \ , \tag{28}$$

in which $\underline{I}_x$ is the (unknown) moment of inertia of the suspension system, it is obvious that a plot of (I_i, t_i^2) data should be linear. A least-squares analysis of the (I_i, t_i^2) data could be made and $\underline{D}$ calculated from the slope. The advantages of the least-squares treatment of the data are readily apparent. All the $(\underline{I}, \underline{t})$ data for the set of cylinders are accorded the same weight and treatment, and the question of inconsistent results from various pairs of cylinders does not arise.

The internal consistency of the $(\underline{I},\underline{t})$ data is easily checked by comparing the experimental periods for a given cylinder with that calculated from the least-squares equation and the calculated moment of inertia.

In an attempt to eliminate any error due to the moment of inertia of the weights, a new set (II) of four cylinders was made. Each of these cylinders has a mass very close to that of the small coil and dimensions (length/radius $=\sqrt{3}$) such that the moment of inertia about a transverse diameter is the same as that about the longitudinal axis (69). This geometry minimizes the change in moment of inertia due to suspension wire attachment or vibrational effects which can cause the mass to oscillate about other than the longitudinal axis. Considerable effort was expended in the careful machining and measuring of these cylinders. The restriction on mass and the requirement that length/radius $=\sqrt{3}$ limit the number of cylinders which can be made from a given material to one. The four cylinders were made from the materials indicated in Table XXII. Stainless steel was also tried, but it had enough residual ferromagnetism to have a preferred orientation in the earth's field.

Table XXIIA gives the calibration data obtained with the new cylinders for the same wire (No. 4) which was used in obtaining the data of Table XIX. Table XXIIB lists the calculated $\underline{D}(a,b)$s. If $\underline{D}(K,L)$ is disregarded with the argument that $(\underline{I}_L - \underline{I}_K)$ is too small to yield a precise value for $\underline{D}$, the remaining values exhibit reasonable consistency, the total range of the $\underline{D}(a,b)$s being less than one per cent. The average value for $\underline{D}$ from Table XXIIB is 0.1162 ± 0.0002 dyne cm/radian which agrees reasonably well with the average value of

TABLE XXII

DETERMINATION OF TORSION CONSTANT OF WIRE NO. 4
USING CALIBRATION CYLINDERS SET II

A

PERIODS OF OSCILLATION

Cylinder	Mass, g	Moment of Inertia I, g cm^2	Period, t, sec
K(Copper)	13.37	2.82461	31.811 ± 0.039
L(Bronze)	13.54	2.98382	32.681 ± 0.051
M(Aluminum)	13.93	6.57283	47.853 ± 0.027
N(Lucite)	13.45	10.81137	61.030 ± 0.019

B

TORSION CONSTANT FOR VARIOUS PAIRS OF CYLINDERS

Cylinder a	Cylinder b	Torsion Constant D dyne cm/radian
K	L	(0.1120)
K	M	0.1158
K	N	0.1162
L	M	0.1160
L	N	0.1163
M	N	0.1166
Average excluding (K-L)		0.1162 ± 0.0002

0.1165 ± 0.0003 dyne cm/radian used for the torsion constant of wire No. 4 in the Series D torque comparison measurements.

The torsion constant for wire No. 4 was also determined by least-squares treatment of the ($\underline{I}$,$\underline{t}$) data from Table XXIIA. The two previous calibrations of wire No. 4 with the first set of weights has also been checked by the least-squares treatment. The torsion constants from these three calibrations are listed in Table XXIII. It is interesting to note that the fortuitous agreement between the values of $\underline{D}$ from series 1 and 2 for wire No. 4 (Table XIX) no longer exists; however, the average for these two values (Table XXIII), 0.1166 dyne cm/radian, is quite close to the previously selected (Table XIX) average of 0.1165 dyne cm/radian. The value for $\underline{D}$ from the new set (II) of cylinders, 0.11624 dyne cm/radian, is lower than the values from set (I), and would produce better agreement between $\underline{T}_w$ and $\underline{T}_z$ in torque comparison measurements, Series D. Whether the deviation of $\underline{D}$ from the values obtained with the first set of weights is really significant remains to be demonstrated by additional data.

<p style="text-align:center">Variation of Torsion Constant with Mass of
Calibrating Cylinder</p>

There is a possibility that the effective torsion constant of a wire will change appreciably with variation in the mass of the object suspended by the wire. The effect of increasing weight would be to lengthen the wire, which would tend to decrease the value of the torsion constant. A concurrent effect would be to work-harden the wire by stretching; work-hardening would tend to increase the torsion constant (67). For small changes in mass, both of these effects might well be small and would tend to cancel.

TABLE XXIII

TORSION CONSTANTS OF WIRE NO. 4 CALCULATED BY LEAST-SQUARES
TREATMENT OF $(\underline{I},\underline{t})$ DATA

Calibration Number	Identification of original (I,t) data	Torsion Constant D, dyne cm/radian
1	Table XIX, Series 1	0.11682
2	Table XIX, Series 2	0.11638
3	Table XXII	0.11624

Two new brass cylinders, R and S, were machined; their masses were 11.01994 and 17.08190 g, compared to 13.57 ± 0.35 g for the calibrating cylinders, set (II). The period of oscillation was measured for each of these six cylinders suspended on wire No. 4. The cylinders were suspended in sequence determined by their masses, lowest mass first. The measured periods and the moments of inertia of cylinders K, L, M, and N were fitted by the least-squares method to a straight line, $Y = 338.880I + 55.5575$, with $Y = t^2$, t = period in seconds, and I, the moment of inertia in g cm^2. With this equation and the value of I for cylinders R and S, Y was calculated for cylinders R and S and compared with the square of the experimental periods. The details of this comparison are given in Table XXIV.

It should be noted first that the data in Table XXIV show the square of the periods of oscillation of the reference cylinders, K, L, M, and N to be consistent within 3 parts in 10^4. The discrepancy between observed and calculated values for cylinders R and S is 7 parts in 10^4 and is in the direction of increased period (lower torsion constant) for smaller mass (R) and decreased period (higher torsion constant) for the larger mass (S). However, the variation of Y, i.e., t^2, with the mass of the cylinder is certainly not sufficient to account for the observed variations among the torsion constants of Tables XIXB and XXIIB.

Anharmonic Oscillation

The possibility exists that the oscillation of the calibrating cylinders is anharmonic. If so, the period of oscillation should vary with amplitude of oscillation. Numerous observations have established,

TABLE XXIV

VARIATION OF PERIOD OF OSCILLATION WITH MASS OF
CALIBRATING CYLINDER

Cylinder	Mass, g	I, g cm^2	$\frac{Y\text{-calc.}}{\sec^2}$	$\frac{Y\text{-obs.}}{\sec^2}$	$\frac{Y_{obs}}{Y_{cal}} - 1$
R	11.02	2.11313	771.655	772.173	+0.00067
K	13.37	2.82461	1012.761	1013.085	+0.00031
L	13.54	2.98382	1066.714	1066.349	-0.00034
M	13.93	6.57283	2282.958	2283.024	+0.00003
N	13.45	10.81137	3719.315	3719.292	-0.00001
S	17.08	4.40645	1548.815	1547.714	-0.00071

*Calculated from $Y = 338.880\ I + 55.5575$.

however, that the period remains constant as the amplitude decreases by a factor of 100. It might be noted, however, that this applies only to observations made during times of relative quiet within the building. During the ten-minute interval for change of classes, the level of vibration increases quite markedly; components of this vibration can and do couple with the oscillations of the calibrating cylinders to cause the amplitude of oscillation of a freely-oscillating cylinder to suddenly increase. These various effects are readily apparent if one determines the variation with time (70) of the logarithmic decrement δ ($\delta = \log X_i/X_{i+1}$; X_i and X_{i+1} are the amplitudes of oscillation on successive periods). The logarithmic decrement should and does remain constant, unless building vibrations couple with the oscillation and cause the amplitude and period to increase.

The torsion constant may also be affected by damping. From the logarithmic decrement one can calculate the damping constant, and its effect on the torsion constant of the wire (70). From a series of measurements with the calibrating cylinders set (II) it was found that the Lucite cylinder had the highest damping constant. However, even for the Lucite cylinder, correction for damping changed the torsion constant by only seven parts in 10^6; the effect of damping is therefore completely negligible.

Alignment of the Electrodynamometer

The alignment of the electrodynamometer before each comparison measurement is accomplished by the built-in circular levels and by sighting through the alignment holes of the large and small coil with a telescope. The circular level used to align the superstructure of the

electrodynamometer was checked with a very precisely machined plumb

bob. The electrodynamometer was adjusted until the plumb bob was

aligned with a pointer inserted in a hole in the center of the base

plate; this alignment was accomplished with two telescopes located at

right angles from one another. The measurements with the plumb bob

indicated that the built-in level was not sufficiently accurate to

produce the desired alignment of the electrodynamometer. Rather than

replace these levels, the electrodynamometer was leveled with the

plumb bob in each of the following comparison measurements.

The axes of the large and the movable coils must be in the same

horizontal plane for the torque expressions (equations 3 and 6) to be

valid. After the electrodynamometer was leveled with the plumb bob,

the movable coil was adjusted until one could sight through the align-

ment holes on the <u>longitudinal</u> <u>axis</u> of both coils. The movable coil

was then rotated 180° and the adjustment checked. Some eclipsing of

the far alignment hole of the large coil was noted. The vertical sup-

port rod for the small coil was found to be bent slightly, and not

attached to the center of the cross bar of the movable coil. A new

Lucite cross bar was constructed and mounted on the small coil. At

this same time the screw clamps which hold the catenary lead wires

on the movable coil were replaced by spring clamps. These clamps

allow the wires to be installed straighter and the small coil to move

with less hinderance.

Three series of comparison measurements were made to determine the

effect of the alignment of the electrodynamometer on the value of the

torque measured. Before each of the three series was begun, the

electrodynamometer and the coils were deliberately misaligned and then

realigned, so that an estimate of reproducibility of alignment could be made. These comparisons were made with wire No. 11 for which the torsion constant was obtained before and after the three comparisons with set (II) calibrating cylinders and the least-squares treatment of (I,t) data. Calibration data obtained for wire No. 11 before, series 1, and after, series 2, the comparison measurements are listed in Table XXV.

The electrodynamometer current and torque data for these comparison measurements are presented in Table XXVI through XXVIII. Table XXIX gives the summary and comparison of these torque values with the torque from wire No. 11. The standard deviation given in Table XXIX for each average value of T_z indicates that, for a given coil alignment, the reproducibility of torque measurements with the electrodynamometer is 0.2-0.3 per cent. The standard deviation of the three average values of T_z shows that the coil alignment is reproducible within about 0.2 per cent. The precision for torsion wire calibration (No. 11) is also about 0.2 per cent. From the precision of these various measurements, the expected agreement between T_z and T_w is ± 0.4 per cent. The results in Table XXIX show that within this expected experimental error, the values of a given torque measured by a carefully calibrated torsion wire and by a carefully aligned electrodynamometer are in good agreement.

Another set of comparison measurements, Series F, was made with wire No. 4; the electrodynamometer was leveled and aligned using the improved procedures. The torsion constant of wire No. 4 was determined before and after the comparison measurements. Duplicate measurements, after the first two, were made of the currents necessary to

TABLE XXV

TORQUE COMPARISON MEASUREMENTS SERIES E
DETERMINATION OF TORSION CONSTANT
WIRE NO. 11

<u>A</u>

PERIODS OF OSCILLATION

Cylinder	Moment of Inertia I, g cm^2	Period t, sec	
		Series 1	Series 2
K(Copper)	2.82461	31.765$\pm$0.020	31.736$\pm$0.026
L(Bronze)	2.98382	32.584$\pm$0.020	32.555$\pm$0.020
M(Aluminum)	6.57283	47.644$\pm$0.050	47.656$\pm$0.040
N(Lucite)	10.81137	60.842$\pm$0.070	60.759$\pm$0.030

<u>B</u>

TORSION CONSTANT

	Series 1	Series 2
Torsion Constant <u>D</u>* (dyne cm/radian)	0.11708	0.11741
Average <u>D</u>	0.11724	

*From least-squares treatment of (<u>I</u>, <u>t</u>) data.

TABLE XXVI

TORQUE COMPARISON MEASUREMENTS SERIES E-I
CURRENTS THROUGH ELECTRODYNAMOMETER
COILS TO COUNTERBALANCE TORQUE OF
$(0.11724\pi/2)$ DYNE CM
WIRE NO. 11

ALIGNMENT I

Expt. No.	Coil Current	Milliamperes Current Direction, j				Torque, T_z dyne cm
		1	2	3	4	
I	i	101.36	101.36	101.36	101.36	
	i'	14.279	12.747	14.579	13.011	0.18468
II	i	101.55	101.55	101.52	101.56	
	i'	14.344	12.802	14.456	12.891	0.18462
III	i	101.67	101.67	101.64	101.62	
	i'	14.308	12.773	14.414	12.879	0.18441
IV	i	101.56	101.64	101.67	101.67	
	i'	14.239	12.721	14.456	12.919	0.18425
V	i	101.39	101.41	101.39	101.40	
	i'	14.283	12.777	14.474	12.919	0.18422
VI	i	101.39	101.56	101.53	101.50	
	i'	14.245	12.712	14.430	12.899	0.18383

TABLE XXVII

TORQUE COMPARISON MEASUREMENTS SERIES E-II
CURRENTS THROUGH ELECTRODYNAMOMETER
COILS TO COUNTERBALANCE TORQUE OF
(0.11724π/2) DYNE CM
WIRE NO. 11

ALIGNMENT II

Expt. No.	Coil Current	Milliamperes Current Direction, j				Torque, T_z dyne cm
		1	2	3	4	
I	i	101.49	101.49	101.49	101.59	
	i'	14.226	12.730	14.644	13.093	0.18523
II	i	101.56	101.57	101.58	101.57	
	i'	14.234	12.746	14.548	13.012	0.18483
III	i	101.53	101.64	101.61	101.62	
	i'	14.212	12.705	14.566	13.029	0.18478
IV	i	101.61	101.61	101.60	101.58	
	i'	14.186	12.692	14.636	13.093	0.18509
V	i	101.51	101.51	101.51	101.47	
	i'	14.194	12.708	14.541	12.992	0.18434
VI	i	101.46	101.43	101.56	101.56	
	i'	14.226	12.709	14.617	13.051	0.18489

TABLE XXVIII

TORQUE COMPARISON MEASUREMENTS SERIES E-III
CURRENTS THROUGH ELECTRODYNAMOMETER
COILS TO COUNTERBALANCE TORQUE OF
$(0.11724\pi/2)$ DYNE CM
WIRE NO. 11

ALIGNMENT III

Expt. No.	Coil Current	Milliamperes				Torque, T_z dyne cm
		Current Direction, j				
		1	2	3	4	
I	i	101.53	101.53	101.54	101.53	
	i'	14.301	12.818	14.499	12.991	0.18503
II	i	101.51	101.51	101.51	101.50	
	i'	14.283	12.803	14.450	12.948	0.18456
III	i	101.51	101.50	101.51	101.50	
	i'	14.398	12.888	14.514	13.017	0.18568
IV	i	101.50	101.49	101.49	101.49	
	i'	14.330	12.846	14.360	12.858	0.18423
V	i	101.47	101.47	101.48	101.47	
	i'	14.396	12.887	14.523	12.992	0.18555
VI	i	101.49	101.47	101.47	101.47	
	i'	14.342	12.847	14.476	12.954	0.18495

TABLE XXIX

SUMMARY OF TORQUES FROM ELECTRODYNAMOMETER COIL CURRENTS
FOR SERIES E-I THROUGH E-III
WIRE NO. 11

Alignment Number	T_z, Average dyne cm	Standard Deviation σ, dyne cm	T_z/T_w*
I	0.18433	0.0003	1.000 ± 0.004
II	0.18486	0.0003	1.003 ± 0.004
III	0.18500	0.0005	1.004 ± 0.004

standard deviation for the three average values of T_z:
$\sigma = 0.0003$

*From Table XXV, $T_w = (0.11724 \, \pi/2) = 0.1843$ dyne cm.

counterbalance the counterclockwise and clockwise rotation of the

torsion wire through $90.00 \pm 0.02^{\circ}$. These duplicate measurements indi-

cate the reproducibility with which a fixed torque in the wire can be

measured by the EDM.

The calibration data obtained for wire No. 4 before and after the

comparison measurements, series 1 and 2, respectively, are given in

Table XXX. The currents through the electrodynamometer coils to

counterbalance the torque in the wire are given in Table XXXI. The

duplicate measurements (a) and (b) of experiments III through VI indi-

cate that the precision with which the electrodynamometer can measure

a torque after it has been introduced in the wire is better than four

parts in 10^4. From the average value for $\underline{D}$ (Table XXX), 0.11651 dyne

cm/radian, $\underline{T}_w$ = 0.18301 dyne cm; from Table XXXII the average $\underline{T}_z$ is

0.18316 dyne cm. Therefore, we have $\underline{T}_z/\underline{T}_w$ = 1.0008 or agreement within

0.1% between the torque calculated from the electrodynamometer data

and that calculated from the torsion constant.

Conclusions and Discussion

The above results indicate that it is possible to measure torques

of 0.1-0.2 dyne cm with an accuracy of $\pm 0.2\%$ using the electrodyna-

mometer. However, as Tables XXIII, XXV, and XXX indicate, determi-

nation of the torsion constant of a 0.00079-inch tungsten wire with an

uncertainty less than $\pm 0.1\%$ is accomplished only by exercising great

care. It may well be that a carefully constructed electrodynamometer

is more nearly accurate for measuring small static torques than is

the usual calibrated torsion wire, especially since the torsion wire

is, of necessity, calibrated under dynamic conditions and used under

TABLE XXX

TORQUE COMPARISON MEASUREMENTS SERIES F
DETERMINATION OF TORSION CONSTANT
WIRE NO. 4

<u>A</u>

PERIODS OF OSCILLATION

Cylinder	Moment of Inertia I, g cm^2	Period, t, sec	
		Series 1	Series 2
K(Copper)	2.82461	31.824±0.012	31.829±0.015
L(Bronze)	2.98382	32.661±0.018	32.655±0.023
M(Aluminum)	6.57283	47.780±0.020	47.781±0.022
N(Lucite)	10.81137	60.981±0.019	60.986±0.026
Torsion Constant <u>D</u>* (dyne cm/radian)		0.11652	0.11650
Average <u>D</u>		0.11651	

*From least-squares treatment of (<u>I</u>, <u>t</u>) data.

TABLE XXXI

TORQUE COMPARISON MEASUREMENTS SERIES F
CURRENTS THROUGH ELECTRODYNAMOMETER
COILS TO COUNTERBALANCE TORQUE
OF $(0.1165\pi/2)$ DYNE CM
WIRE NO. 4

Expt. No.	Coil Current	Milliamperes Current Direction, j			
		1	2	3	4
I	i	100.99	101.05	101.06	101.06
	i'	14.184	12.837	14.328	12.967
II	i	101.05	101.05	101.05	101.06
	i'	14.179	12.858	14.304	12.972
III (a)	i	101.08	101.10	101.09	101.07
	i'	14.180	12.858	14.272	12.947
III (b)	i	101.09	101.08	101.09	101.10
	i'	14.180	12.858	14.269	12.941
IV (a)	i	101.11	101.11	101.10	101.10
	i'	14.194	12.859	14.257	12.927
IV (b)	i	101.11	101.10	101.10	101.10
	i'	14.197	12.863	14.260	12.931
V (a)	i	101.11	101.11	101.13	101.13
	i'	14.188	12.861	14.275	12.923
V (b)	i	101.14	101.13	101.13	101.13
	i'	14.180	12.854	14.272	12.925
VI (a)	i	101.14	101.14	101.15	101.15
	i'	14.180	12.857	14.254	12.917
VI (b)	i	101.15	101.13	101.16	101.16
	i'	14.180	12.857	14.251	12.915

TABLE XXXII

TORQUE COMPARISON MEASUREMENTS SERIES F
TORQUE PRODUCED BY ELECTRODYNAMOMETER*
WITH CURRENTS GIVEN BY TABLE XXXI
WIRE NO. 4

Expt.	δ/K	milliamperes		(milliamperes)^2		Torque, dyne cm		
		ρ_{12}	ρ_{34}	i_x^2	i_z^2	$T_x{}'$	T_x	T_z
I	0.0048	5.02	5.05	1368.6	1368.6	0.18324	0.18324	0.18324
II	0.0048	4.95	4.94	1368.8	1368.8	0.18327	0.18327	0.18327
III	0.0041	4.95	4.94	1367.9	1367.9	0.18315	0.18315	0.18315
IV	0.0027	5.00	4.96	1367.6	1367.6	0.18310	0.18311	0.18311
V	0.0037	4.98	5.04	1367.8	1367.8	0.18313	0.18313	0.18313
VI	0.0027	4.96	4.99	1367.4	1367.4	0.18308	0.18307	0.18307
Average	0.0038	4.97	4.98			0.18316 ± 0.00006	0.18316 ± 0.00006	0.18316 ± 0.00006

*Torque from torsion constant: $T_W = 0.11651\pi/2 = 0.18301$ dyne cm.

static ones (67). One should be particularly wary of attempting to determine the torsion constant by equation (26) with moments of inertia and periods for only two cylinders.

The results of these comparison measurements, in particular the value of the ratio T_z/T_w, are pertinent to questions which have been raised, in several laboratories (68,71-74) where the torsion Knudsen effusion recoil (Torker) technique (61) is employed, about possible inequality of static and dynamic torsion constants and about torsional anisotropy of small tungsten wires. The value of the torque T_z calculated from the EDM coil currents is a measure of the static torsion constant, while the value of the torque T_w is a measure of the dynamic torsion constant. For the comparison measurements which have been made with various wires, the ratio T_z/T_w consistently fell within the range 0.998-1.004. The results strongly support the validity of the usual assumption that static and dynamic torsion constants are equal.

Unfortunately, in the operation of the EDM it is necessary to measure the torque when the wire is rotated in clockwise (cw) and counterclockwise (ccw) directions; this and the ensuing calculations are done to eliminate any effect which might be caused by stray magnetic fields, especially those arising from currents in lead wires to the EDM (64,65). If the torsion wire were anisotropic, such that the torque which the wire exerted on being rotated 90° cw differed in magnitude from the torque exerted on being rotated 90° ccw, the effect on the EDM measurements would be obscured by the procedure required to eliminate the lead wire effects. Therefore, from any single comparison measurement one can obtain no definite information about torsional anisotropy of a wire.

However, we can make some reasonable inferences. It is shown in Appendix C that the anisotropy of the wire is defined as $\underline{s} = \underline{T}_w$ (cw) $- \underline{T}_w$ (ccw) and if the lead wire effect $\underline{\delta}$ is defined by equations (16) and (17), the following relations may be deduced:

if $\underline{s}$ is negligible: $\delta/K = (i_{34}^2 - i_{12}^2)/(i_{12}^2 + i_{34}^2)$;

if $\underline{\delta}$ is negligible: $s/T_{12} = -(i_{34}^2 - i_{12}^2)/i_{12}^2$.

The critical quantity is obviously $(\underline{i}_{34}^2 - \underline{i}_{12}^2)$. With the exception of one sequence of six comparison measurements, values for $(\underline{i}_{34}^2 - \underline{i}_{12}^2)$ for all our measurements fall in the range 0 ± 40 ma^2, have an algebraic average very near zero and an average magnitude of ~ 20 ma^2; typical values for $\underline{i}_{12}^2$ and $(\underline{i}_{12}^2 + \underline{i}_{34}^2)$ are 1400 and 2810 ma^2, respectively. Therefore, if the lead wire effect is negligible, $\underline{s}/\underline{T}_{12}$ cannot be much larger than 0.015; if anisotropy is negligible, the lead wire effect is $\underline{\delta}/K \approx 0.007$. The values of $(\underline{i}_{34}^2 - \underline{i}_{12}^2)$ are found to vary with no apparent pattern from run to run; typical values of $(\underline{i}_{34}^2 - \underline{i}_{12}^2)$ for successive sequences with the same wire are +38, -4, +37, -57, -19, -36, -12. If the wire were anisotropic, one would not expect $\underline{s}$ to be positive in one sequence, and negative in the next. Further, in one sequence of comparison measurements, the source of dc current for the EDM was changed in the middle of the sequence, with consequent rearrangement of lead wires around the EDM: the values of $(\underline{i}_{34}^2 - \underline{i}_{12}^2)$ before the change in power supplies was ~ -15, and after the change $\sim +50$. It is concluded that, for the wires used in this work, the major fraction of the variation in $(\underline{i}_{34}^2 - \underline{i}_{12}^2)$ arose from lead wire effects and experimental error and that the anisotropy (i.e.,

the quantity s/T_{12}) of the wires was less than 0.5% of the total torque.

As was stated earlier, the electrodynamometer was intended for measurements of momentum distribution in molecular beams, and average molecular weight determinations by measurement of beam momentum coupled with weight-loss data from the Knudsen cell-source. While the electro-dynamometer appears to be applicable in the 0.1-0.2 dyne cm range, it is rather doubtful that the necessary precision and accuracy can be maintained in the lower range of 0.01-0.001 dyne cm. For measurements in this range the application of a torque measuring device more sensi-tive than the electrodynamometer appears to be needed (76). Further, more sophisticated, and potentially more accurate, measurements of angular distribution of momentum are expected on the near future from other workers (77). A new technique, the Microbalance-Inverted Knudsen Effusion-Recoil Technique, appears to have much more promise for studies of average molecular weights of the species effusing from a Knudsen cell at elevated temperatures than does the electrodynamometer (78). For these reasons, it is concluded that further development of the electrodynamometer momentum detector is not profitable at the present time.

SELECTED BIBLIOGRAPHY

(1)   Le Chatelier, H.   (1887).   Bull. soc. franc. mineral. 10, 204.

(2)   Smothers, W. J., and Y. Chiang.   (1958).   "Differential Thermal
         Analysis." Chemical Publ. Co., New York.

(3)   Eyraud, C.   (1954).   Compt. rend. 238, 1511.

(4)   Borchardt, H. J., and F. Daniels.   (1957).   J. Am. Chem. Soc.
         79, 41.

(5)   Sturm, E.   (1961).   J. Phys. Chem. 65, 1935.

(6)   Vold, M. J. (1949).   Anal. Chem. 21, 683.

(7)   Wittig, F. E.   (1950).   J. Electrochem. 54, 288.

(8)   Deeg, E.   (1956).   Ber. deut. keram. Ges. 33, 321.

(9)   Spiel, S.   (1944).   U. S. Bur. Mines Rept. Invest. No. 3764.

(10) Speros, D. M., and R. L. Woodhouse.   (1963).   J. Phys. Chem.
         67, 2161.

(11) Brewer, L. and J. S. Kane.   (1955).   J. Phys. Chem. 59, 105.

(12) McAdams, W. H.   (1942).   "Heat Transmission." pp. 22. McGraw
         Hill Book Co., Inc., New York.

(13) Kissinger, H. E.   (1957).   Anal. Chem. 29, 1702.

(14) Freeman, E. S., and B. Carroll.   (1958).   J. Phys. Chem. 62,
         394.

(15) Horowitz, H. H., and G. Metzger.   (1963).   Anal. Chem. 35, 1464.

(16) Brindley, G. W., J. H. Sharp and B. N. Narahari Achar.   (1965).
         In "Proceedings of The First International Conference on
         Thermal Analysis." J. P. Redfern, editor, Macmillan and
         Co. Ltd. London.

(17) Hughes, M. A.   (1965).   In "Proceedings of The First Internation-
         al Conference on Thermal Analysis." J. P. Redfern, editor,
         Macmillan and Co. Ltd. London.

(18) Garner, W. E. (1955). "Chemistry of The Solid State." pp. 184-211. Academic Press, New York.

(19) Dollimore, D., J. Dollimore, and D. Nicholson. (1960). "Reactivity of Solids." 4th International Conference, pp. 627.

(20) Jacobs, P. W. M., and A. R. T. Kureishy. (1962). Trans. Faraday Soc. 58, 551.

(21) Handbook of Operational Amplifier Applications, Burr-Brown Research Corporation, P.O. Box 11400 Tucson, Arizona, 85706.

(22) Kelley, K. K. (1960). "Contributions to the Data on Theoretical Metallurgy XIII. High-Temperature Heat-Content, Heat-Capacity, and Entropy Data for the Elements and Inorganic Compounds." U. S. Bur. Mines Bull. 584. U. S. Government Printing Office, Washington, D. C.

(23) Ruff, O., and R. Wallstein. (1923). Z. anorg. allgem. Chem. 128, 96.

(24) Young, R. C. (1931). J. Am. Chem. Soc. 53, 2148.

(25) Larsen, E. N. and J. J. Leddy. (1956). J. Am. Chem. Soc. 78, 5983.

(26) Swaroop, B., and S. N. Flengas. (1964). Can. J. Chem. 42, 1495.

(27) Newnham, I. E., and J. A. Watts. (1960). J. Am. Chem. Soc. 82, 2113.

(28) Schumb, W. C., and R. F. Sundstrom. (1933). J. Am. Chem. Soc. 55, 596.

(29) Vogel, A. I. (1961). "Quantitative Inorganic Analysis." third edition, pp. 547. Longmans, Green and Co. Ltd. London.

(30) Swaroop, B., and S. N. Flengas. (1964). Can. J. Phys. 42, 1886.

(31) Dahl, L. F., Tao-I Chiang, P. W. Seabaugh, and E. M. Larsen. (1964). J. Inorg. Chem. 3, No. 9, 1236.

(32) Grisafe, D. A. and W. B. White. (1964). Am. Mineralogist. 49, 1184.

(33) Warne, S. ST. J. and P. Bayliss. (1962). Am. Mineralogist. 47, 1011.

(34) Garn, P. D., and J. E. Kessler. (1960). Anal. Chem. 32, 1563.

(35) Glasner, A., and I. Hodara. (1958). Bull. Res. Council Israel. 7A, 66.

(36) Peretti, E. A. (1957). J. Am. Ceram. Soc. 40, 171.

(37) Lamure, J. (1953). Compt. rend. 236, 926.

(38) Beck, C. W. (1950). Am. Mineral. 35, 985.

(39) Nicol, A. (1948). Compt. rend. 226, 670.

(40) Cuthbert, F. L. and R. A. Rowland. (1947). Am. Mineral. 32, 111.

(41) Centnerswer, M., G. Falk and A. Averbuch. (1925). Z. Phys. Chem. 115, 29.

(42) Collins, G. A., and A. G. Swan. (1954). Canadian Min. Met. Bull. 47, 533.

(43) Kauffman, A. J. and E. O. Dilling. (1950). Econ. Geol. 45, 222.

(44) Bruzs, B. (1926). J. Phys. Chem. 30, 680.

(45) Gruver, R. M. (1950). J. Am. Ceram. Soc. 33, 96.

(46) "International Critical Tables of Numerical Data, Physics, Chemistry and Technology." (1930). Ed. by National Research Council, 1st ed., Vol. 7, McGraw-Hill, New York.

(47) Wagman, D. D., W. H. Evans, I. Halow, V. B. Parker, S. M. Bailey and, R. H. Schumm. (1965). "Selected Values of Chemical Thermodynamic Properties, Part 2. Tables for the Elements Twenty-Three Through Thirty-Two in The Standard Order of Arrangement." U. S. National Bureau of Standards Technical Note. 270-2.

(48) Kadlec, O. and M. M. Dubinin. (1958). Izvest. Akad. Nauk. S.S.S.R., Otdel. Khim. Nauk. 1031.

(49) Samal, G. I. (1961). Geterogennye Khim. Reaktsii, 92.

(50) Tuccarbasi, S. (1962). Istanbul Univ. Fen. Fak. Mecmuasi Ser. C 27, 1.

(51) Erofeev, B. V. (1961). "Reactivity of Solids." Proceedings of the 4th International Symposium on the Reactivity of Solids, pp. 273, J. H. De Boer Editor-in-Chief. Elsevier Publishing Company, Amsterdam.

(52) Lewis, G. N. (1905). Z. Phys. Chem. 52, 310.

(53) Rossini, F. D., D. D. Wagman, W. H. Evans, S. Levine, and I.
      Jaffe. (1952). "Selected Values of Chemical Thermodynamic
      Properties." U. S. National Bureau of Standards Circ. 500.
      U. S. Government Printing Office, Washington, D. C.

(54) JANAF Thermochemical Tables. (1965). The Dow Chemical Co.,
      Midland, Michigan.

(55) Markowitz, M. M., and D. A. Boryta. (1962). J. Phys. Chem.
      66, 1477.

(56) Popov, M. M., and G. L. Galchenko. (Moscow State Univ.) (1951).
      Zhur. Obschci Khim. (J. Gen. Chem.) 21, 2489.

(57) Arell, A. (1960). Ann. Acad. Sci. Fennicae Ser. A VI, No. 57,
      42.

(58) Schultz, R. D., and A. O. Dekker. (1956). J. Phys. Chem. 60,
      1095.

(59) Chaiken, R. F., D. J. Sibbett, J. E. Sutherland, D. K. Van De
      Mark, and A. Wheeler. (1962). J. Chem. Phys. 37, 2311.

(60) Schultz, R. D., and A. O. Dekker. (1954). "The Absolute Thermal
      Decomposition Rates of Solids, Part I." In Fifth Inter-
      national Combustion Symposium, Pittsburgh, Reinhold Publish-
      ing Corp. Also, Aerojet-General Technical Note (OSR-TN-55-
      117) Prepared for the Office of Scientific Research.

(61) Freeman, R. D. (1966). "Momentum Sensors." in Characterization
      of High Temperature Vapors. J. L. Margrave, Ed. John Wiley
      and Sons, Inc., New York.

(62) Knudsen, M. (1909). Ann. Physik. 28, 999.

(63) Guthe, K. E. (1906). Bull. Bureau of Standards. 2, 33.

(64) Dawson, J. P. (1960). M. S. Thesis, Oklahoma State University,
      Stillwater.

(65) Freeman, R. D. (1962). ASD-TDR-62-204, part 1, submitted by
      A. D. Little, Inc., under Contract AF 33(616)-7427.

(66) Driscoll, R. L. (1958). J. Res. NBS. 60, 287.

(67) Bearden, J. A. (1939). Phys. Rev. 56, 1023.

(68) Rosenblatt, G. M. (1960). Ph.D. Thesis, Princeton University.

(69) Limb, C. (1892). Compt. rend. 114, 1057.

(70) Page, L. (1928). "Intro. To Theoretical Physics." pp. 64, 142,
      D. Van Nostrand, Inc., New York.

(71) Rosenblatt, G. M., and C. E. Birchenall. (1961). $\underline{J}$. $\underline{Chem}$. $\underline{Phys}$. 35, 788.

(72) Schulz, D. A., and A. W. Searcy. (1963). $\underline{J}$. $\underline{Phys}$. $\underline{Chem}$. 67, 103.

(73) Schulz, D. A. (1962). Ph.D. Thesis, University of California, Berkeley.

(74) Hollahan, J. R., and N. W. Gregory. (1964). $\underline{J}$. $\underline{Phys}$. $\underline{Chem}$. 68, 2346.

(75) Humphrey, F. B., and A. R. Johnston. (1963). $\underline{Rev}$. $\underline{Sci}$. $\underline{Instr}$. 34, 348.

(76) Wahlbeck, P. G. (1962). Private Communication.

(77) Bennett, J. E. (1965). Ph.D. Thesis, Oklahoma State University, Stillwater.

(78) Caldwell, J. R., and H. V. Moyer. (1935). $\underline{Ind}$. $\underline{Eng}$. $\underline{Chem}$., $\underline{Anal}$. $\underline{Ed}$. 7, 38.

(79) Newnham, I. E. (1957). $\underline{J}$. $\underline{Amer}$. $\underline{Chem}$. $\underline{Soc}$. 79, 5415.

(80) Turnbull, A. G., and J. A. Watts. (1963). $\underline{Aust}$. $\underline{J}$. $\underline{Chem}$. 16, 947.

APPENDIX A

COMPUTER PROGRAM FOR DTA/DSC KINETIC DATA

The computer program which was used to determine the best repre-
sentation of the kinetic data is listed in this appendix. The program
is written in FORTRAN IV language for the IBM 7040 computer.

The program will determine the Arrhenius activation energy from
computed values for ln k and 1/T, using peak data from either DTA or
DSC. For DTA the rate constant k is calculated from the equation
Borchardt and Daniels (4) derived for studying solution reactions with
DTA. The equation for k,

$$k = \left[\frac{KAV}{n_o}\right]^{x-1} \frac{C_p \frac{d\Delta T}{dt} + K\Delta T}{\left[K(A-a) - C_p \Delta T\right]^x}$$

contains known quantities, quantities that may be obtained from the DTA
peak, and the order of the reaction for which one assumes values. A
listing of these quantities follows:

K - Heat transfer coefficient for the DTA cells

A - Total integrated area of DTA peak

V - Volume of solution in DTA cell

n_o - Initial number of moles of reactant

x - The order of the reaction

C_p - Heat capacity of solution in DTA cell

ΔT   -   Difference in temperature between the sample and reference cells, the ordinate of the DTA peak at time $\underline{t}$

$d\Delta T/dt$ -   Slope of the DTA peak at time $\underline{t}$

a   -   Area under DTA peak from beginning of reaction to time $\underline{t}$

The program reads in values for all these quantities except $\underline{a}$, $\underline{A}$, and $d\Delta T/dt$. The input data consists of data pairs $(T, \Delta T)$, since for a linear heating rate temperature $\underline{T}$ is a more convenient absissa than time $\underline{t}$. For DSC $\underline{k}$ is calculated from an equation used by Erofeev (51) and by Lewis (52) to describe some solid decomposition reaction kinetics. The equation for $\underline{k}$,

$$k = \frac{1}{A} \frac{dH}{dt} \left(\frac{a}{A}\right)^{-\alpha} (1 - a/A)^{-\beta}$$

contains quantities that may be obtained from the DSC peak, and $\underline{\alpha}$ and $\underline{\beta}$ for which values are assumed. The quantities in this equation are defined as follows:

A   -   Total integrated area of DSC peak

dH/dt -   Ordinate of DSC peak at a given time $\underline{t}$

a   -   Area under DSC peak from beginning of reaction to time $\underline{t}$

α -   Order of reaction for product phase

β -   Order of reaction for reactant phase

The input data consists of data pairs $(T, dH/dt)$, since, just as with DTA, temperature $\underline{T}$ is a more convenient absissa than time $\underline{t}$.

The program consists of three major parts:

(1)   Integration of the peak to obtain the total area, and integration to obtain the area from the start of the reaction to the point represented by each data pair. The integration is accomplished by fitting three points at a time to a quadratic

equation which is then integrated over the three point in-
terval.

(2) Calculation of $\underline{k}$ from the appropriate equation given above.
Values for the order of reaction are assumed, and these ini-
tial values incremented to their final values. A set of $\underline{k}$'s
are determined for each of the assumed values for the order.

(3) A least-squares linear analysis of ln $\underline{k}$ vs. 1/$\underline{T}$ is made for
each set of $\underline{k}$'s from (2) above. The program utilizes all the
data pairs in the least-squares analysis, or only those in a
specified range, depending upon the input options. For each
set of $\underline{k}$'s values for the Arrhenius activation energy, the
slope and the standard deviation of the slope, the intercept
and its standard deviation, and the standard deviation of a
single ln $\underline{k}$ are computed.

The program is designed to analyze more than one DTA/DSC peak, by
simply placing the input data cards for these peaks in sequence at the
end of the program.

Input

Four information cards precede the set of data cards for each peak.
The first card is used to identify the data, i.e., the compound, note-
book page number where reaction conditions are described, etc. The
second and third cards contain the following information, beginning in
column one for each card:

Format	Input Information
	Second Card
I2	DTA 01, DSC 00
I2	Number of data cards
F7.4	Temperature at start of peak
F7.4	Temperature at end of peak
F7.4	Temperature increment
F7.4	Total area of peak (if known)
F7.4	Volume of solution in DTA cell
F7.4	Concentration of solution in DTA cell
F7.4	Heat transfer coefficient of DTA cell
F7.4	Heat capacity of solution in DTA cell
F4.2	Starting value for alpha
F4.2	Ending value for alpha
F4.2	Increment by which alpha is increased
	Third Card
F4.2	Starting value for beta
F4.2	Ending value for beta
F4.2	Increment by which beta is increased

The fourth card in 2I2 format indicates the first point and last point of the data which is to be used in the least-squares analysis. The data cards are in 4F8.4 format, and the order on the card is temperature, area, dH/dt, and ΔT.

Two options concerning area and temperature should be noted. If the total area and the area up to the point where the ordinate is taken are known, these may be read-in and the integration routine will then

be omitted. For linear temperature increase the temperature data may
be generated by giving the starting temperature, the temperature incre-
ment, and the temperature at the end. If these options are not desired
it is only necessary to leave the appropriate spaces on the second in-
put card blank.

FORTRAN IV Words and Their English Equivalents

FORTRAN IV Word	English Equivalent
ANAME	Used to read-in Alphameric information for peak identification
TEMP(I)	Temperature corresponding to ordinate H(I)
AR(I)	Area up to point where dH/dt is taken
H(I)	dH/dt, ordinate of DSC peak
DELT	ΔT, ordinate of DTA peak
DENOM	Denominator
DNUM	Numerator
RTCNST	Rate Constant, $\underline{k}$
TSTART	Temperature at start of peak
TEND	Temperature at end of peak
TINC	Temperature increment
ATOT	Total area of peak
V	Volume of solution in DTA cell
CONC	Concentration of solution in DTA cell
U	Heat transfer coefficient of DTA cell
CP	Heat capacity of solution in DTA cell
ORDST1	Initial value of alpha
ALPHND	Final value of alpha
DORD1	Increment by which alpha is increased

ORDST2   Initial value of beta

BETEND   Final value of beta

DORD2   Increment by which beta is increased

NA,NB   Number of first and last data points in range
                            to be used in least-squares analysis

NPTS   Number of data pairs

GARB1, GARB2   Incremental areas used in integration routine

XX(I)   Ratio of AR(I) to ATOT, represents fraction
                            of product formed

HCHNG   Function used to correct ordinates to a drift-
                            ing base line

CON   Used to help evaluate the constants for the
                            quadratic equation in the integration routine

```
      DIMENSION ANAME (8),TEMP(30),AR(30),H(30),DELT(30),DENOM(30),
     1DNUM(30),RTCNST(30),X(30),Y(30),YCALC(30),T(30),XX(35)
   60 FORMAT(37H ARRHENIUS  ACTIVATION ENERGY,KCAL/MOLE15.8//8H    SLOPE=E1
     14.8,5X,10HINTERCEPT=E14.8//)
   70 FORMAT(28H  STD DEV OF A SINGLE LN K =E14.8/20H  STD DEV OF SLOPE
     1=E14.8/24H  STD DEV OF INTERCEPT =E14.8//)
  200 FORMAT(18H  REJECTED POINT =15,E19.8)
  300 FORMAT(9H NEG AREA)
  400 FORMAT(11H NEG RATE K)
 1000 FORMAT(8A6/2I2,8F7.4,3F4.2/3F4.2)
 1001 FORMAT(4F8.4)
 2000 FORMAT(49H1ARRHENIUS ACTIVATION ENERGY FROM DSC OR DTA DATA///1X,8
     1A6)
 2002 FORMAT(3H M=I2,18H (M=1,DTA/M=0,DSC)/8H NO PTS=I2/8H T AREA=F9.4/5
     1H VOL=F9.4/7H MOLES=F9.4/15H HT TRANS COEF=F9.4/13H HT CAPACITY=F9
     2.4/17H ALPHA AT START =F6.2/15H ALPHA AT END =F6.2/18H ALPHA INCRE
     3ment = F6.2/16H BETA AT START =F6.2/14H BETA AT END =F6.2/17H BETA
     4INCREMENT =F6.2/11H TEMP INCR=F8.4/12H START TEMP=F8.4/10H END Tem
     5MP=F8.4//)
 2001 FORMAT(5H   NO5X,4HTIME8X,4HAREA9X,5HDH/DT5X,8HDEL TEMP,5X,15HAREA
     1/TOTAL AREA/(I5,5F12.4))
 2003 FORMAT(28H1ARRHENIUS PLOT FOR ALPHA = F6.2,6X,7HBETA = F6.2/)
 2004 FORMAT(3X,2HNO3X,4HTEMP9X,6HRATE K11X,4HLN K9X,9HLN K,CALC6X,9H100
     10/TEMP6X,9HDIFF LN K/(I5,F10.5,5E16.8))
 2005 FORMAT(5H   NO5X,4HTIME8X,4HAREA9X,5HDH/DT5X,8HDEL TEMP/(I5,4F12.4))
     1))
 3000 FORMAT(1H1)
 4000 FORMAT(15,5E16.8)
 2222 FORMAT(2I2)
 2224 FORMAT(2X,4HNA =I2,3X,4HNB = I2///)

    1 READ(5,1000)(ANAME(I),(I=1,8),M,NPTS,TSTART,TEND,TINC,ATOT,V,CONC,U
     1,CP,ORDST1,ALPHND,DORD1,ORDST2,BETEND,DORD2
      READ(5,2222)NA,NB
```

```
      READ(5,1001)(TEMP(I),AR(I),H(I),DELT(I),I=1,NPTS)
      WRITE(6,2000)(ANAME(I),I=1,8)
      WRITE(6,2002)M,NPTS,ATOT,V,CONC,U,CP,ORDST1,ALPHND,DDRD1,ORDST2,BE
     2TEND,DORD2,TINC,TSTART,TEND
      WRITE(6,2224) NA,NB
      WRITE(6,2005)(I,TEMP(I),AR(I),H(I),DELT(I),I=1,NPTS)
      WRITE(6,3000)
      JJJ = 1
      IF(TSTART.EQ.0.0)JJJ=2
      TDIFF = TEMP(NPTS) - TEMP(1)
      NS = NPTS
      N = NPTS
      NNN = 1
      CONV = 1.0
      IF (ATOT.NE.0.0)GO TO 12
C     IF ATOT IS ZERO THEN MUST INTEGRATE TO GET AREA
      NS = NPTS - 2
      N = NPTS - 1
      NNN = 2
      HDIFF = H(NPTS) - H(1)
  401 IF(TINC.EQ.0.0)GO TO 9
C     IF TINC HAS A VALUE THEN ALL INCREMENTS ARE EQUAL AND HAVE THIS VALUE
      PTS = NPTS
      TDIFF = (PTS-1.0)*TINC
    9 DO 7 J = 2,NPTS
      IF (TINC.EQ.0.0) GO TO 11
      TEMP(J) = TEMP(J-1) + TINC
   11 HCHNG = (HDIFF/TDIFF)*(TEMP(J) - TEMP(1))
    7 H(J) = H(J) - H(1) - HCHNG
      H(1) = 0.0
      AR(1) = 0.0
      L = 1
      DO 500 J = 1,NS,2
      I = J
  700 T(4) = TEMP(I+1)-TEMP(I)
```

```
      T(5) = TEMP(I+2)-TEMP(I+1)
      CON = (TEMP(I)*TEMP(I))*(-T(5)) -
     1(TEMP(I+1)*TEMP(I+1))*(TEMP(I)-TEMP(I+2)) +
     2(TEMP(I+2)*TEMP(I+2))*(-T(4))
      A = (H(I)*(-T(5)) - H(I+1)*(TEMP(I)-TEMP(I+2)) +
     1H(I+2)*(-T(4)))/CON
      B = ((H(I+1)-H(I))-A*(TEMP(I+1)*TEMP(I+1)-TEMP(I)*TEMP(I))) /T(4)
      C = H(I+2)-(A*TEMP(I+2)+B)*TEMP(I+2)
      K = I-1
      DO 600 M=1,3
      K = K + 1
  600 T(M) = ((A*TEMP(K)/3.0+B/2.0)*TEMP(K)+C)*TEMP(K)
   31 GO TO (901,902),L
  901 GARB1 = T(2) -T(1)
      IF(GARB1.LT.0.0) GO TO 903
  902 GARB2 = T(3) - T(2)
      IF(GARB2.LT.0.0) GO TO 903
      GO TO (904,905),L
  904 AR(I+1) = AR(I)+GARB1
  905 AR(I+2) = AR(I+1)+GARB2
      IF((I+2).EQ.NPTS)GO TO 800
      IF((I+3).NE.NPTS)GO TO 500
      L = 2
      I = I + 1
      GO TO 700
  903 WRITE(6,300)
      WRITE(6,4000)I,GARB1,GARB2
      GARB1 = ((H(I+1)-H(I))*(T(4))/2.0)+H(I)*(T(4))
      GARB2=((H(I+2)-H(I+1))*(T(5))/2.0)+H(I+1)*(T(5))
      WRITE(6,4000)I,GARB1,GARB2
      WRITE(6,3000)
      GO TO (904,905),L
  500 CONTINUE
  800 ATOT = AR(NPTS)
      T(1) = 0.0
```

```
      DO301I=1,N
  301 XX(I)=AR(I)/ATOT
      WRITE(6,2002)M,NPTS,ATOT,V,CONC,U,CP,ORDST1,ALPHND,DORD1,ORDST2,BE
     2TEND,DORD2,TINC,TSTART,TEND
      WRITE(6,2001)(I,TEMP(I),AR(I),H(I),DELT(I),XX(I),I=1,NPTS)
      WRITE(6,3000)
   12 GO TO (406,4),JJJ
C     CONVERT TIME TO TEMPERATURE IF TSTART HAS A VALUE
  406 DO 13 I = 1,NPTS
   13 TEMP(I) = TEND =((TEND-TSTART)/TDIFF)*(TEMP(NPTS)-TEMP(I))
    4 NSAVE = N
      NFIT = NS
      IF(MTYPE.EQ.1)GOTO3
      DO 10 JI = 1,100
      AJ = JI
      ALPHA=ORDST1+DORD1*(AJ-1.)
      DO303JJ=1,100
      AJJ=JJ
      BETA=ORDST2+DORD2*(AJJ-1.)
      DO 6 I=NNN,N
      RTCNST(I)=H(I)/(ATOT*XX(I)**ALPHA*(1.0-XX(I))**BETA)
      Y(I) = ALOG(RTCNST(I))
    6 X(I) = 1000.0/TEMP(I)
      WRITE(6,2003)ALPHA,BETA
      NS=NB-NA+1
      GOTO14
00003 CONST=(U*ATOT*V)/CONC
      ORD=ORDST
      DO5I=NNN,N
      DENOM(I)=U*(ATOT-AR(I))-CP*DELT(I)
00005 DNUM(I)=(CP*H(I)+U*DELT(I))*CONV
      DO10II=1,100
      CONPWR=CONST**(ORD-1.0)
      DO6I=NNN,N
      RTCNST(I)=CONPWR*DNUM(I)/(DENOM(I)**ORD)
```

```
      IF(RTCNST(I).GT.0.0)GOTO407
      WRITE(3,400)
      WRITE(3,4000)I,RTCNST(I),CONPWR,DNUM(I),DENOM(I),ORD
      IF(RTCNST(I).EQ.0.0)GOTO115
      RTCNST(I)=ABS(RTCNST(I))
00407 Y(I)=ALOG(RTCNST(I))
00006 X(I)=1000.0/TEMP(I)
      WRITE(3,2003)ORD
   14 SUMX=0.0
      SUMY=0.0
      SUMXY=0.0
      SUMX2=0.0
      SUMY2=0.0
   40 DO50I=NA,NB
      SUMX=SUMX+X(I)
      SUMY=SUMY+Y(I)
      SUMXY=SUMXY+X(I)*Y(I)
      SUMX2=SUMX2+X(I)*X(I)
   50 SUMY2=SUMY2+Y(I)*Y(I)
      FN = NS
      SUMXSQ = SUMX*SUMX
      A=(FN*SUMXY-SUMX*SUMY)/(FN*SUMX2-SUMXSQ)
      B=(SUMY*SUMX2-SUMXY*SUMX)/(FN*SUMX2-SUMXSQ)
      ENERG = -A*1.987
      WRITE(6,60)ENERG,A,B
      FRACT=((SUMXY-SUMX*SUMX*SUMY/FN)**2)/(SUMX2-SUMXSQ/FN)
      E=SUMY2-(SUMY*SUMY/FN)- FRACT
      S2=E/(FN-2.0)
      S=SQRT(S2)
      SA2=S2/(SUMX2-(SUMXSQ/FN))
      SA=SQRT(SA2)
      SB2=S2*SUMX2/(FN*SUMX2-SUMX3Q)
      SB=SQRT(SB2)
      WRITE(6,70)S,SA,SB
      DO80I=NA,NB
      YCALC(I)=A*X(I)+B
```

```
 80 T(I)=Y(I)-YCALC(I)
    VMAX=ABS(T(I))
    DO89I=NA,NB
    TEST=VMAX-ABS(T(I))
    IF(TEST.GE.0.0)GOTO89
    VMAX=ABS(T(I))
    JAM=I
 89 CONTINUE
    DEV=ABS(T(JAM))-3.0*S
    IF(DEV.LT.0.0)GOTO115
100 WRITE(6,200)JAM,Y(JAM)
    DO110I=JAM,NB
    X(I)=X(I+1)
110 Y(I)=Y(I+1)
    NS = NS - 1
    NB=NB-1
    GOTO14
115 WRITE(6,2004)(I,TEMP(I),RTCNST(I),Y(I),YCALC(I),X(I),T(I),I=1,N)
    IF(BETA.GE.BETEND)GOTO305
    N = NSAVE
    NN = NOUT
303 CONTINUE
305 IF(ALPHA.GE.ALPHND)GOTO1
    N=NSAVE
    NN=NOUT
 10 CONTINUE
    END
```

TABLE XXXIII

LEAD CARBONATE, FIRST PEAK. RATE CONSTANT DATA FOR ARRHENIUS ACTIVATION ENERGY PLOT

$\alpha = 0.4$, $\beta = 0.6$ Slope $= (-33.83 \pm 0.986)10^3$ $E_a = 67.23$ kcal/mole

Standard Deviation of a Single lnk $= 0.0676$

Number	Temp	Rate K*	LN K	LN K, CALC	1000/Temp
1	583.00000	0.30860035E-01	-0.34782933E 01	-0.35627384E 01	0.17152659E 01
2	585.00000	0.35009851E-01	-0.33521258E 01	-0.33643356E 01	0.17094017E 01
3	586.50000	0.38108709E-01	-0.32673125E 01	-0.32164212E 01	0.17050298E 01
4	588.00000	0.43112610E-01	-0.31439398E 01	-0.30692621E 01	0.17006803E 01
5	589.50000	0.50270481E-01	-0.29903372E 01	-0.29228511E 01	0.16963528E 01
6	591.00000	0.60657123E-01	-0.28025182E 01	-0.27771835E 01	0.16920474E 01
7	593.00000	0.73978072E-01	-0.26039866E 01	-0.25841065E 01	0.16863406E 01
8	595.00000	0.90358973E-01	-0.24039650E 01	-0.23923278E 01	0.16806723E 01
9	596.00000	0.10774043E 00	-0.22280304E 01	-0.22969213E 01	0.16778523E 01
10	597.00000	0.12344781E 00	-0.20919368E 01	-0.22018338E 01	0.16750419E 01
11	599.00000	0.14154876E 00	-0.19551110E 01	-0.20126119E 01	0.16694491E 01
12	601.00000	0.16536960E 00	-0.17995723E 01	-0.18246493E 01	0.16638935E 01
13	602.50000	0.18386417E 00	-0.16935580E 01	-0.16844964E 01	0.16597510E 01
14	604.00000	0.19278688E 00	-0.16461699E 01	-0.15450397E 01	0.16556291E 01

*Must be multiplied by 3 deg/minute to convert to per minute.

TABLE XXXIV

LEAD CARBONATE, SECOND PEAK. RATE CONSTANT DATA FOR ARRHENIUS ACTIVATION ENERGY PLOT

$\alpha = 0.20$, $\beta = 1.60$ Slope $= (-36.960 \pm 1.799)10^3$ $E_a = 73.45$ kcal/mole

Standard Deviation of a Single lnk $= 0.107$

Number	Temp	Rate K*	LN K	LN K, CALC	1000/Temp
1	655.00000	0.68264879E-01	-0.26843599E 01	-0.25539942E 01	0.15267175E 01
2	659.00000	0.11052057E 00	-0.22025536E 01	-0.22114496E 01	0.15174507E 01
3	662.00000	0.16679705E 00	-0.17909775E 01	-0.19572577E 01	0.15105740E 01
4	664.00000	0.18703440E 00	-0.16764627E 01	-0.17890725E 01	0.15060241E 01
5	667.00000	0.21205871E 00	-0.15508921E 01	-0.15386853E 01	0.14992504E 01
6	671.00000	0.29309800E 00	-0.12272483E 01	-0.12083192E 01	0.14903130E 01
7	673.00000	0.31571556E 00	-0.11529136E 01	-0.10446086E 01	0.14858841E 01
8	676.00000	0.41017146E 00	-0.89118001E 00	-0.80085897E 00	0.14792899E 01
9	679.00000	0.55019600E 00	-0.59748070E 00	-0.55926323E 00	0.14727540E 01
10	682.00000	0.81176453E 00	-0.20854497E 00	-0.31979323E 00	0.14662756E 01

*Must be multiplied by 3 deg/minute to convert to per minute.

TABLE XXXV

LEAD CARBONATE, THIRD PEAK. RATE CONSTANT DATA FOR ARRHENIUS ACTIVATION ENERGY PLOT

$\alpha = 0.60, \quad \beta = 1.0$ $\qquad$ Slope $= (-39.97 \pm 5.490)10^3$ $\qquad$ $E_a = 79.42$ kcal/mole

Standard Deviation of a Single lnk = 0.0951

Number	Temp	Rate K[*]	LN K	LN K, CALC	1000/Temp
1	723.00000	0.21675650E 00	-0.15289807E 01	-0.14236889E 01	0.13831259E 01
2	724.00000	0.30035672E 00	-0.12027845E 01	-0.13473325E 01	0.13812155E 01
3	726.00000	0.29217202E 00	-0.12304126E 01	-0.11952500E 01	0.13774105E 01
4	728.00000	0.32312972E 00	-0.11297015E 01	-0.10440040E 01	0.13736264E 01
5	729.00000	0.40343920E 00	-0.90772949E 00	-0.96869183E 00	0.13717421E 01
6	730.00000	0.44558517E 00	-0.80836687E 00	-0.89358616E 00	0.13698630E 01
7	731.00000	0.42447495E 00	-0.85690229E 00	-0.81868601E 00	0.13679890E 01
8	733.00000	0.49892202E 00	-0.69530548E 00	-0.66949844E 00	0.13642565E 01

*Must be multiplied by 3 deg/minute to convert to per minute.

TABLE XXXVI

AMMONIUM CHLORIDE RATE CONSTANT DATA FOR ARRHENIUS ACTIVATION ENERGY PLOT

$\alpha = 0.2$, $\beta = 0.2$ Slope $= (-13,830 \pm 0.123)10^3$ $E_a = 27.49$ Kcal/mole

Standard Deviation of a Single lnk $= 0.0318$

Number	Temp	Rate K*	LN K	LN K, Calc	1000/Temp
1	543.00000	0.38857521E-02	-0.55504387E 01	-0.55612852E 01	0.18416206E 01
2	550.00000	0.49598892E-02	-0.53063719E 01	-0.52370362E 01	0.18181818E 01
3	556.00000	0.72311841E-02	-0.49293525E 01	-0.49656067E 01	0.17985611E 01
4	559.00000	0.81085291E-02	-0.48148388E 01	-0.48320773E 01	0.17889088E 01
5	562.00000	0.92850496E-02	-0.46793497E 01	-0.46999731E 01	0.17793594E 01
6	565.00000	0.10886125E-01	-0.45202662E 01	-0.45692718E 01	0.17699115E 01
7	568.00000	0.12044533E-01	-0.44191444E 01	-0.44399512E 01	0.17605634E 01
8	571.00000	0.13468622E-01	-0.43073926E 01	-0.43119896E 01	0.17513135E 01
9	575.00000	0.15222028E-01	-0.41850117E 01	-0.41434510E 01	0.17391304E 01
10	578.00000	0.17417852E-01	-0.40502596E 01	-0.40185781E 01	0.17301038E 01
11	581.00000	0.19677436E-01	-0.39282827E 01	-0.38949945E 01	0.17211704E 01
12	583.00000	0.22383725E-01	-0.37994212E 01	-0.38133121E 01	0.17152659E 01
13	587.00000	0.25441524E-01	-0.36713727E 01	-0.36516171E 01	0.17035775E 01
14	590.00000	0.28891815E-01	-0.35441970E 01	-0.35317848E 01	0.16949152E 01
15	593.00000	0.32992283E-01	-0.34114816E 01	-0.34131647E 01	0.16863406E 01
16	596.00000	0.37080447E-01	-0.32946655E 01	-0.32957390E 01	0.16778523E 01
17	600.00000	0.42973043E-01	-0.31471823E 01	-0.31409977E 01	0.16666667E 01
18	602.00000	0.45348303E-01	-0.30933825E 01	-0.30643985E 01	0.16611296E 01
19	603.00000	0.48563131E-01	-0.30248907E 01	-0.30262892E 01	0.16583748E 01
20	605.00000	0.53079374E-01	-0.29359669E 01	-0.29504490E 01	0.16528926E 01
21	606.00000	0.57183104E-01	-0.28614968E 01	-0.29127164E 01	0.16501650E 01

*Must be multiplied by 3 deg/minute to convert to per minute.

APPENDIX B

EQUIPMENT AND PARTS

Item and Description	Manufacturer or Source of Supply
Antibacklash Gear Assembly, P13-7-260	PIC Design Corp. East Rockaway, New York 11518
Bantam Speed Reducer, 11-C1000 R	Metron Instruments, Inc. Littleton, Colorado
C.A.T. Control Unit Series 60, Model C-1	Leeds and Northrup Co. 4901 Stenton Avenue Philadelphia 44, Pa.
Collet 10-Turn Counter Dials 116-208-1	E. F. Johnson Company Waseca, Minnesota
Cubical Mirrors 1/4 by 1/4 inch Cubes	A. D. Jones Optical Works 2400 Massachusetts Avenue Cambridge, Mass.
Diffusion Pump, Metal Oil MCF-60	Consolidated Vacuum Corp. 7900 Carpenter Freeway Dallas 7, Texas
Fixed Field Electric Clutch FFC-30, 24 VDC	Simplatrol Products Crop. Worcester, Mass.
Furnace Element Hevi-duty Type, 2712SP	Hevi-Duty Heating Equipment Division Basic Products Corp. Watertown, Wisconsin
Glove Bags, Model 3X	I^2R Instruments for Research and Industry, 108 Franklin Avenue Cheltenham, Pa.
Hall Multiplier Type MB 26-EI38-Mu	Instrument Systems Corp. 129-07 18th Avenue College Point 56, L.I., New York
Hastings Vacuum Gauge Type DV-6M	Hastings-Raydist, Inc. Hampton, Virginia

Item and Description	Manufacturer or Source of Supply
High Temperature Cement Norton RA 1139	Norton Company Worcester 6, Mass..
Miller Cold Cathode Gauge Tube and Magnet Type T-100	Miller Laboratories P. O. Box 97 Brea, California
Null-Detector, DC Amplifier	Leeds and Northrup 4901 Stenton Avenue Philadelphia 44, Pa.
Operational Amplifier Burr-Brown 1605	Burr-Brown Research Corp. P. O. Box 11400 Tucson, Arizona 85706
Permacel-423 Teflon Film Tape	Permacel, U. S. Highway No. 1 New Brunswick, N. J.
Reference Cell, D-845 (1.0194 Volts at 25°C) Serial No. 379804	Muirhead and Co., Ltd. Beckenham, Kent, England
Sauereisen No. P-7 Insu-Lute Hi-Temp Cement	Sauereisen Cements Co. Pittsburgh 15, Pa.
Silicontrol, Types VS6431CF and VS6332AF	Vectrol Engineering Division Sprague Electric Co. North Adams, Mass.
Standard Resistor 10-Kohm	Electro Scientific Industries Portland, Oregon
Stepping Motor, Type SS250 and Translator Module STM 250	Superior Electric Co. Bristol, Connecticut
Transformer, High Voltage T21P77	Thordarson Meissner Mt. Carmel, Illinois
Tungsten Wire 0.00079-inch Diameter	North American Phillips Co., Inc. Lewiston, Maine
Tuning Fork Oscillator Model T/f - 0, 1000 Hz	Time and Frequency Batavia, Illinois
Valor Voltage Regulator	Valor Instruments, Inc. 13214 Crenshaw Boulevard Gardena, California
Welch Duo-Seal Mechanical Pump 1402-B	E. H. Sargent and Co. 5919 Peeler St. Dallas 35, Texas

APPENDIX C

DERIVATION OF EXPRESSIONS FOR TORSION WIRE ANISOTROPY

Torsion wire anisotropy results when the clockwise (cw) and counterclockwise (ccw) torque exerted by a wire differ in magnitude for the same angle of rotation. The anisotropy, $\underline{s}$, of a wire may be defined as

$$s = T_w(cw) - T_w(ccw) \tag{1}$$

in which $\underline{T}_w(cw)$ and $\underline{T}_w(ccw)$ represent the magnitude of the torque exerted by the wire when rotated through the same angle clockwise and counterclockwise.

The expressions derived for the clockwise and counterclockwise balancing torque exerted by the elctrodynamometer are

$$T_{12} = (K + \delta)i^2_{12}, \tag{2}$$

and

$$T_{34} = (K - \delta)i^2_{34}. \tag{3}$$

When the torque exerted by the wire is balanced by the electrodynamom-eter, one may equate the following:

$$T_w(cw) = T_{12} = (K + \delta)i^2_{12} \tag{4}$$

$$T_w(ccw) = T_{34} = (K - \delta)i^2_{34} \tag{5}$$

which when substituted into equation (1) yields,

$$s = T_{12} - T_{34} = (K + \delta)i_{12}^2 - (K - \delta)i_{34}^2. \tag{6}$$

Equation (6) may be rearranged to

$$s = K(i_{12}^2 - i_{34}^2) + \delta(i_{12}^2 + i_{34}^2). \tag{7}$$

If the lead wire effect, $\underline{\delta}$, is negligible, equation (7) reduces to

$$s = K(i_{12}^2 - i_{34}^2) \tag{8}$$

which may be divided by $\underline{T}_{12} = (K + \delta)i_{12}^2 \cong Ki_{12}^2$ to give

$$s/T_{12} = \frac{i_{12}^2 - i_{34}^2}{i_{12}^2}. \tag{9}$$

From equation (7), if $\underline{s}$ is negligible one obtains

$$\frac{\delta}{K} = \frac{i_{34}^2 - i_{12}^2}{i_{12}^2 + i_{34}^2}. \tag{10}$$

VITA

Paul Dean Gwinup

Candidate for the Degree of

Doctor of Philosophy

Thesis: DIFFERENTIAL SCANNING CALORIMETRY IN HIGH TEMPERATURE CHEMISTRY

Major Field: Chemistry

Biographical:

Personal Data: Born at Shawnee, Oklahoma, October 13, 1931, the son of Charles Franklin and Nola Marie Gwinup.

Education: Graduated from Pocahontas High School in 1950; attended Southern Baptist College, Walnut Ridge, Arkansas; received the Bachelor of Science degree from Oklahoma State University, with a major in Chemistry, in May, 1957; completed requirements for the Doctor of Philosophy degree in July, 1967.

Professional Experience: Research Chemist with Jersey Production Research Company, Tulsa, Oklahoma, 1957-1959; Assistant Professor of Chemistry, Arkansas State University, 1965 to present.